STATE OF CALIFORNIA • DEPARTMENT OF TRANSPORTATION

TECHNICAL REPORT DOCUMENTATION PAGE

TR0003 (REV 10/98)

ADA Notice

For individuals with sensory disabilities, this document is available in alternate formats. For information call (916) 654-6410 or TDD (916) 654-3880 or write Records and Forms Management, 1120 N Street, MS-89, Sacramento, CA 95814.

1. REPORT NUMBER	2. GOVERNMENT ASSOCIATION NUMBER	3. RECIPIENT'S CATALOG NUMBER
CA16-2532		

4. TITLE AND SUBTITLE	5. REPORT DATE
Assessment of Soil Arching Factor for Retaining Wall Pile Foundations	03/31/2017
	6. PERFORMING ORGANIZATION CODE

7. AUTHOR	8. PERFORMING ORGANIZATION REPORT NO.
Andre R. Barbosa, Scott A. Ashford, Henry B. Mason, Andre F. V. Belejo	

9. PERFORMING ORGANIZATION NAME AND ADDRESS	10. WORK UNIT NUMBER
School of Civil and Construction Engineering 101 Kearney Hall Oregon State University Corvallis, OR 97331-3212	11. CONTRACT OR GRANT NUMBER 65A0497

12. SPONSORING AGENCY AND ADDRESS	13. TYPE OF REPORT AND PERIOD COVERED
Department to California Department of Transportation, Division of Engineering Services, 1801 30th Street, MS #9-2/5I, Sacramento, CA 95816	Final Report
	14. SPONSORING AGENCY CODE

15. SUPPLEMENTARY NOTES

16. ABSTRACT

Despite the prevalence of the soldier piles retaining wall systems as temporary and even permanent shoring systems along state highways, relatively little is known on the effect of the foreslope bench width and the slope inclination on the arching capability factor used in design codes and standards. A review of literature indicated that no full-scale tests were conducted for soldier pile systems and only a few components have been modeled analytically, often using 2-D analyses that cannot capture the complex 3-D behavior of the arching behavior in active and passive regions of soldier pile retaining wall systems. To help address this gap in knowledge, an analytical research program is developed herein to assess the current design procedures on soldier pile walls and make recommendations for improvement, specifically with respect to 3-D effects of soil arching, foreslope sloping ground, and bench width, based on a parametric study supported on advanced nonlinear finite element models of the soldier pile systems. Discussions on how to account for 3-D effects based on 2-D analyses and on how to account for bench width effects when classical soil theories are used in design are provided. Finally, a proposed experimental program is simulated using the modeling approaches developed in this study.

17. KEY WORDS	18. DISTRIBUTION STATEMENT
Soil arching, soldier pile walls, lagging, retaining systems, soil slope, modeling	No restrictions. This document is available to the public through the National Technical Information Service, Springfield, Virginia 22161

19. SECURITY CLASSIFICATION *(of this report)*	20. NUMBER OF PAGES	21. COST OF REPORT CHARGED
None	179	

Reproduction of completed page authorized.

ASSESSMENT OF SOIL ARCHING FACTOR FOR RETAINING WALL PILE FOUNDATIONS

FINAL PROJECT REPORT

by

Andre R. Barbosa, Ph.D.
Scott A. Ashford, Ph.D.
Henry B. Mason, Ph.D.

and

Andre F.V. Belejo

Oregon State University

May 2017

CALIFORNIA DEPARTMENT OF TRANSPORTATION

DISCLAIMER

This document is disseminated in the interest of information exchange. The contents of this report reflect the views of the authors who are responsible for the facts and accuracy of the data presented herein. The contents do not necessarily reflect the official views or policies of the State of California or the Federal Highway Administration. This publication does not constitute a standard, specification or regulation. This report does not constitute an endorsement by the Department of any product described herein.

For individuals with sensory disabilities, this document is available in Braille, large print, audiocassette, or compact disk. To obtain a copy of this document in one of these alternate formats, please contact: the Division of Research and Innovation MS-83, California Department of Transportation, P.O. Box 942873, Sacramento, CA 94273-0001.

ACKNOWLEDGMENTS

Input and comments from the technical advisory team are sincerely appreciated. The team would like to thank Frank McKenna and Pedro Arduino for working on improving the OpenSees models and tools needed for the research developed herein. In addition, the team would like to thank Dr. Minjie Zhu for discussions and developments of Paraview used extensively in the visualization of the results of the numerical models. This work was funded by California Department of Transportation under Agreement #65A0497.

EXECUTIVE SUMMARY

Despite the prevalence of the soldier piles retaining wall systems as temporary and even permanent shoring systems along state highways, relatively little is known on the effect of the foreslope bench width and the slope inclination on the arching capability factor used in design codes and standards. A review of literature indicated that no full-scale tests were conducted for soldier pile systems and only a few components have been modeled analytically, often using 2-D analyses that cannot capture the complex 3-D behavior of the arching behavior in active and passive regions of soldier pile retaining wall systems. To help address this gap in knowledge, an analytical research program is developed herein to assess the current design procedures on soldier pile walls and make recommendations for improvement, specifically with regard to 3-D effects of soil arching, foreslope sloping ground and bench width, based on a parametric study supported on advanced nonlinear finite element models of the soldier pile systems. Discussions on how to account for 3-D effects based on 2-D analyses and on how to account for bench width effects when classical soil theories are used in design are provided. Finally, a proposed experimental program is simulated using the modeling approaches developed in this study.

TABLE OF CONTENTS

Page

1 INTRODUCTION 11

1.1 OBJECTIVE OF THIS STUDY 11

1.2 ORGANIZATION OF THIS REPORT 12

2 LITERATURE REVIEW 14

2.1 OVERVIEW 14

2.2 EFFECTS OF SOIL ARCHING AND SLOPE ON PILES AND RETAINING WALLS 14

2.2.1 Soil Arching Theory and Experimental Tests 14

2.2.2 Soil Arching and Slopes 16

2.2.3 Effects of Soil Slope on Lateral Capacity of Piles 21

2.3 CRITERIA FOR DESIGN AND ANALYSIS 25

2.3.1 Design Procedures 25

2.3.2 Analysis Procedures 26

2.4 SUMMARY 28

3 METHODOLOGY FOR ASSESSMENT OF THE ARCHING FACTOR 31

3.1 OVERVIEW 31

3.2 DEFINITION OF CASE STUDIES 31

3.2.1 Soil Definition 31

3.2.2 Parameter Selection 33
3.3 PARAMETRIC CASE STUDY 34
3.3.1 Soldier Pile Design 34
3.3.2 Development of Numerical Models 39
3.3.3 Pushover Analysis Methodology 47
3.3.4 Analysis of Results / Post-processing 49
3.3.5 Assessment of the Arching Capability Factor 50
4 FINITE ELEMENT RESULTS AND DISCUSSION 52
4.1 OVERVIEW 52
4.2 SOLDIER PILE DESIGN 52
4.3 THEORETICAL PASSIVE RESISTANCE VALUES 56
4.4 2-D PLAN ANALYSIS RESULTS 58
4.5 3-D MODEL RESULTS 63
4.5.1 Effect of load distribution and detachment effects 63
4.5.2 Validation of the 3-D Modeling Approach 67
4.5.3 Nonlinear Static Pushover Analysis Results 72
5 ARCHING CAPABILITY FACTOR ASSESSMENT 83
5.1 Overview 83
5.2 Effect of Bench Width 83
5.3 Effect of Soldier Pile Retaining Wall Geometry: Wall height and pile spacing 86

5.4 Effect of Analysis Dimensionality: 2-D versus 3-D analysis 90

6 PROPOSED REVISIONS TO THE PASSIVE RESISTANCE EQUATION 93

7 SIMULATION OF A PROPOSED EXPERIMENTAL PROGRAM 96

7.1 OVERVIEW 96

7.2 PROPOSED EXPERIMENTAL PROGRAM 96

7.3 SIMULATION OF AN EXAMPLE OF A PROPOSED EXPERIMENT 97

7.4 EFFECT OF LOAD DISTRIBUTION 99

8 SUMMARY, CONCLUSIONS, AND SUGGESTIONS FOR FURTHER RESEARCH 100

9 REFERENCES 103

APPENDICES AP-1

LIST OF FIGURES

Page

Figure 2-1: Load acting on the pile versus soil movement (Liang and Zeng 2002). 18

Figure 2-2: Effect of variation in internal frictional angle: cohesionless soil (Liang and Zeng 2002). 18

Figure 2-3: Effect of variation in cohesion (Liang and Zeng 2002). 19

Figure 2-4: Effect of pile diameter (Liang and Zeng 2002). 19

Figure 2-5: Measured load versus measured pile displacement at 3 ft from ground surface for 0*d*, 2*d*, 4*d*, 8*d* piles (Nimityongsukul et al. 2012). 24

Figure 2-6: Comparison of Caltrans method and measured results for 0*d*, 2*d*, 4*d* and 8*d* piles (Nimityongsukul et al. 2012). 24

Figure 2-7: Cantilever retaining walls (Caltrans 2011): (a) wall deformation; (b) load distribution, (c) load simplification. 27

Figure 3-1: Load diagram for a single layer (Caltrans 2011): (a) granular soil; (b) cohesive soil. 36

Figure 3-2: Load distribution for cohesive backfill (Caltrans 2011). 36

Figure 3-3: Cross-section of the embedded pile. 37

Figure 3-4: Passive earth pressure coefficient (Caquot and Kerisel 1948). 38

Figure 3-5: 2-D Modeled soil meshes (plan view); (a) considering one strip; (b) considering three strips. 40

Figure 3-6: 3-D model mesh: (a) 3-D view; (b) zoom over region of the pile; (c) elevation view 42

Figure 3-7: Part of the numerical model created in *OpenSeesPL* and adjusted using TCL scripts for modeling the HP section above the excavation line. 42

Figure 3-8: Schematic of constitutive model response of a PressureDependMultiYield material showing shear stress, effective confinement, and shear strain relationship. 44
Figure 3-9: Schematic of constitutive model response of a PressureIndependMultiYield material showing shear stress, effective confinement, and shear strain relationship. 44
Figure 3-10: Fiber section: (a) embedded pile; (b) pile above the dredge line. 45
Figure 3-11: Constitutive models used in fiber sections: (a) steel01; (b) concrete04. 46
Figure 3-12: Mohr-Coulomb friction model. 47
Figure 3-13: Pushover analysis scheme. 48
Figure 4-1: 2-D plan analysis scheme for: (a) 1 pile/soil strip; (b) 3 pile/soil strips. *s* is the center-to-center pile distance. 60
Figure 4-2: Capacity curves from 2-D plan analyses considering 1 and 3 pile/soil strips for the medium-stiff clay. 60
Figure 4-3: Effect of pile spacing on capacity curves from 2-D plan analyses: (a) medium-stiff clay; (b) medium-dense sand. 61
Figure 4-4: Plan model for medium-dense sand with width = 4*d*: (a) displacements in X direction; (b) displacements in Y direction. 61
Figure 4-5: Plan model for medium-dense sand with s = 4*d*: (a) stresses in X-direction; (b) stresses in Y-direction; (c) stresses in XY direction. 62
Figure 4-6: Plan model for medium-stiff clay with s = 3*d*: (a) displacements in X-direction; (b) displacements in Y-direction. 62
Figure 4-7: Plan model for medium-stiff clay with s = 3*d*: (a) stresses in X-direction; (b) stresses in Y-direction; (c) stresses in XY direction. 63
Figure 4-8: Load distributions considered: (a) concentrated load; (b) triangular load. 64

Figure 4-9: Comparison between capacity obtained with different load distribution: (a) medium-dense sand; (b) medium-stiff clay; (c) granular cohesive soil. 65
Figure 4-10: Capacity of medium-stiff clay considering gap behind the pile. 66
Figure 4-11: Numerical models developed in Plaxis 3D by Nimityongsukul et al. (2012): (a) baseline model; (b) 4D pile model. 68
Figure 4-12: Numerical models in OpenSees: (a) baseline model; (b) 4D pile model. 68
Figure 4-13: Comparison of capacity curves between the values measured, values obtained in *Plaxis 3D* and values obtained in *Open Sees*: (a) baseline model; (b) 4D pile model. 70
Figure 4-14: Deflection and rotation measured in the field (markers) and obtained from the *OpenSees* models (continuous lines): (a) baseline model; (b) 4D pile model. 71
Figure 4-15: Stresses in Y direction obtained with the *Open Sees* model: (a) baseline model; (b) 4D pile model. 72
Figure 4-16: Effect of embedment depth on capacity curves for a soldier pile retaining wall with h_w = 10 ft and s = 4d. Soil type is medium-dense sand. 73
Figure 4-17: Effect of slope on capacity curves for a soldier pile retaining wall with h_w = 10 ft and s = 4d. Soil type is medium-dense sand. 73
Figure 4-18: Effect of bench width on capacity curves for a soldier pile retaining wall with h_w = 10 ft and s = 4d. Soil type is medium-dense sand. 74
Figure 4-19: 3-D model – 3-D view of σ_{yy} stresses and deformed shape for a pile-head displacement = 2 in. Case: medium-dense sand, h_w=10 ft, s=4d, and no slope. 75
Figure 4-20: 3-D model – Plan view of σ_{yy} stresses at depth = -2d, for pile-head displacement = 2 in. Case: medium-dense sand, h_w=10 ft, s=4d, and no slope. 75

Figure 4-21: 3-D model – Elevation view of σ_1 stresses for a pile-head displacement = 2 in. Case: medium-dense sand, h_w=10 ft, s=4d, and no slope. 76

Figure 4-22: 3-D model – Elevation view of σ_{YZ} stresses in YZ direction and deformed shape for pile-head displacement = 2 in, Case: medium-dense sand, h_w=10 ft, s=4d, and no slope. 76

Figure 4-23: Capacity curves for soldier pile retaining wall system. Case: medium stiff clay, hw = 10 ft and s = 4d. 77

Figure 4-24: 3-D model – 3-D view of stresses in σ_{yy} for a pile-head displacement = 2 in. Case: medium-stiff clay, h_w = 10 ft, s = 4d, no slope. 78

Figure 4-25: Plan view of stresses in σ_{yy} at z = - 2d, for a pile-head displacement = 2 in. Case: medium-stiff clay, h_w = 10 ft, s = 4d, no slope. 78

Figure 4-26: Elevation view of σ_1 stresses for a pile-head displacement = 2 in. Case: medium-stiff clay, h_w = 10 ft, s = 4d, no slope. 79

Figure 4-27: Capacity curves different embedment depths. 80

Figure 4-28: Capacity curves for different slope conditions. 80

Figure 4-29: Capacity curves for different bench widths. 81

Figure 4-30: 3-D view of σ_{yy} stresses for a pile-head displacement = 2 in. Case: granular cohesive soil, h_w = 10 ft, s = 4d, no slope. 82

Figure 4-31: Plan view of σ_{yy} stresses for a pile-head displacement = 2 in at z = -2d. Case: granular cohesive soil, h_w = 10 ft, s = 4d, no slope. 82

Figure 5-1: Arching capability factor assessment for medium-dense sand: (a) h_w = 10 ft and s = 4d; (b) h_w = 10 ft and s = 3d; (c) h_w = 15 ft and s = 4d; (d) h_w = 15 ft and s = 3d. 84

Figure 5-2: Arching capability factor assessment for medium-stiff clay: (a) h_w = 10 ft and s = 4d; (b) h_w = 10 ft and s = 3d; (c) h_w = 15 ft and s = 4d; (d) h_w = 15 ft and s = 3d. 85

Figure 5-3: Arching capability factor assessment for medium-stiff clay: (a) h_w = 10 ft and s = 4d; (b) h_w = 10 ft and s = 3d; (c) h_w = 15 ft and s = 4d; (d) h_w = 15 ft and s = 3d. 86

Figure 5-4: Effect of wall height on arching capability factor for medium-dense sand case: (a) s = 4d, with no slope; (b) s = 4d, 3:2 slope, and bench width = 8d. 87

Figure 5-5: Effect of wall height on arching capability factor for medium-stiff clay soil case: *s* = 4*d*, no slope. 88

Figure 5-6: Effect of wall height on arching capability factor for granular cohesive soil case: (a) *s* = 4*d*, no slope; (b) *s* = 4*d*, 2:1 slope, and 4*d* bench width. 88

Figure 5-7: Effect of pile spacing on arching capability factor for medium-dense sand case: (a) h_w=10 ft, no slope; (b) h_w=10 ft, 2:1 slope, and 4d bench width. 89

Figure 5-8: Effect of pile spacing on arching capability factor for medium-stiff clay case: h_w=10 ft, no slope..... 89

Figure 5-9: Effect of pile spacing on arching capability factor for granular cohesive soil case: (a) h_w=10 ft, no slope; (b) h_w=10 ft, 3:2 slope, and 8d bench. 90

Figure 5-10: Effect of analysis dimensionality on system capacity and arching capability factor for medium-dense sand: (a) h_w = 10 ft, s = 4d, no slope; (b) h_w = 10 ft, s = 4d, 2:1 slope, and 4d bench width. 91

Figure 5-11: Effect of analysis dimensionality on system capacity and arching capability factor for medium-stiff clay: (a) h_w = 10 ft, s = 4d, no slope; (b) h_w = 10 ft, s = 4d, 2:1 slope, and 4d bench width. 91

Figure 5-12: Effect of analysis dimensionality on system capacity and arching capability factor for granular cohesive soil: (a) h_w = 10 ft, s = 4d, no slope; (b) h_w = 10 ft, s = 4d, 3:2 slope, 8d bench width. 92

Figure 6-1: Plot to determine bench width effect factor, f_B. 95

Figure 7-1: Plan view of the proposed test set-up for combined single pile and system tests..... 97

Figure 7-2: Profile view of proposed test set-up for combined single pile and system tests..... 98

Figure 7-3: Schematic representation of the experimental simulation. 98

Figure 7-4: Capacity curves obtained from the experiment simulation, hw = 10 ft, s = 4d. 99

LIST OF TABLES

Page

Table 2-1: Arching capability factor for cohesionless soils 28

Table 2-2: Arching capability factor for cohesive soils 28

Table 3-1: Selected Soils 32

Table 3-2: Parameter definition 34

Table 4-1: Pile embedment depths considered for the medium dense sand study cases 53

Table 4-2: Pile embedment depths considered for the medium-stiff clay study cases 54

Table 4-3: Pile embedment depths considered for granular cohesive soil study cases 55

Table 4-4: Pile embedment depth for the medium dense sand study cases 56

Table 4-5: Pile embedment depth for the medium-stiff clay study cases 57

Table 4-6: Pile embedment depth for the granular cohesive soil study cases 58

Table 4-7: Soil parameters 69

Table 4-8: Pile parameters 69

1 INTRODUCTION

Retaining wall soldier pile foundations consist of two basic components, soldier piles and lagging. The soldier piles carry the full earth pressure load while the lagging, which spans the distance between the soldier piles, resists relatively small earth pressure loads. Soldier piles are either installed with pile driving equipment or are set in pre-excavated holes and then concreted in place. The most common soldier piles are rolled steel sections, normally wide flange. Lagging can be treated timber, reinforced shotcrete, reinforced cast in place concrete, precast concrete panels, or steel plates. This type of wall depends on the passive resistance of the foundation material and on the moment resisting capacity of the vertical structural members for stability. When these retaining wall pile foundations are temporary in nature, most often the lagging consists of treated timber boards.

Despite the prevalent usage of soldier pile walls to resist the anticipated loads and deformations, upon close inspection of the "Trenching and Shoring Manual" (Caltrans 2000, Caltrans 2011) "AASHTO LRFD Bridge Design Specifications" (AASHTO, 2012), and based on experience gathered by CALTRANS engineers, it was concluded that the current methods may be overly conservative and a better approach could be adopted, specifically in what concerns the use of arching capability factor used in the design of soldier retaining wall systems.

1.1 OBJECTIVE OF THIS STUDY

The main objective of this research project is to assess the current design procedures on soldier pile walls and make recommendations for improvement, specifically with regard to 3-D effects of soil arching, sloping ground and bench width, based on an advanced nonlinear finite element parametric study developed herein. This work is also used to provide information on a proposed testing program for future full-scale testing to study these topics.

1.2 ORGANIZATION OF THIS REPORT

The document is divided into eight (8) chapters.

Chapter 2 provides a literature review that describes previous studies on soldier pile retaining walls. The discussion focuses on the arching effects and influence of the proximity to slopes in the estimation of earth pressures in soldier pile walls. Following a critical review of relevant technical literature where an exhaustive worldwide literature review search is performed, the main findings are used to define the numerical research program developed herein in order to evaluate the effect of the soil arching on performance of soldier piles.

Chapter 3 presents the methodology developed for assessment of the arching capability factor. A three-dimensional finite element modeling approach is proposed for the soldier piles retaining systems, in order to capture complexities of soil arching, soil movement between piles, settlement of back-fill, and anisotropy of lagging. *OpenSees* (Mazzoni, et al., 2009) is used to model the soldier piles and wall lagging. Linear and non-linear static (displacement-based) pushover analyses were performed. In these analyses, both stiffness and strength of the main components are explicitly modeled.

Chapter 4 presents the results of the finite element parametric study. All analytical studies considered a soldier pile with a foundation consisting of HP14x89 piles set in 24-inch diameter drilled holes with the annulus filled with concrete. Focus is placed on the effect of modeling options on the response of the soldier piles modeled, and main parameters changed include soil type, embedment depth, distance between piles, slope angle in front of the soldier piles retaining wall, and presence of a bench and its width.

Chapter 5 presents the main findings of the effects of slope angle and bench width on the arching capability factor. In addition, the effect of performing 3-D versus 2-D analyses are also addressed in this chapter.

Chapter 6 presents a new design equation that considers the effects of the bench width in the capacity of soldier pile wall systems. This equation is proposed for granular soils, since for clays, based on the results of the 3-D analytical program, changes to the expressions are not needed.

Chapter 7 presents the analysis of a proposed future experimental program, needed to support some of the numerical findings reported. The proposed experimental program could also be used to estimate the factor of safety of the proposed simplified analysis procedure developed herein.

Chapter 8 presents a summary of the work and the main conclusions. In addition, proposed future work is also listed to aid follow on researchers.

2 LITERATURE REVIEW

2.1 OVERVIEW

This chapter presents a literature review of previous studies on the effects of soil arching and piles on retaining walls and on criteria typically used in analysis and design. Section 2.2 presents a review of soil arching theory, soil arching on drilled shaft stabilized slopes, and effects of soil slope on lateral capacity of piles. The availability of loading test data was determined to be relatively limited for soldier pile retaining systems and effects of soil arching. Section 2.3 summarizes the existing criteria for design and analysis of soldier pile retaining wall systems. The literature review concludes with a summary of the review, including the identification of areas where information available in the literature is limited.

2.2 EFFECTS OF SOIL ARCHING AND SLOPE ON PILES AND RETAINING WALLS

In this section, first, studies focused on the theory behind soil arching are reviewed. Second, several analytical and experimental studies that focused on studying the effects of soil arching on pile and piles on slopes are also assessed. Finally, studies addressing effective forces measured on piles in the presence of soil arching and of slope proximity are discussed.

2.2.1 Soil Arching Theory and Experimental Tests

Soil arching is defined as the transfer of pressure from a yielding mass of soil onto adjacent stationary parts of soil. In the transition zone between moving and stationary soil masses, shear stresses develop due to the relative displacement between the two masses. Since the shearing resistance tends to maintain the yielding mass in its original position, the pressure on the support of the yielding part is reduced while the pressure on the adjoining stationary part in increased. Arching occurs whenever there is a localized displacement along any restraining structure, horizontal or vertical, which confines a soil mass.

In soil arching, passive arching occurs when the soil is more compressible than the structure and as a result the soil undergoes large displacements. In this latter case, assuming the structural deformations are uniform, the stresses are highest at the edges and lowest at the centerline of the moving soil mass. When analyzing soldier pile walls, with or without lagging, passive arching can be developed, as the soil masses are restrained by stiffer structural elements (piles or supports)

Soil arching was first investigated and defined by Terzaghi, (1936). The classic studies of soil arching (Terzaghi 1936, Terzaghi, 1943) consisted on predicting pressures on a trap door, when this trap door was displaced from under a soil mass. Based on these studies, soil arching has been applied in designs of silos, bins, and underground structures. Using elastic theory, Chelapati (1964) studied the soil arching phenomenon. Finn (1963) was the first to use plasticity methods, having recognized that elasticity methods in soils are only valid for small deformations and small strains, whereas soil arching is accompanied by large deformations and would thus need to be studied using plastic methods.

The study of the soil arching was integrated with the analysis of slope stability by Wang and Yen (1974). Ito and Matsui (1978) provided a good understanding of the arching effects, developing an analytical procedure to derive closed-form equations used in the determination of earth pressure acting on the soil between the piles. Wang and Liang (1979) and Wang and Salmassian (1978) presented procedures for calculating lateral forces on soldier beams/piles. They analyzed the stability of an unsheathed mass of soil between the soldier beams/piles, using idealized free-body diagrams. The analysis conducted by Wang and Liang (1979), for example, can be used to predict the moment produced by the friction between moving soil masses between fixed vertical supports or soldier piles and stationary masses behind the supports.

Bosscher and Gray (1986) conducted a laboratory test to experimentally model soil arching for a sandy slope. In these tests, fixed gates and swing gates were used to simulate embedded vertical piles and the soil mass between piles, respectively. The authors concluded that: (1) discrete piles embedded into a firm, non-yielding, base in a slope could provide significant additional stability to a slope, (2) the loose soil is still capable of transferring stress, not precluding the possibility of mobilizing soil arching or side friction, and (3) in soldier pile and lagging systems, material costs, strengths, and sizes could be optimized in order to achieve maximum benefit from soil arching.

Wang and Reese, (1986) presented a method for designing drilled shaft retaining walls. The method considers the height of the wall, the soil characteristics, the diameter, length and reinforcing of the drilled shaft, and the spacing between drilled shafts. Other experimental studies (Adachi, et al. 1989, Low, et al. 1994, Chen, et al. 1997) also indicated that the effects of soil arching were observed experimentally and that these significantly increased slope stability, depending on the soil and pile conditions.

In a different context, Atkinson and Potts (1977) and Bolton (1979) studied soil arching in connection with the stability with tunnels. Other works in design of culverts also account for the effect of soil arching in determining the loads on structures, although these are not revised in this report since they fall somewhat outside the scope of the work discussed.

2.2.2 Soil Arching and Slopes

Soil arching effects in drilled shaft stabilized slopes has been studied by several authors. Liang and Zeng (2002), Kahyaoglu et al. (2009), Liang amd Yamin (2010), Liu and Zhang (2010), Yue et al. (2011) and Kourkoulis et al. (2011) are among authors that performed studies on the influence of parameters regarding pile geometry and soil characteristics. Others studies such as Liang et al.

(2010) and Kourkoulis et al. (2012) developed methods for analysis and design of slope-stabilizing piles.

Liang and Zeng (2002) investigated soil arching in drilled shaft stabilized slopes using two-dimensional finite element analyses. The authors assumed rigid-plastic soil behavior, plane strain conditions, and uniform soil movement with respect to shaft length. The formation of soil arching was simulated by applying a triangular displacement field occurring in the soil between the drilled shafts. The model was validated through experimental testing done in the 1980's (Bosscher and Gray 1986, Adachi et al. 1989). It was found that soil arching is highly dependent on the magnitude of soil movement, soil properties (strength parameters), and mainly geometric properties of the drilled shafts (spacing and diameter) as illustrated in Figure 2-1 to Figure 2-4.

Figure 2-1, from Liang and Zeng (2002), shows the load acting on a single pile as a function of the soil movement. It can be observed from this figure that for pile spacing greater than 8*d*, where *d* is the diameter of the pile, the single pile results are identical to the ones obtained using the pile spacing of 8*d*. Figure 2-2 shows the variation of the friction angle with the pile spacing ratio and various soil friction angles for cohesionless soils. It can be observed that the percentage of residual load acting on the soil between piles decreases with increasing friction angle, but increases with increasing pile spacing ratio (in the range of 2*d* to 4*d*). Figure 2-3 highlights the effect of variation of soil cohesion. For low values of cohesion, the load acting between piles decreases with increasing friction angle, and decreases linearly as the soil cohesion increases. Figure 2-4 shows that for the same pile spacing ratio, the diameter of the pile also plays an effect. In this figure it can be seen that the pressures carried by the soil decrease with the increase in the pile diameter.

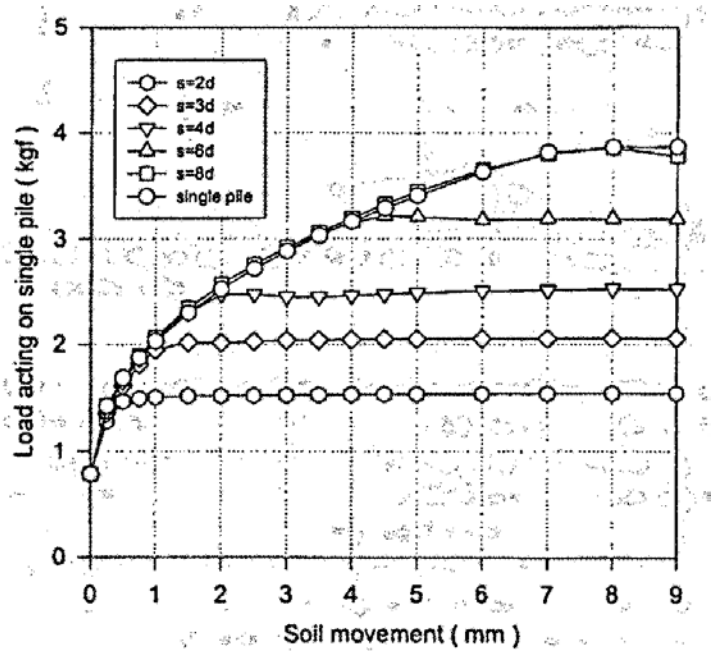

Figure 2-1: Load acting on the pile versus soil movement (Liang and Zeng 2002).

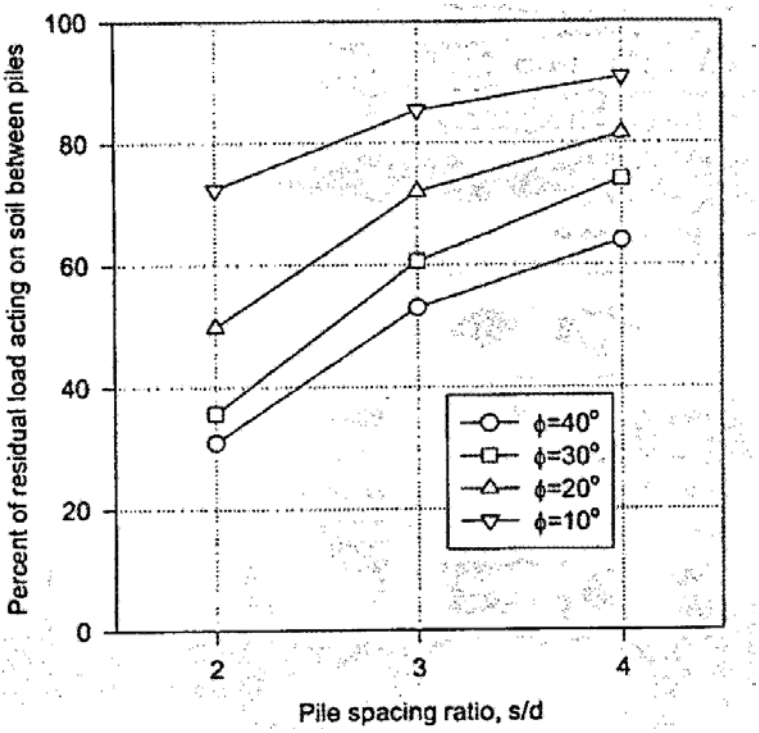

Figure 2-2: Effect of variation in internal frictional angle: cohesionless soil (Liang and Zeng 2002).

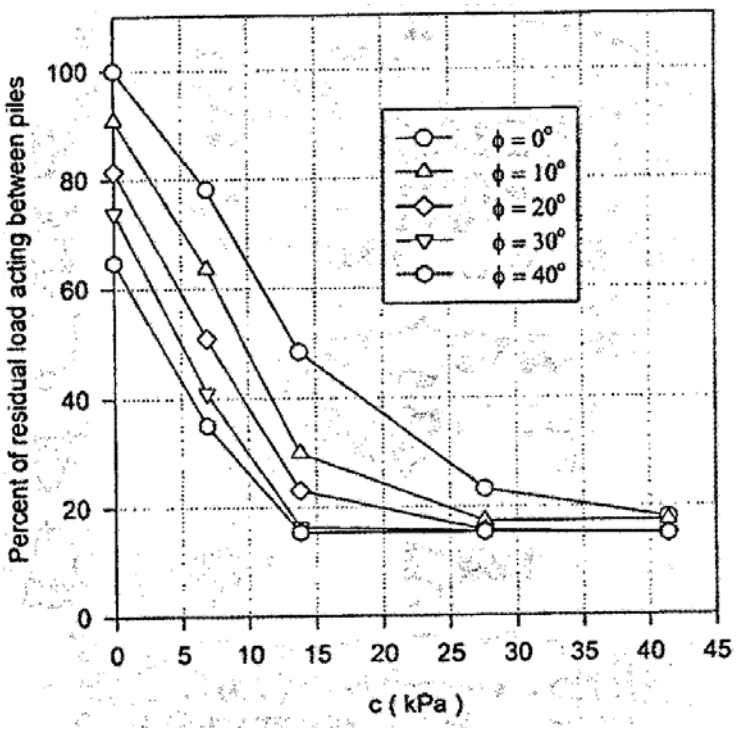

Figure 2-3: Effect of variation in cohesion (Liang and Zeng 2002).

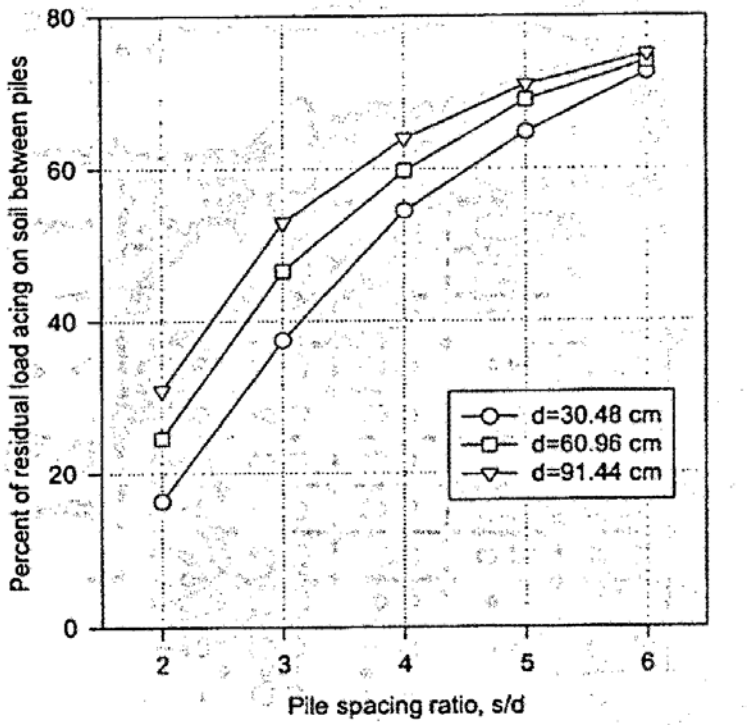

Figure 2-4: Effect of pile diameter (Liang and Zeng 2002).

Liang et al. (2010a) developed an analysis method to obtain the factor of safety of a drilled shaft on a slope system as well as to determine the earth thrust on the drilled shafts for structural design. The concept of the analysis is based on the limiting equilibrium approach, while incorporating the arching effects as the soil mass moved downslope and around the drilled shafts.

Kourkoulis et al. (2012) developed a hybrid method for designing slope-stabilizing piles, combining the accuracy of rigorous three-dimensional (3-D) finite element simulation with the simplicity of widely accepted analytical techniques. The hybrid method consists of two steps: (1) evaluation of the lateral resisting force needed to increase the safety factor of the precarious slope to the desired value, and (2) estimation of the optimum pile configuration that offers the required resisting force for a prescribed deformation level. The first step utilizes the results of conventional slope-stability analysis. A novel approach was proposed for the second step, which consists in decoupling the slope geometry from the computation of pile lateral capacity, thus allowing for numerical simulation of only a limited region of soil around the piles.

Liang et al. (2010b) used a 3-D finite element modeling approach to study soil arching between piles on slopes. The nonlinear and plastic nature of the soil, the elastic behavior of the drilled shafts, and interface friction, were modeled to gain a better understanding of the arching mechanisms in a slope with evenly spaced drilled shafts. The influence of various factors in both load transfer and lateral shaft movement was evaluated through a parametric study. The stiffness of the drilled shafts, shafts spacing and location on the slope, the material properties of rock and the socket length of shaft, and the soil movement and strength parameters were assessed. The simulation results showed evidences of soil arching and reduction in the stresses and displacements through load transfer mechanisms due to the presence of the drilled shafts. The different parameters analyzed were ranked in decreasing order of influence, as follows: (1) shaft diameter; (2) depth ratio along

the drilled shaft; (3) soil cohesion; (4) shaft length; (5) location in the slope; (6) rock-socket length ratio; (7) spacing-to-diameter ratio; and (8) rock elastic modulus.

Other studies that used 3-D finite element analysis to study the effect of soil arching include: Kahyaoglu et al. (2009), Liu and Zhang (2010), Yue et al. (2011), and Kourkoulis et al. (2011). Parameters included in these studies are pile spacing, pile diameter, soil characteristics (e.g. cohesion, friction angle). Overall conclusions for these papers are: (1) pile spacing is the main influencing factor for soil arching effects, and it was observed that as pile spacing increases, the effects of soil arching become less pronounced; (2) soil arching is not effective when spacing between piles is larger than 8*d*; (3) soil elastic modulus and Poisson's ratio have negligible influence in soil arching; (4) the arching effects increase with increasing friction angle; (5) soil inhomogeneity (in terms of shear stiffness) was found to be unimportant, because the response is primarily affected by the strength of the unstable soil layer.

2.2.3 Effects of Soil Slope on Lateral Capacity of Piles

Even though there is available research on the effects of soil slope on lateral capacity of piles using small-scale model tests, centrifuge tests, finite element analyses, and full-scale lateral pile loading tests, the studies reviewed in this section address three main topics regarding to the effect of soil slope on the lateral capacity of piles: (1) distance between the pile and the slope crest (bench width) at which slope effects are insignificant (Poulos 1976, Terashi et al. 1991, Ogata and Gose 1995, Boufia and Bouguerra 1996, Nimityongsukul et al. 2012); and (2) depth from the ground surface, z_{max}, at which slope effect is negligible (Brown and Shie 1991, Georgiadis and Georgiadis 2010), and (3) scale factors to be applied to the p-component of the p-y curves in level ground, p_{mult} (Terashi et al. 1991, Mezazigh and Levacher 1998). In addition, the effects of soil slope when the piles are subjected to displacements, as well as the soil slope effects on *p-y* curves, are also

reviewed (Chae et al. 2004, Brown and Shie 1991, Georgiadis and Georgiadis 2010, Nimityongsukul et al. 2012).

Poulos (1976) conducted small-scale laboratory tests on piles in clay to study the effects of slope on lateral response of piles. The study suggests that the distance between the slope crest and the pile after which the slope has negligible effect on the lateral pile response, t_{lim}, is approximately 5d.

Terashi, et al. (1991) performed centrifuge tests to investigate the behavior of laterally loaded piles in dense sand for different slope angles. The test results suggest that t_{lim} is approximately 2.5d. The same study also reported that p_{mult} for pile installed at the crest of the slope is 0.44, 0.63, and 0.64 for slopes 3:2 (β = 33.7deg), 2:1 (β = 26.5deg) and 3:1 (β = 18.4deg), respectively, indicating that slope effects are function of the slope angle.

Brown and Shie (1991) conducted 3-D elasto-plastic finite element analyses to study the effects of in-situ soil stresses, pile/soil interface friction, and sloping ground for laterally loaded piles in saturated clay. The study reported that the coefficient of earth pressure at rest (varying ratio of horizontal to vertical stress from 0.5 to 1.5) was not a major factor affecting *p-y* curves. However, pile/soil interface friction was observed to have significant effect on the lateral pile response. The effects of soil slope on the ultimate soil resistance are maxima at the ground surface. The study suggests that z_{max} is 4d. In addition, the study reported that the initial stiffness of the load-displacement curve as well as *p-y* curves are independent of ground slope.

Boufia and Bouguerra (1996) used a centrifuge to study the effects of the pile distance from slope crest on the lateral response of piles in sand. The study suggests that the range of t_{lim} is between 10d and 20d.

Ogata and Gose (1995) reported that the presence of a soil slope affected the modulus of subgrade reaction, especially close to the ground surface.

Chae et al. (2004) performed a series of 3-D finite element analyses, as well as small scale testing, to study the effects of soil slope on the lateral resistance of short single piles. The study concluded that the reduction of the lateral resistance due to slope effects is more significant for a small range of pile displacement and remain constant as the pile displacement increases.

Georgiadis and Georgiadis (2010) proposed new criteria for the initial slope of *p-y* curves and ultimate soil resistance for piles on a slope crest. The study suggests that z_{max} is 6d from the ground surface. For undrained static lateral loading of a pile in level ground, the study proposed analytical methods for the ultimate soil resistance and the initial stiffness of hyperbolic *p-y* curves. The proposed *p-y* criteria take into account the soil slope and the adhesion of the pile-slope interface.

Nimityongsukul et al. (2012) conducted a series of full-scale lateral loading tests for instrumented piles in cohesive and cohesionless soils to assess the lateral response of piles in free field and near slope conditions. For tests of piles in cohesive soils, it was found that: (1) for small pile head displacements (less than 1.0 inch) the proximity of slope has insignificant effects on piles at a distance of 2*d* or further from the slope crest; (2) for the piles on the slope crest, the effects of the soil slope should always be considered; (3) the presence of the slope has insignificant effects for piles installed at distances of 8*d* or greater from the crest. For piles in cohesionless soils: (1) the effects of slope on lateral pile capacity are insignificant at displacements of less than 2 inches for piles located at a distance 2*d* and further from the crest; (2) for piles located at a distance 4*d* or greater from the slope crest, the effects of slope on *p-y* curves are insignificant. Figure 2-5 and Figure 2-6 display the load-displacement curves between different distances from the slope crest and Caltrans method as well.

For design, Mezazigh and Levacher (1998) proposed p-multipliers to account for slope effects as a function of (1) the distance between the pile and the slope crest, and (2) the slope angle. The study suggests that t_{lim} is *8d* and *12d* for slope angle of *2:1* and *3:2*, respectively.

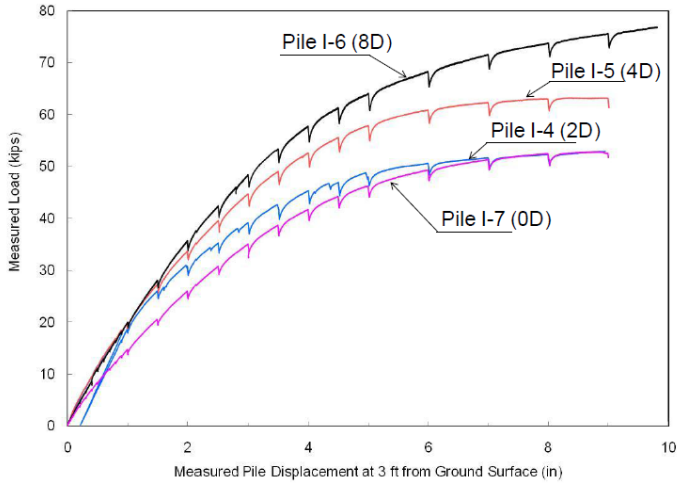

Figure 2-5: Measured load versus measured pile displacement at 3 ft. from ground surface for 0*d*, 2*d*, 4*d*, 8*d* piles (Nimityongsukul et al. 2012).

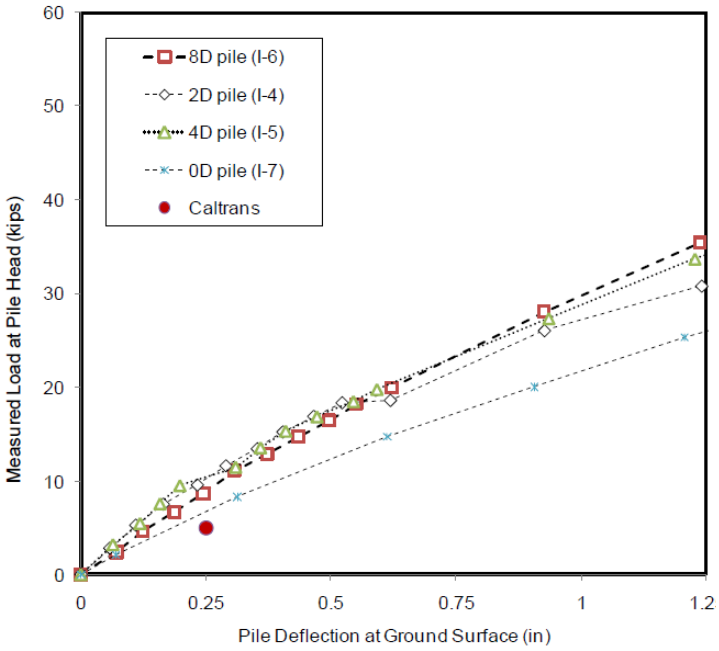

Figure 2-6: Comparison of Caltrans method and measured results for 0*d*, 2*d*, 4*d* and 8*d* piles (Nimityongsukul et al. 2012).

2.3 CRITERIA FOR DESIGN AND ANALYSIS

The pile tests in the previous section provide information on the effect of some of the design variables on the resistance of soldier piles. However, the capacity of piles must be predicted before a loading event in order for these to resist the possible load of the backfill. Thus, some discussion of the available design methodologies is warranted.

2.3.1 Design Procedures

In general, the design of shoring systems that make use of soldier pile walls is performed using well-established theories developed from structural mechanics. The members of the shoring system are checked for flexure, shear, compression, and bearing strength, as well the stability of the shoring system considering the soil stiffness and loads. Driven piles, drilled shafts, and auger-cast piles are among the vertical elements that are designed to support the full design earth, surcharge, and water pressures. Approximate calculations are satisfactory for most shoring systems, so common structural mechanics formulas are used for design of all members. The maximum spacing between vertical wall elements are determined based on the relative stiffness of the vertical elements and lagging, and characteristics of soil. For the steel members, lateral buckling is typically not checked since lateral and lateral-torsional buckling of piles is avoided since the entire length of the vertical element is laterally supported due to the presence of lagging.

Lagging is designed assuming simple span between elements or assuming continuous support over several elements. The soil arching induces a redistribution of soil pressure away from the center of the lagging toward the much stiffer soldier pile, minimizing the soil pressure behind the lagging. Hence a reduction factor is applied to the theoretical or calculated earth pressures. A simple span model, where a factor of 0.6 is applied, is suggested by Caltrans to account for soil arching, and the bending moment in the lagging is given by:

$$M = 0.6\frac{pL^2}{8} \tag{2-1}$$

where p is the applied pressure and L is the support span. On the other hand, AASHTO, for both simple span model and continuous beam model, suggest the application of a different reduction factor leading to the expression:

$$M = 0.083pL^2 \tag{2-2}$$

In AASHTO LRFD (AASHTO 2012), the overall stability of the retaining wall, retained slope, and foundation soil or rock is evaluated using limiting equilibrium methods of analysis. A *Service I Load Combination* is used in the evaluation of the overall stability of temporary cut slopes and capacities are affected by an appropriate resistance factor. The resistance factor may be taken as 0.75 where the geotechnical parameters are well defined, and the slope does not support or contain a structural element, and the resistance factor of 0.65 where the geotechnical parameters are based on limited information, or the slope contains or supports a structure, such as a bridge, retaining wall, sound wall, or building. The Modified Bishop, simplified Janbu, and Spencer methods of analysis (Bishop 1955, Janbu et al. 1956, and Spencer 1967) can also be used in order to analyze the overall stability of the retaining wall, retained slope, and foundation soil or rock.

2.3.2 Analysis Procedures

This type of walls, being non-gravity cantilever retaining walls, are analyzed by assuming that the vertical structural element rotates at a point below the excavation line. The point is labeled here as Point O, as shown in Figure 2-7. The realistic and simplified load distributions are also shown in this figure. Force R is assumed at Point O to compensate the resultant between active and passive pressure below point of rotation at Point O. The calculated depth, D, is determined by increasing D_0 by 20% in order to approximate the total embedment depth of the vertical wall element and to

accounting for the rotation of the length of vertical wall element below Point O. More details can be found on this procedure in CALTRANS (2011) and AASHTO (2012).

In determining earth pressures, Caltrans uses the concept of *Adjusted Pile Width*, recognizing that the width of soil contributing to the passive earth pressures can be greatly increased due to soil arching between soldier piles. The adjusted pile width is computed as the product of the effective pile width, *d*, and the *Arching Capability Factor*, *f*. The effective pile width *d* of a soldier pile is generally considered to be the dimension of the soldier pile taken parallel to the line of the wall for driven piles or drilled piles backfilled with material other than concrete, and can be taken as the diameter of the drilled-hole when 4-sack or better concrete is used.

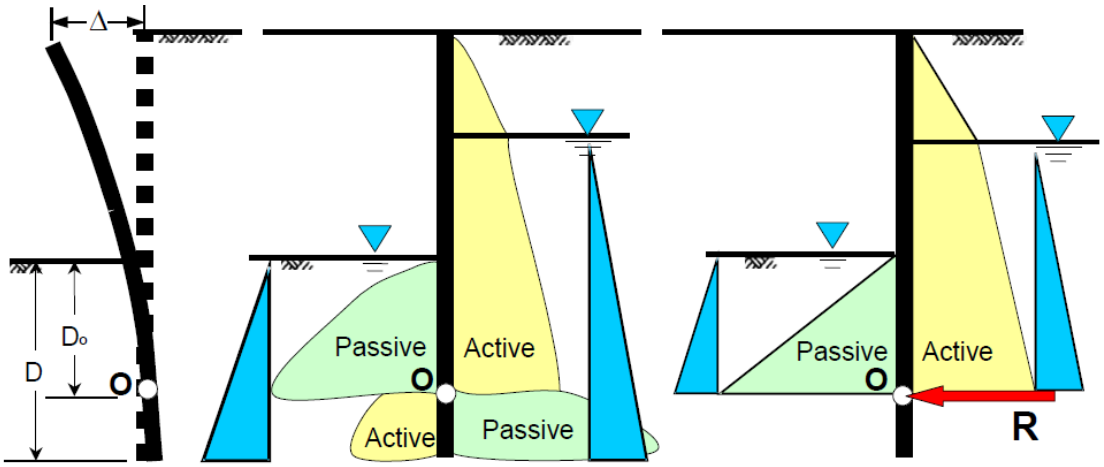

Figure 2-7: Cantilever retaining walls (Caltrans 2011): (a) wall deformation; (b) load distribution, (c) load simplification.

For cohesionless soils the arching capability factor is a function of the friction angle, determined according with Table 2-1 and for cohesive soils depends on consistency of the soil. The values of arching capability factor for cohesive soils are defined in Table 2-2. The adjusted pile width is used for the passive resistance in front of the pile as for any active loadings (including surcharge

loadings) on the back of the pile below the excavation depth. Obviously, the adjusted pile width should not be greater than the pile spacing, otherwise the system can be analyzed in the same manner as sheet pile systems.

Table 2-1: Arching capability factor for cohesionless soils

Pile spacing, *s*	**Arching capability factor, *f***
$\leq 3 \cdot d$	3
$> 3 \cdot d$	$0.08\ \phi (\leq 3)$

Table 2-2: Arching capability factor for cohesive soils

Consistency	**Very Soft**	**Soft**	**Medium**	**Stiff**	**Very Stiff**	**Hard**
q_u = unconfined comp. strength (psf)	500	1000	2000	4000	8000	
Unit Weight (pcf)	100-120	110-130		120-140	130+	
Arching Capability factor	1 to 2	1 to 2	2	2	2	

2.4 SUMMARY

This chapter presented a discussion on the effects of soil arching on the load developed in piles as well as the effects of slopes. Most of the literature reported address testing numerical work on piles and shafts. However, few loading tests were found in literature on soldier pile retaining systems. The main consensual conclusions reported in the literature include:

(1) Discrete piles can provide significant additional stability to a slope;

(2) In soldier pile and lagging systems, material costs, strengths, and sizes can be optimized to achieve maximum benefit from soil arching;

(3) Pile spacing is the main influencing factor for soil arching: as pile spacing increases, soil arching effects weaken gradually. In addition, several studies also highlight the importance of pile stiffness, embedment, soil's cohesion, and friction angle. On the other hand soil elastic modulus and Poisson's ratio have negligible influence in the soil arching effects;

(4) For small head displacements, in cohesive soil, for distances from the slope crest greater than 2*d*, the proximity of slope on the pile forces and displacements has insignificant effects;

(5) For the piles on the slope crest, the effects of the soil slope should always be considered;

(6) The presence of the slope has insignificant effects for piles installed at distances of 8*d* or greater from the crest;

(7) For piles located at 4*d* or greater from the slope crest, the effects of slope on *p-y* curves are insignificant.

Regarding to the criteria established for design and analysis of retaining wall systems:

(1) The design is performed using well-established theories from structural mechanics;

(2) The soil arching is taken into account in the *Adjusted Pile Width* affecting the arching factor which depends on the soil friction angle;

(3) No explicit consideration is given to the effect of the

This summary serves as groundwork to study effects of soil arching on analysis and design of soldier piles. Unfortunately, no load transfer observations were reported for any of the full-scale tests, limiting our understanding of the contributions of soil arching and slopes on soldier pile retaining systems. Therefore, full-scale tests on soldier pile system instrumented to measure load transfer in and soil arching effects would address a major need for engineers concerned with topic. To further understand the points listed above for pile and shaft systems but now on soldier pile retaining systems a parametric study will be performed to inform designers and future testing

programs. The main parameters to be considered in the analyses include: (1) at least two soil types (cohesive and cohesionless); (2) soldier pile spacing (3*d* and 4*d*); (3) pile position relative to slope crest (bench width). These will be studied using 2-D and 3-D Finite Element models that will be developed accounting for symmetry and plain strain assumptions to reduce model complexity.

3 METHODOLOGY FOR ASSESSMENT OF THE ARCHING FACTOR

3.1 OVERVIEW

In order to develop confidence in the modeling approach for capturing the effects related to soil arching capability and its effect on the passive earth pressures, both 2-D and 3-D nonlinear modeling approaches are developed and results of the finite element models are compared to experimental test results when possible to gain an understanding of the arching capability factor and effects of different parameters on the estimates of the arching capability factor. First, the 2-D analyses are developed, in which the tools needed for assessment of soil arching capability factor taking into account the effects of soil slope and bench width are defined. In particular, the 2-D analyses are first performed to aid in: (1) the selection of reference soil materials; (2) definition of geometry of the numerical models, element sizes, number of elements in each direction, type of elements, materials, and other modeling options. Furthermore, mesh sensitivity studies and extensive parametric studies are developed as part of the validation of the modeling approach, which uses *Open Sees* as the primary nonlinear finite element modeling tool. Finally, the same parameters are considered in the 3-D analyses performed, based on the findings of the 2-D analyses. In the interest of brevity mesh sensitivity studies and convergence of the finite element responses are not shown in this report, but could be made available upon request.

3.2 DEFINITION OF CASE STUDIES

3.2.1 Soil Definition

The selection of the soils used in this study was developed selecting soils expected to be found on site. Three different soils are selected from the set of tested soils available in Duncan, et al. (1980): a medium-dense sand, a medium-stiff clay, and a granular cohesive soil. The Table 3-1 shows the soils parameters selected.

Table 3-1: Selected Soils

Soil Description	**Medium-Dense Sand** *"Sacramento River Sand"*	**Medium-Stiff Clay** *Sandy Clay (Somerville Dam)*	**Granular Cohesive Soil** *Silty Clayey Sand (Mica Dam Core)*
Bulk Modulus, tsf (kPa)	1,305 (125,000)	1,514 (145,000)	1,514 (145,000)
Shear Modulus, tsf (kPa)	627 (60,000)	679 (65,000)	679 (65,000)
Unit Weight, γ_{soil}, pcf (kN/m^3)	94.0 (14.8)	106.7 (16.8)	114.9 (18.0)
Friction Angle, ϕ', deg	37	-	33
Cohesion, c_u, psf (kPa)	-	1,817 (87)	794 (38)

The values of shear and bulk moduli listed Table 3-1 were estimated as follows:

(1) The SPT value N_{60} were estimated using relationships in Kulhawy and Mayne (1990) that correlate N_{60} with friction angle and undrained cohesion for granular and cohesive soils, and are respectively given by:

$$\phi' = \tan^{-1}\left(\frac{N_{60}}{12.2 + 20.3\left(\frac{\sigma'}{p_a}\right)}\right)^{0.34} \tag{3-1}$$

$$\frac{c_u}{p_a} = 0.06 N_{60} \tag{3-2}$$

where p_a is the atmospheric pressure.

(2) The shear wave velocity is estimated using N_{60} and equations from Wair et al. (2012) for granular and cohesive soils, respectively,

$$V_S = 30.0 \cdot N_{60}^{0.23} \cdot \sigma_v^{'0.25} \quad (3\text{-}3)$$

$$V_S = 26.0 \cdot N_{60}^{0.17} \cdot \sigma_v^{'0.32} \quad (3\text{-}4)$$

(3) The maximum shear modulus is determined using:

$$G_{\max} = \gamma_{soil} \cdot V_S \quad (3\text{-}5)$$

where G_{max} is the maximum shear, V_S is the shear wave velocity, and γ_{soil} is the unit weight of the soil. To estimate the shear wave velocity, the following steps were performed:

(4) Estimate the shear modulus and the bulk modulus for isotropic materials, considering the G_{max} estimated in Step 3, and assuming Poisson's ratios defined in Kulhawy & Mayne (1990).

3.2.2 Parameter Selection

The following parameters were defined to be of interest in the analysis: (1) height of the wall; (2) spacing between piles; (3) slope angle; and, (4) bench width. These parameters have an important contribution in the capacity of soldier pile wall system and consequently in the arching capability factor. Table 3-2 shows the values considered in the analysis and design of the numerical specimens. As listed in Table 3-2, for each type of soil, four base situations are defined combining the two wall heights (10-ft and 15-ft) and the two assumed pile spacings (3d and 4d), and for each situation five different slope conditions are analyzed. A total of 60 different analyses are performed with the objective of performing the assessment of the arching capability factor.

Table 3-2: Parameter definition

Type of Soil (3 levels)	**Height of the wall, h_w** (2 levels)	**Spacing between piles, *s*** (2 levels)	**Slope conditions** (5 levels) **Ratio horiz.:vert.**	**Bench width, b_w**
Med. Stiff Clay			None ("*slno*")	
Med. Dense Sand	10 ft	3*d*	3:2 ("*sl32*")	2*d* ("*b2d*")
				4*d* ("*b4d*")
	15 ft	4*d*		8*d* ("*b8d*")
Granular Cohesive			2:1 ("*sl21*")	4*d* ("*b4d*")

Note: the text in quote is the code name assigned to the variable

3.3 PARAMETRIC CASE STUDY

In order to develop the most realistic condition for the analysis steps, the following steps were performed for each analysis case: (1) Soldier pile design; (2) develop the numerical models for each study case; (3) Perform the pushover analysis; (4) post-process the analysis results; and, (5) develop an assessment of the arching capability factor. The methods defined in each of steps is described in detail in this section.

3.3.1 Soldier Pile Design

For each one of the 60 study cases defined, the soldier pile embedment depth was designed on a case-by-case basis. All cases consider the use of an HP14x89 pile embedded below the wedge line in a 2-ft diameter circular pile consisting of structural concrete. Regarding the pile embedment depth, the following procedure is applied for each case study:

(1) Obtain active and passive earth pressure load distributions as a function of the embedment depth, $D_{0,}$ according to Figure 3-1.

a. Figure 3-1 shows the distributions for each soil type considered. For cohesive soils, the height of the tension zone, h_{cr} (see Figure 3-2) is ignored and the simplified lateral earth pressure distribution acting along the entire wall height, *h*, including presence of water pressure within the tension zone as shown in Figure 3-2 was used.

b. The active lateral earth pressure (σ_a) acting over the wall height, *h*, should not be less than 0.25 times the effective vertical stress ($\sigma_v = \gamma h$) at any depth. The Active Earth Pressure is given by:

$$P_a = \frac{1}{2}\gamma_{soil} K_a D_0^{\,2} - 2c\sqrt{K_a} D_0 \tag{3-6}$$

c. The Passive Earth Pressure is given by:

$$P_p = \frac{1}{2}\gamma_{soil} K_p D_0^{\,2} + 2c\sqrt{K_p} D_0 \tag{3-7}$$

where γ_{soil} is the soil density, *c* corresponds to the apparent cohesion, and K_p is the passive earth pressure coefficient. For Granular Soils ($\phi>0$) K_p was obtained using the (Caquot and Kerisel 1948) graphs (Figure 3-4), which is based on the Log-Spiral earth pressure theory. For Clays, K_p was considered to be equal to 1. It is worth noting that this methodology and does not take into account the presence of a slope crest (bench width = 0), and thus the bench width was neglected in the design.

(2) Compute the Driving Moment (M_{DR}) and Resisting Moment (M_{RS}) about the toe of the pile as a function of the embedment depth, D_0.

a. The driving moment accounts for the spacing between piles which corresponds to the total influence length of the pile and is given by:

$$M_{DR} = \sum DrivingForce \cdot Arm = \sum P_a \cdot s \cdot Arm \quad (3\text{-}8)$$

b. The resisting moment accounts for the adjusted pile width which is the product of the capability arching factor, f with the pile effective width, d

$$M_{RS} = \sum ResistingForce \cdot Arm = \sum P_p \cdot f \cdot d \cdot Arm \quad (3\text{-}9)$$

c. The width d for this study corresponds to the diameter of the embedded pile which is 2 feet, as shown in Figure 3-3.

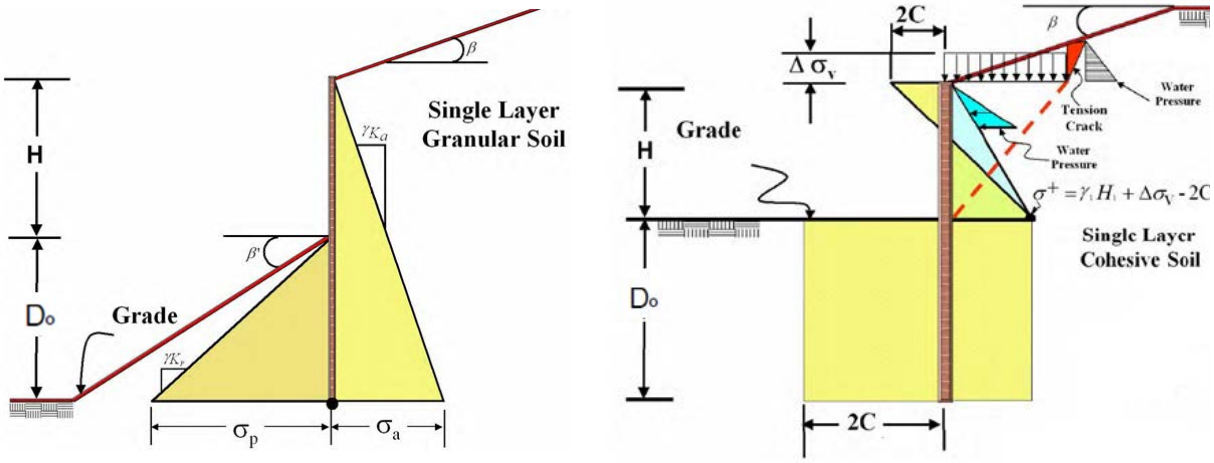

(a) (b)

Figure 3-1: Load diagram for a single layer (Caltrans 2011): (a) granular soil; (b) cohesive soil.

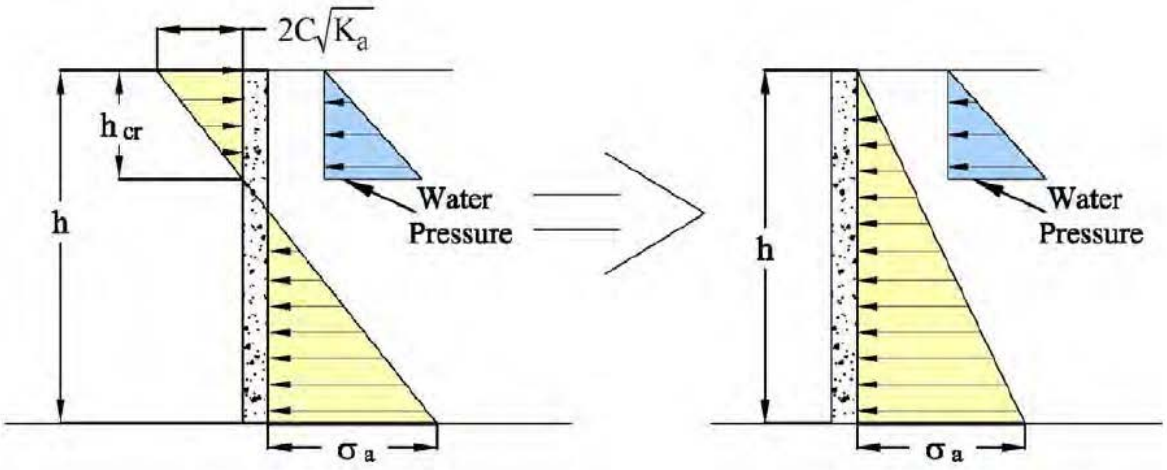

Figure 3-2: Load distribution for cohesive backfill (Caltrans 2011).

(3) Solve for D_0 using a factor of safety (FS) equal to 1.3, given by:

$$\frac{M_{RS}}{M_{DR}} \geq 1.3 \tag{3-10}$$

(4) Increase D_0 by 20%. Note that the calculated depth, D, is determined by increasing D_0 by 20% to approximate the total embedment depth of the vertical wall element. The 20% increase is not a factor of safety, it accounts for the rotation of the length of vertical wall element below Point O.

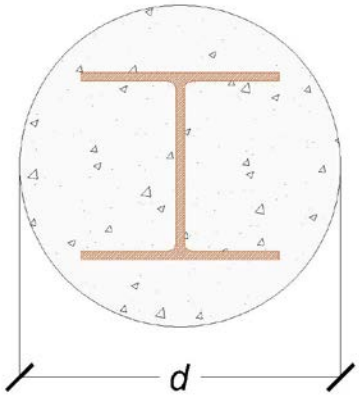

Figure 3-3: Cross-section of the embedded pile.

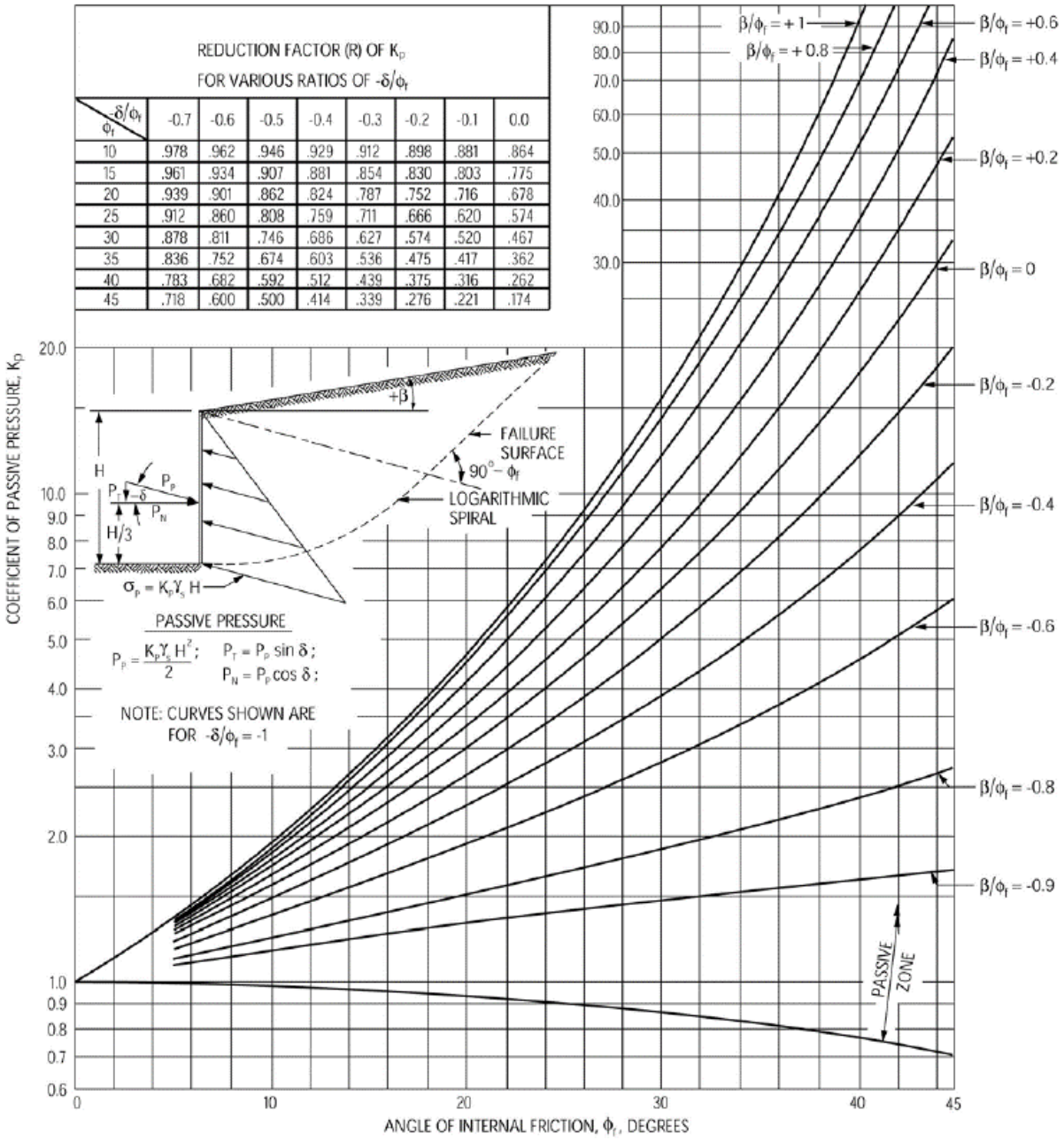

Figure 3-4: Passive earth pressure coefficient (Caquot and Kerisel 1948).

3.3.2 Development of Numerical Models

The development of the numerical models is of crucial importance in the study. *Open Sees* was selected as the analysis software due to the extensive capabilities built in for modeling geotechnical and structural engineering problems. The model development included the following stages. First, 2-D plan view analyses were performed to establish mesh sizes and the extension of the model, and if identical results can be obtained when using a single strip of soil-pile (between mid-distances of two adjacent piles) versus multiple soil-pile strips. Second, all case studies were analyzed using 2-D elevation models, and finally, 3-D analyses were performed. Since the methods and approaches are similar for the 2-D elevation analyses and 3-D analyses, on the latter are described here in this section.

3.3.2.1 2-D Plan Models

Figure 3-5 shows the plan geometries tested. The models were developed (along with other mesh geometries not shown) to study: (1) differences that would be obtained when considering different spacing between piles; (2) if one soil-pile strip (Figure 3-5a) can reproduce the identical responses and soil behavior obtained when using 3 (Figure 3-5b) or 5 strips, and (3) observe the stress distribution and deformation patterns in front of the pile.

Figure 3-5 shows the soil mesh, which is the mesh generated for the soil, which was automatically generated using scripts developed in *TCL*. The pile was modeled using linear elastic quadrilateral elements (not shown in the figures). It can be seen in the figure, that for this analysis type, only the passive side was modeled. Uniform distributed loads are applied on the pile elements, into the direction of the soil elements. The models have a dimension of 10 ft (3 m) along X-direction, two levels for the width of the strip equal to the space between piles adopted in the model along Y-direction (s = 3d and 4d). In terms of restraints in the model, both horizontal boundaries

are restrained in Y-direction, and the vertical boundary located on the opposite side of the pile is restrained in the X direction, all through pinned supports. The UC San Diego soil models *PressureIndependMultiYield* and *PressureDependMultiYield* materials were used for cohesive and cohesionless soils, respectively. More details on the models can found elsewhere (Parra 1996, Yang 2000, Elgamal et al. 2002, Yang and Elgamal 2002, Yang et al. 2003, and Elgamal and Yang 2003). The pile was modeled using linear elastic quadrangular elements.

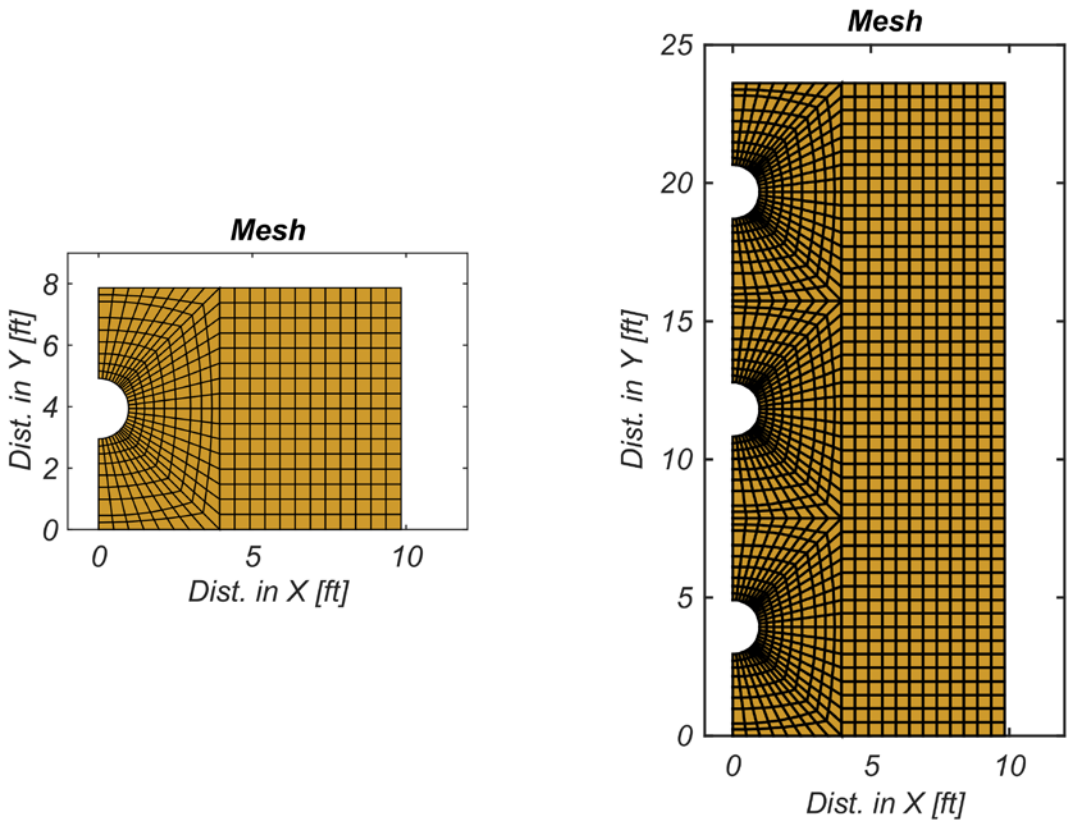

(a) (b)

Figure 3-5: 2-D Modeled soil meshes (plan view); (a) considering one strip; (b) considering three strips.

3.3.2.2 2-D Elevation and 3-D Models: Meshing

The global models developed refers here either to the 3-D model or for the 2-D model in elevation. Figure 3-6 displays a reference 3-D model. In terms of numerical model dimensions, the difference between 2-D and 3-D models lies on the width. For the 2-D models, *Quad* elements are used and a plane-strain condition is assumed. In the 3-D numerical models, 8-node brick elements are used. The dimensions on the numerical models are: (1) in the Y-direction, 24 feet of soil-active side (see for example, Figure 3-6c) and 40 to 50 feet of passive side, depending on the slope and bench width considered; (2) in the Z-direction, the total dimension accounts for the height of the wall, the embedment depth, and 10 to 15 feet below the toe of the pile; and (3) 6 feet or 8 feet for the X-direction for the 3-D numerical models, depending if the distance between piles considered is 3*d* or 4*d*, while for the 2-D cases, the width assigned to the elements is the *adjusted pile width* is given by:

$$adjusted\ \ pile\ width = f \cdot d \tag{3-11}$$

where the arching capability factor, *f*, is defined in Table 2-1 for cohesionless soils and Table 2-2 for cohesive soils.

For the 3-D model, the finite element meshes were developed using a combination of *OpenSeesPL* (Lu et al. 2011), to generate a refined mesh around the pile, and *TCL* language scripts developed within the scope of this project to model the remain soil domain. Since OpenSeesPL does not generate meshes for HP piles, all the elements that lie between a distance of 4 feet in front of the pile and 4 feet behind the pile, along the whole width and height of the model, as displayed in Figure 3-7 were also developed using an automated mesh generator implemented by the authors.

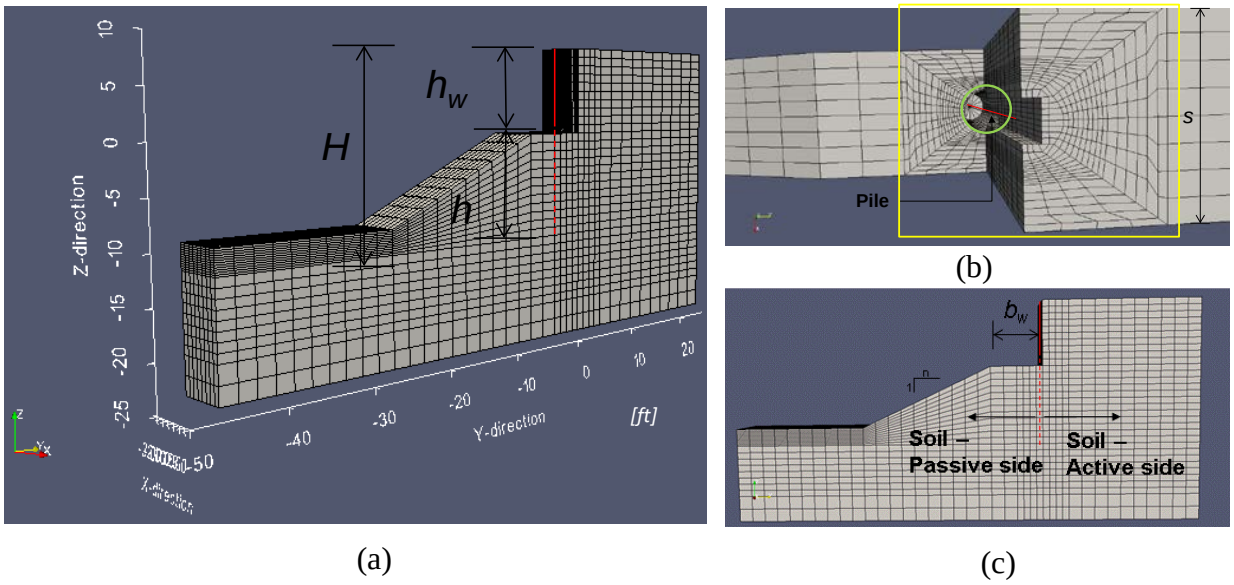

Figure 3-6: 3-D model mesh: (a) 3-D view; (b) zoom over region of the pile; (c) elevation view

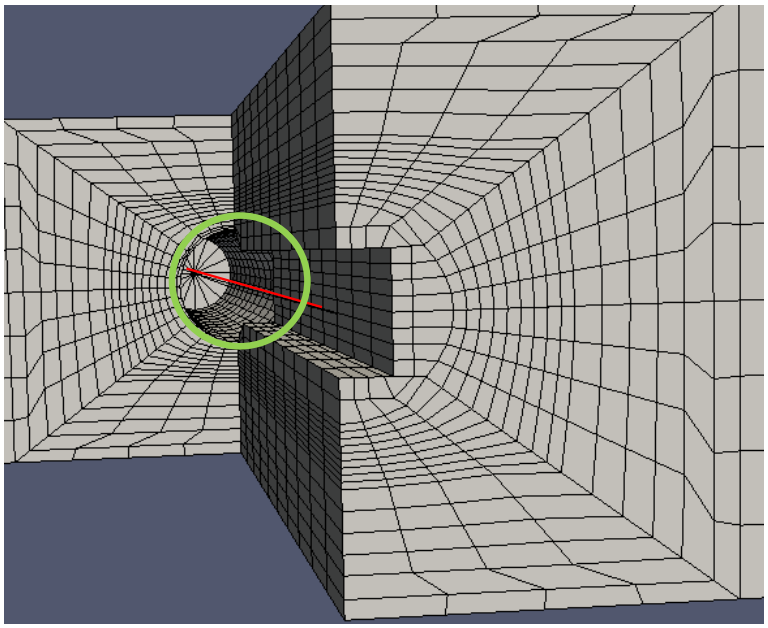

Figure 3-7: Part of the numerical model created in *OpenSeesPL* and adjusted using TCL scripts for modeling the HP section above the excavation line.

3.3.2.3 Material Models

In terms of selection of the most appropriate materials to assign soil elements, several materials were tested. Depending on the soils, among the tested materials in Open Sees, are the University

of Washington implemented *Manzari Dafalias* material (Dafalias and Manzari 2004), the *Drucker Prager* material (Drucker and Prager 1952), and the UC San Diego soil models *PressureIndependMultiYield* and *PressureDependMultiYield* materials for cohesive and cohesionless soils, respectively.

For cohesionless soils, initially two models were tested. First, the *Manzari Dafalias* material was tested, but the version of the model which was implemented in Open Sees by August 2015 had several convergence issues. After personal communications by the authors of this report with the team implementing the models in Open Sees, several improvements have been made since, which seem to have addressed the issues detected. However, these improvements were only completed after the first draft of this report was completed. The *Drucker Prager* material model was also tested, but in the case of low to negligible cohesion the model implemented in Open Sees also seemed to provide several challenges when running analyses that simulated cohesionless soils. The models that were seen to be most appropriate and stable for this work were the UC San Diego soil models. The *PressureDependMultiYield* material model was therefore used in this study. The *PressureDependMultiYield* material was assigned to cohesionless soils. It is an elastic-plastic material for simulating the essential response characteristics of pressure sensitive soil materials under general loading conditions.

For cohesive soils, the *PressureIndependMultiYield* material was used. This model is an elastic-plastic material in which plasticity exhibits only in the deviatoric stress-strain response. The volumetric stress-strain response is linear-elastic and is independent of the deviatoric response. This material is implemented to simulate monotonic or cyclic response of materials whose shear behavior is insensitive to the confinement change.

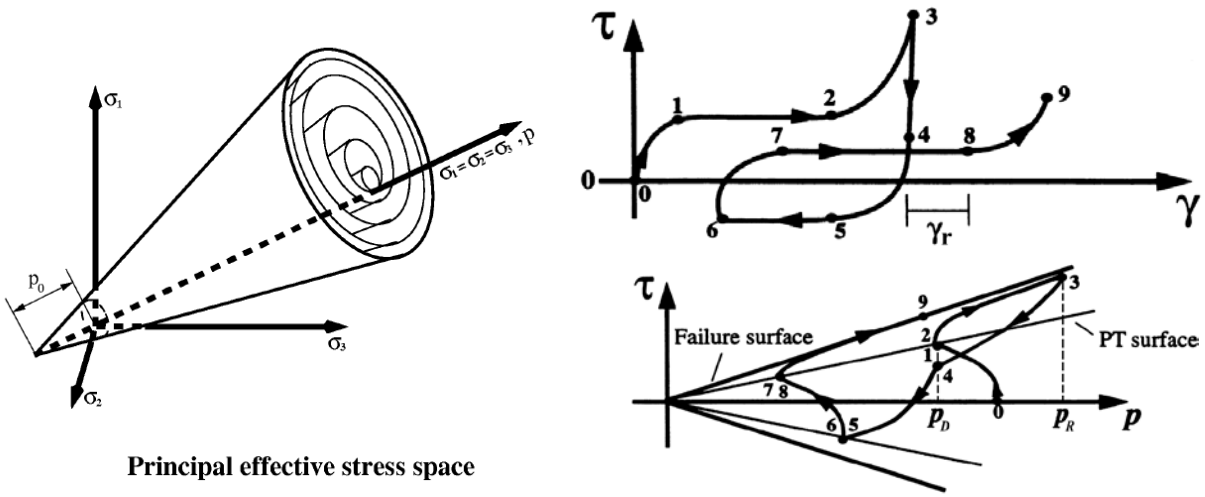

Figure 3-8: Schematic of constitutive model response of a PressureDependMultiYield material showing shear stress, effective confinement, and shear strain relationship.

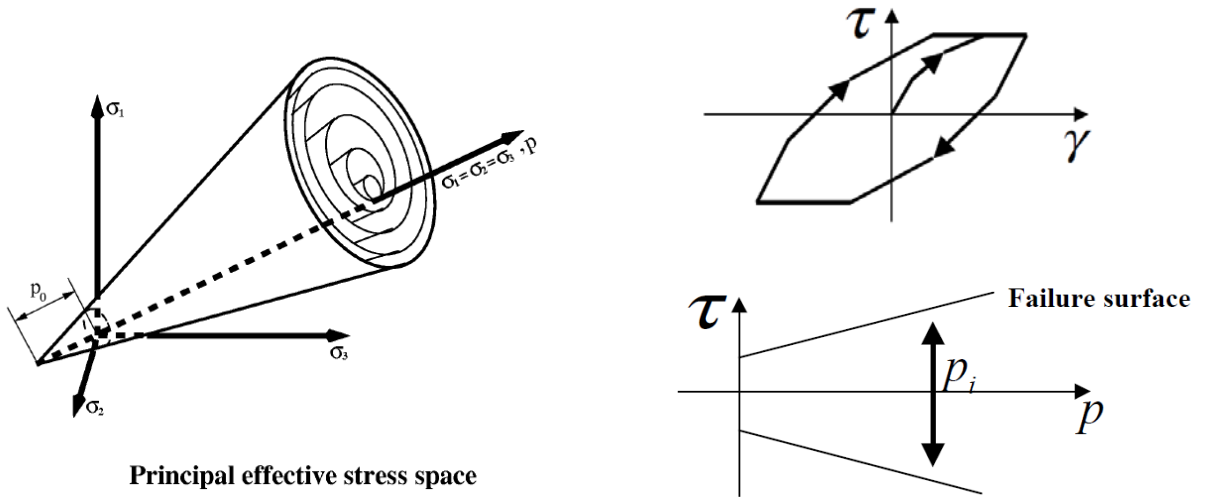

Figure 3-9: Schematic of constitutive model response of a PressureIndependMultiYield material showing shear stress, effective confinement, and shear strain relationship.

3.3.2.4 Soil Element Types

The *FourNodeQuad* elements were used to model the soil domain in 2-D analyses. The *FourNodeQuad* element is a quadrilateral element that uses use a bilinear isoparametric formulation. For 3-D analyses, the *Bbarbrick* element was used to model the soil. The *Bbarbrick*

element is an eight-node mixed volume/pressure brick element object that uses a trilinear isoparametric formulation. In both type of elements, the solid-fluid coupling is not considered in the pushover analyses performed in this study.

3.3.2.5 Pile Element Types

The soldier pile considered were defined as an HP14x89 steel section, which was grouted with structural concrete below the dredge line. The whole pile was modeled using *Displacement-based BeamColumn* elements with 3 integration points per element. Figure 3-10a shows the fiber section discretization for the pile embedded in concrete, while Figure 3-10b shows the discretization of the steel section above the dredge line.

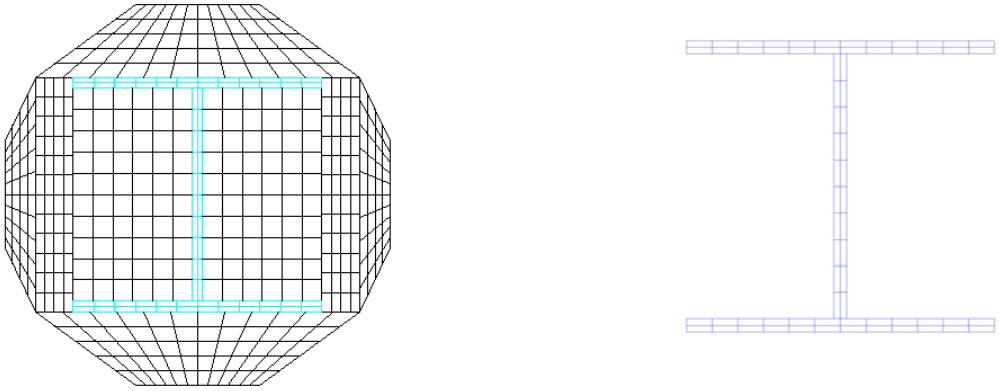

(a) (b)

Figure 3-10: Fiber section: (a) embedded pile; (b) pile above the dredge line.

Both linear and nonlinear material behavior was assumed to assess the influence of the pile nonlinearity in this study. When nonlinear behavior was considered, the bilinear steel material (*Steel01*) was assumed for the steel fibers and the *Popovics* concrete material model (*Concrete04*) (Popovics 1973) was used to model the concrete fibers, respectively.

A compressive strength of about 3500 psi was considered for the concrete and 50 ksi for the yield strength of steel (assumed A36 steel).

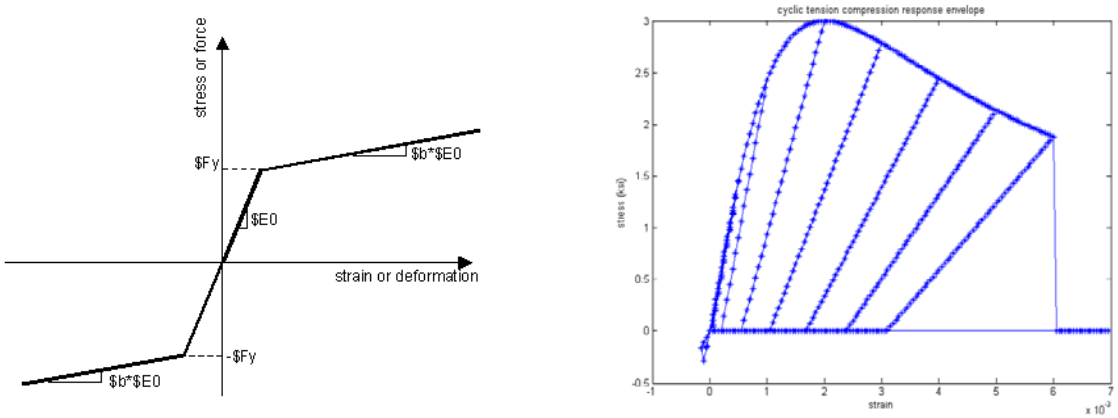

(a) (b)

Figure 3-11: Constitutive models used in fiber sections: (a) steel01; (b) concrete04.

3.3.2.6 Interface Elements

In order to model the interface between the soldier pile and the soil, two different modeling options were considered: (1) the nodes of the pile were restrained to the soil nodes located at the same elevation, using a master-slave algorithm (*equalDOF* in Open Sees), and (2) beam contact elements, providing interaction between the beam element and the soil elements.

In the 2-D analyses, *BeamContact2D* elements were used, while in the 3-D analyses *BeamContact3D* and *BeamEndContact3D* elements (Petek 2006, Arduino et al. 2007) were used. These beam contact elements provide the beam-to-node interaction, defining a frictional contact interface between a beam element and a separate body which follows the form shown in Figure 3-12 and is given by (Wriggers 2006):

$$f = \|\mathbf{t}_s\| - \mu \cdot t_n - c \leq 0 \tag{3-12}$$

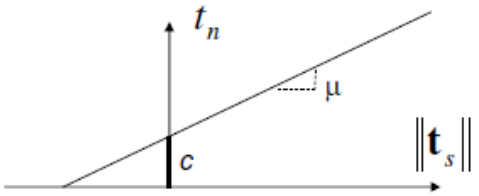

Figure 3-12: Mohr-Coulomb friction model.

Equation (3-12 defined a regularized Coulomb frictional law that is implemented in Open Sees as a *ContactMaterial2D/3D*. This material assigned to the interface elements between two adjacent bodies in contact. The interface defined by this material object allows for sticking, frictional slip, and separation between the two bodies. The values used recommended in NAVFAC (1986) are applied to model both the *ContactMaterial2D* and *ContactMaterial3D* material models.

3.3.3 Pushover Analysis Methodology

A displacement controlled nonlinear pushover analysis is performed applying an incremental load on the pile. The application of the load has an extreme importance on this study, because depending how it is applied, the system capacity can vary considerably as can be evaluated in the subsection below. Using the appropriate load pattern, a nonlinear pushover analysis is performed, in which the horizontal pile-head displacement at each step and the load total force applied is recorded at each step. Figure 3-13 shows the analysis scheme for the case of cohesionless soils.

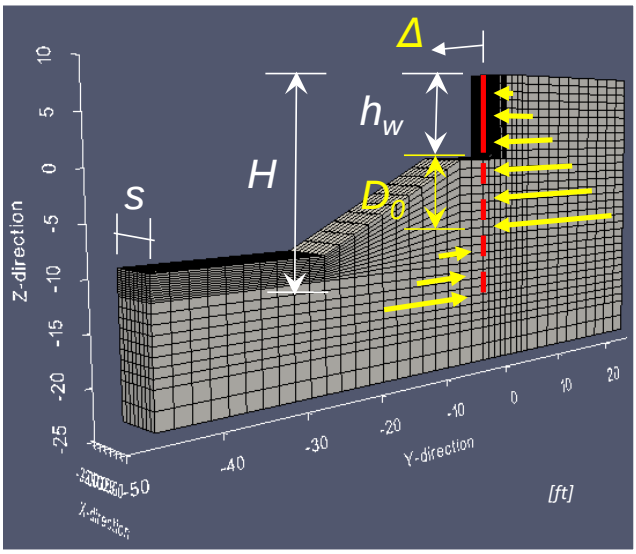

Figure 3-13: Pushover analysis scheme.

The following parameters were adopted for nonlinear finite element static pushover analysis. First, for the gravity load analysis, the *Load Control* algorithm is used to set the initial state of stress in the model. Second, the pushover analysis is performed using a displacement controlled analysis. In both gravity and pushover analyses, OpenSeesSP is used and the solver of for the system of equations used is *Mumps*, which is a multifrontal massively parallel sparse direct solve. The use of OpenSeesSP and the Mumps solver allow for efficient parallel computation of the large nonlinear finite element models. The type of convergence test selected was the *NormDispIncr*. The algorithm used in the analysis of the nonlinear system of equilibrium equations was *KrylovNewton* (Scott and Fenves 2010), which uses a Krylov subspace accelerator to accelerate the convergence of the modified newton method. The constraints in the model are enforced using a *Penalty* constraint handler.

Each case study corresponds to a *TCL* file, including node location, element connectivity, and assigned material properties. Node and element recorders are defined to outputs results of analysis, for nodal displacements as well as strains and stresses at gauss points.

3.3.4 Analysis of Results / Post-processing

A *Matlab* code was developed to parse input and output Open Sees model data to generate a file for visualization in *Paraview*, which is used to visualize the results in terms of displacement shapes and stresses, both in model Cartesian directions as well as in the principal stress directions. For 2-D analyses, the principal stresses are obtained using the expressions:

$$\sigma_I = \frac{\sigma_{11} + \sigma_{22}}{2} + \sqrt{\left(\frac{\sigma_{11} - \sigma_{22}}{2}\right)^2 + \sigma_{12}^2} \tag{3-13}$$

$$\sigma_{II} = \frac{\sigma_{11} + \sigma_{22}}{2} - \sqrt{\left(\frac{\sigma_{11} - \sigma_{22}}{2}\right)^2 + \sigma_{12}^2} \tag{3-14}$$

For the 3-D analyses, the principal stresses in three orthogonal directions I, II, and III are respectively given by:

$$\sigma_I = \frac{I_1}{3} + \frac{2}{3}\left(\sqrt{I_1^2 + 3I_2}\right) \cdot cos\,\phi \tag{3-15}$$

$$\sigma_{II} = \frac{I_1}{3} + \frac{2}{3}\left(\sqrt{I_1^2 + 3I_2}\right) \cdot cos\left(\phi + \frac{2\pi}{3}\right) \tag{3-16}$$

$$\sigma_{III} = \frac{I_1}{3} + \frac{2}{3}\left(\sqrt{I_1^2 + 3I_2}\right) \cdot cos\left(\phi + \frac{4\pi}{3}\right) \tag{3-17}$$

where terms in equations (3-15), (3-16), and (3-17) are given by:

$$\phi = \frac{1}{3} cos^{-1}\left(\frac{2I_1^3 - 9I_1 I_2 + 27I_3}{2(I_1^2 - 3I_2)^{3/2}} \right) \tag{3-18}$$

$$I_1 = \sigma_{11} + \sigma_{22} + \sigma_{33} \tag{3-19}$$

$$I_2 = \sigma_{11}\sigma_{22} + \sigma_{22}\sigma_{33} + \sigma_{33}\sigma_{11} - \sigma_{12}^2 - \sigma_{23}^2 - \sigma_{31}^2 \tag{3-20}$$

$$I_3 = \sigma_{11}\sigma_{22}\sigma_{33} - \sigma_{11}\sigma_{23}^2 - \sigma_{22}\sigma_{31}^2 - \sigma_{33}\sigma_{12}^2 + 2\sigma_{12}\sigma_{23}\sigma_{31} \tag{3-21}$$

and where the quantities I_1, I_2 and I_3 are the stress invariants.

3.3.5 Assessment of the Arching Capability Factor

The assessment of the arching capability factor has the following steps.

(1) Determine the passive resistance, R_p, in front of a soldier pile based on accepted analytical expressions. The passive earth pressure is given by

$$R_p = P_{p_theory} \cdot d \cdot f \tag{3-22}$$

where the arching capability factor, f, is given in Table 2-1 and Table 2-2, d is the pile diameter, and P_{p_theory} is the theoretical passive earth pressure. For a given embedment length, P_{p_theory} is obtained from Figure 3-4 (Caquot and Kerisel 1948) neglecting the bench width and using the nominal slope values. For clayey soils, when $\phi = 0$, Rankine earth pressure theory is used to estimate the passive earth pressure.

(2) Determine the pushover load as a function of the tracked horizontal displacement horizontal, $F(\Delta)$

(3) Determine the ratio of the pushover load to the passive resistance obtained in Step 1. This ratio is assigned the variable n and it is a function of the level of displacement, being given by:

$$n(\Delta) = \frac{F(\Delta)}{R_p} \tag{3-23}$$

Note that for values of n higher than 1, the capacity obtained from the pushover analysis is greater than the theoretical passive resistance, which means that the definition of capability factor is conservative using logspiral theories.

4 FINITE ELEMENT RESULTS AND DISCUSSION

4.1 OVERVIEW

This chapter first presents the results for the soldier pile design and the theoretical passive resistance, which are needed to define the numerical models and to evaluate the ratio of the resistance obtained from the computational models with the one obtain from the theory. Then, results on the 2-D plan models are performed to illustrate effect of pile spacing and number of piles/soil strips needed for consideration in the 3-D models. Next, results of the nonlinear static pushover analyses for the three soil types and for all model permutations considered are shown. Differences between the results obtained using 2-D and 3-D analyses are highlighted for future modelers and designers. Finally, the arching capability factor assessment based on the numerical analyses is presented.

4.2 SOLDIER PILE DESIGN

The embedment depth of the soldier pile was designed for each specific study case, resulting in different embedment depths for most of the cases when considering different slopes. However, in order to be able to compare the effect of the slope characteristics in front of the wall, equal values of embedment depth were also considered in the analyses. Table 4-1, Table 4-2, and Table 4-3 show the values obtained in design and consequently used in the study cases considered, for medium-dense sand, medium-stiff clay, and granular cohesive soils, respectively. In some cases, the design calculations required very small embedment depths. For those cases, the embedment depth h was assumed be at least equal to the wall height, i.e. $h \geq h_w$.

Table 4-1: Pile embedment depths considered for the medium dense sand study cases

Wall Height h_w	**Pile Spacing,** s	**Slope, H:V**	**Bench width,** b_w	**Embedment depth,** h
10 ft	4*d*	No slope (*slno*)		12 ft *30 ft
		2:1 (*sl21*)	4d (*b4d*)	18 ft *30 ft
		3:2 (*sl32*)	2d (b2d) 4d (b4d) 8d (b8d)	30 ft
	3*d*	No slope (*slno*)		10 ft *22 ft
		2:1 (*sl21*)	4d (b4d)	14 ft *22 ft
		3:2 (*sl32*)	2d (b2d) 4d (b4d) 8d (b8d)	22ft
15 ft	4*d*	No slope (slno)		20 ft *42 ft
		2:1 (*sl21*)	4d (b4d)	26 ft *42 ft
		3:2 (*sl32*)	2d (b2d) 4d (b4d) 8d (b8d)	42 ft
	3*d*	No slope (slno)		16 ft *32 ft
		2:1 (*sl21*)	4d (b4d)	22 ft *32 ft
		3:2 (*sl32*)	2d (b2d) 4d (b4d) 8*d* (*b8d*)	32 ft

*equal to the maximum obtained for the same type of soil. These analyses results will be denoted using the "_eqh" as an identifier.

Table 4-2: Pile embedment depths considered for the medium-stiff clay study cases

Wall Height h_w	**Pile Spacing, *s***	**Slope, H:V**	**Bench width, b_w**	**Embedment depth, *h***
10 ft	4*d*	No slope (*slno*)		14 ft
		2:1 (*sl21*)	4d (*b4d*)	
		3:2 (*sl32*)	2d (b2d) 4d (b4d) 8d (b8d)	
	3*d*	No slope (*slno*)		12 ft
		2:1 (*sl21*)	4d (b4d)	
		3:2 (*sl32*)	2d (b2d) 4d (b4d) 8d (b8d)	
15 ft	4*d*	No slope (slno)		16 ft
		2:1 (*sl21*)	4d (b4d)	
		3:2 (*sl32*)	2d (b2d) 4d (b4d) 8d (b8d)	
	3*d*	No slope (slno)		16 ft
		2:1 (*sl21*)	4d (b4d)	
		3:2 (*sl32*)	2d (b2d) 4d (b4d) 8*d* (*b8d*)	

Table 4-3: Pile embedment depths considered for granular cohesive soil study cases

Wall Height h_w	**Pile Spacing, *s***	**Slope, H:V**	**Bench width, b_w**	**Embedment depth, *h***
10 ft	4*d*	No slope (*slno*)		12 ft *16 ft
		2:1 (*sl21*)	4d (*b4d*)	12 ft *16 ft
		3:2 (*sl32*)	2d (b2d) 4d (b4d) 8d (b8d)	16 ft
	3*d*	No slope (*slno*)		10 ft *12 ft
		2:1 (*sl21*)	4d (b4d)	12 ft
		3:2 (*sl32*)	2d (b2d) 4d (b4d) 8d (b8d)	12 ft
15 ft	4*d*	No slope (slno)		16 ft *40 ft
		2:1 (*sl21*)	4d (b4d)	26 ft *40 ft
		3:2 (*sl32*)	2d (b2d) 4d (b4d) 8d (b8d)	40 ft
	3*d*	No slope (slno)		16 ft *24 ft
		2:1 (*sl21*)	4d (b4d)	16 ft *24 ft
		3:2 (*sl32*)	2d (b2d) 4d (b4d) 8*d* (*b8d*)	24 ft

*equal to the maximum obtained for the same type of soil. These analyses results will be denoted using the "_eqh" as an identifier.

4.3 THEORETICAL PASSIVE RESISTANCE VALUES

Table 4-4, Table 4-5, and Table 4-6 list the values of the arching capability factor estimated using expressions in Caltrans (2011) and the theoretical passive resistance obtained using the methodology listed in section 3.3.5, for medium-dense sand, medium-stiff clay and granular cohesive soil, respectively.

Table 4-4: Pile embedment depth for the medium dense sand study cases

h_w	s	Slope	b_w	f	R_p
10 ft	4*d*	No slope (slno)		2.96	275 kip
		2:1 (*sl21*)	4*d* (*b4d*)		120 kip
		3:2 (*sl32*)	2*d* (*b2d*) 4*d* (*b4d*) 8*d* (*b8d*)		110 kip
	3*d*	No slope (slno)		3.0	70 kip
		2:1 (*sl21*)	4*d* (*b4d*)		65 kip
		3:2 (*sl32*)	2*d* (*b2d*) 4*d* (*b4d*) 8*d* (*b8d*)		90 kip
15 ft	4*d*	No slope (slno)		2.96	285 kip
		2:1 (*sl21*)	4*d* (*b4d*)		240 kip
		3:2 (*sl32*)	2*d* (*b2d*) 4*d* (*b4d*) 8*d* (*b8d*)		320 kip
	3*d*	No slope (slno)		3.0	200 kip
		2:1 (*sl21*)	4*d* (*b4d*)		180 kip
		3:2 (*sl32*)	2*d* (*b2d*) 4*d* (*b4d*) 8*d* (*b8d*)		190 kip

Table 4-5: Pile embedment depth for the medium-stiff clay study cases

h_w	s	Slope	b_w	f	R_p
10 ft	4*d*	No slope (slno)		2.0	180 kip
		2:1 (*sl21*)	4*d* (*b4d*)		
		3:2 (*sl32*)	2*d* (*b2d*) 4*d* (*b4d*) 8*d* (*b8d*)		
	3*d*	No slope (slno)			160 kip
		2:1 (*sl21*)	4*d* (*b4d*)		
		3:2 (*sl32*)	2*d* (*b2d*) 4*d* (*b4d*) 8*d* (*b8d*)		
15 ft	4*d*	No slope (slno)			220 kip
		2:1 (*sl21*)	4*d* (*b4d*)		
		3:2 (*sl32*)	2*d* (*b2d*) 4*d* (*b4d*) 8*d* (*b8d*)		
	3*d*	No slope (slno)			220 kip
		2:1 (*sl21*)	4*d* (*b4d*)		
		3:2 (*sl32*)	2*d* (*b2d*) 4*d* (*b4d*) 8*d* (*b8d*)		

Table 4-6: Pile embedment depth for the granular cohesive soil study cases

h_w	s	Slope	b_w	f	R_p
10 ft	4*d*	No slope (slno)		2.0	275 kip
		2:1 (*sl21*)	4*d* (*b4d*)		120 kip
		3:2 (*sl32*)	2*d* (*b2d*) 4*d* (*b4d*) 8*d* (*b8d*)		110 kip
	3*d*	No slope (slno)			210 kip
		2:1 (*sl21*)	4*d* (*b4d*)		120 kip
		3:2 (*sl32*)	2*d* (*b2d*) 4*d* (*b4d*) 8*d* (*b8d*)		80 kip
15 ft	4*d*	No slope (slno)			390 kip
		2:1 (*sl21*)	4*d* (*b4d*)		220 kip
		3:2 (*sl32*)	2*d* (*b2d*) 4*d* (*b4d*) 8*d* (*b8d*)		360 kip
	3*d*	No slope (slno)			380 kip
		2:1 (*sl21*)	4*d* (*b4d*)		170 kip
		3:2 (*sl32*)	2*d* (*b2d*) 4*d* (*b4d*) 8*d* (*b8d*)		180 kip

4.4 2-D PLAN ANALYSIS RESULTS

The analysis performed using the plan geometry is conceptually illustrated in Figure 4-1. First, the incremental force, *F*, is applied as a pushover analysis. The capacity is provided by the numerical "passive resistance" developed in the soil model that resist the pushover. A unit passive earth pressure is computed and load-deformation plots are obtained. The effect of the number of strips used in the analysis is evaluated running an example with one and three soil-pile strips shown in Figure 4-1.

Figure 4-2 shows that the pushover curves of the force required to push one pile/soil strip of shows negligible differences when compared to the three pile/soil strip model. These results are shown for a medium-stiff clay soil using parameters defined in Chapter 3.

Figure 4-3 shows the results when $s = 4d$ and $s = 3d$ are considered. It can be seen that higher capacities are achieved when a smaller spacing between piles are considered, even though for medium-dense clay the differences are negligible.

Figure 4-4 and Figure 4-5 show representative results of displacements and stresses, respectively, at 1 inch of displacement of the pile, for a medium-dense sand and spacing between piles of $4d$. Note that no smoothing of the results are done. Figure 4-6 and Figure 4-7 also show representative results of displacements and stresses, respectively, at 1 inch of displacement of the pile, for medium-stiff clay with spacing between piles equal to $3d$. The results in these four figures illustrate the pressure bulbs in front of the wall, which are well captured in this analysis.

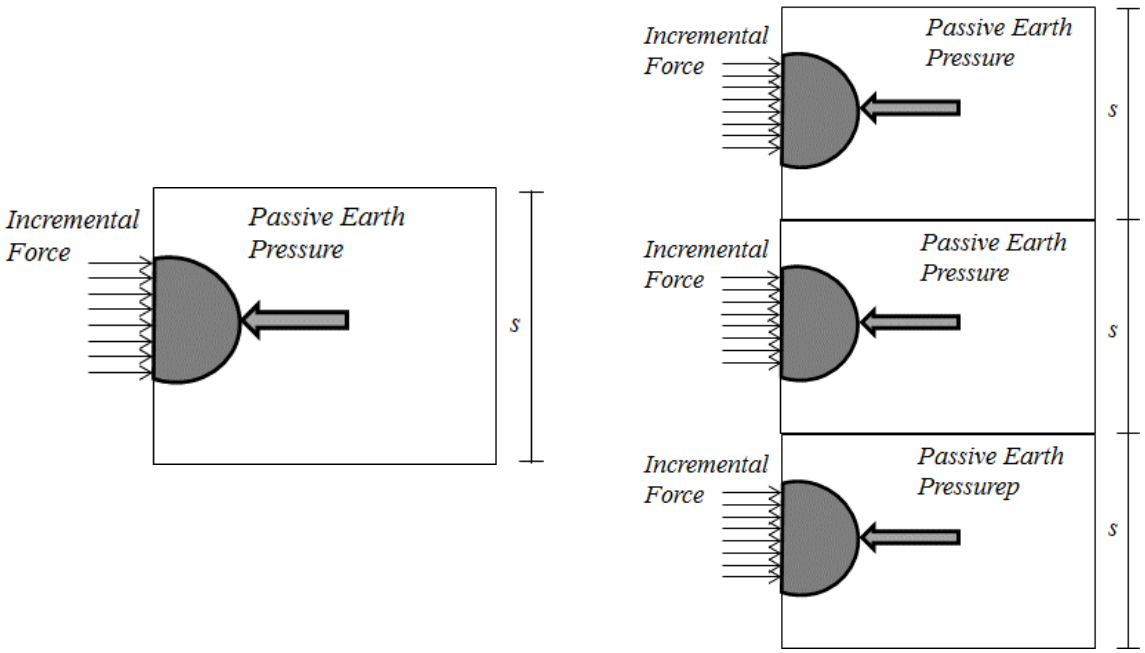

(a) (b)

Figure 4-1: 2-D plan analysis scheme for: (a) 1 pile/soil strip; (b) 3 pile/soil strips. *s* is the center-to-center pile distance.

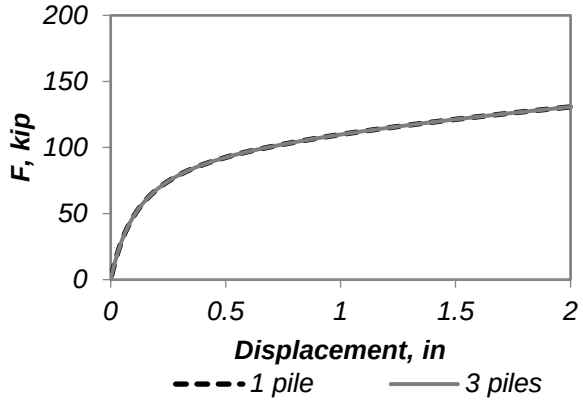

Figure 4-2: Capacity curves from 2-D plan analyses considering 1 and 3 pile/soil strips for the medium-stiff clay.

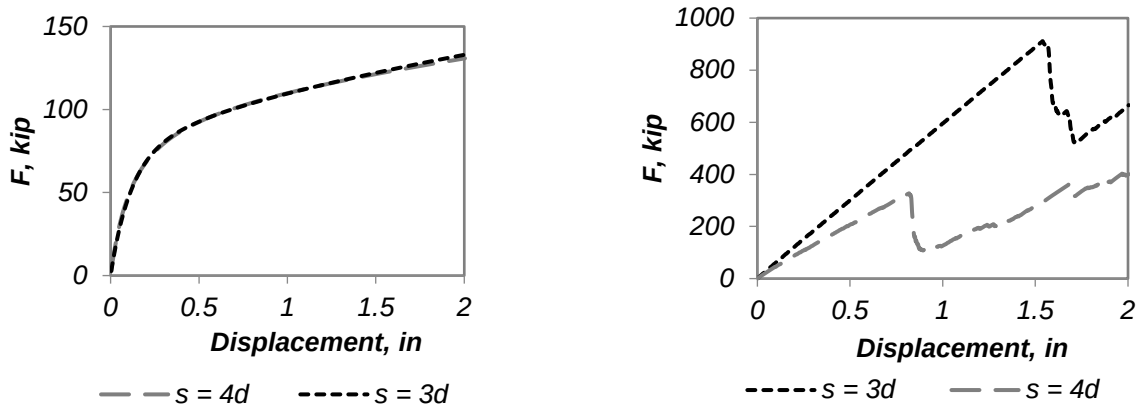

(a) (b)

Figure 4-3: Effect of pile spacing on capacity curves from 2-D plan analyses: (a) medium-stiff clay; (b) medium-dense sand.

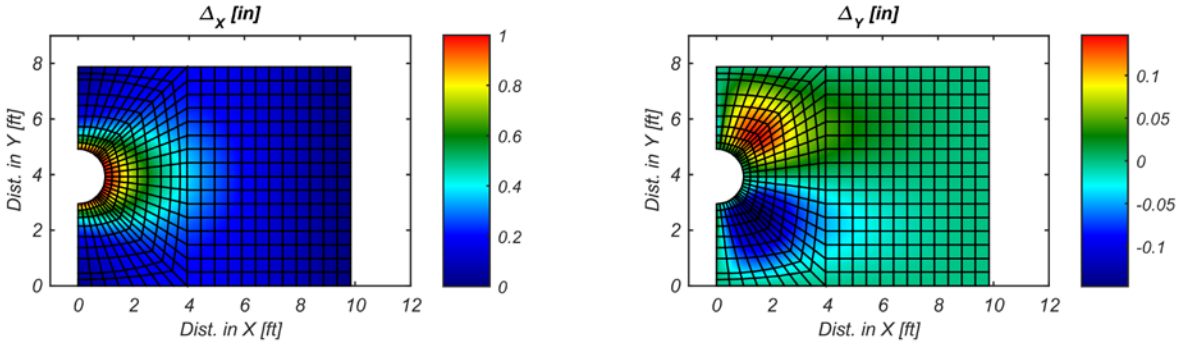

(a) (b)

Figure 4-4: Plan model for medium-dense sand with width = 4*d*: (a) displacements in X direction; (b) displacements in Y direction.

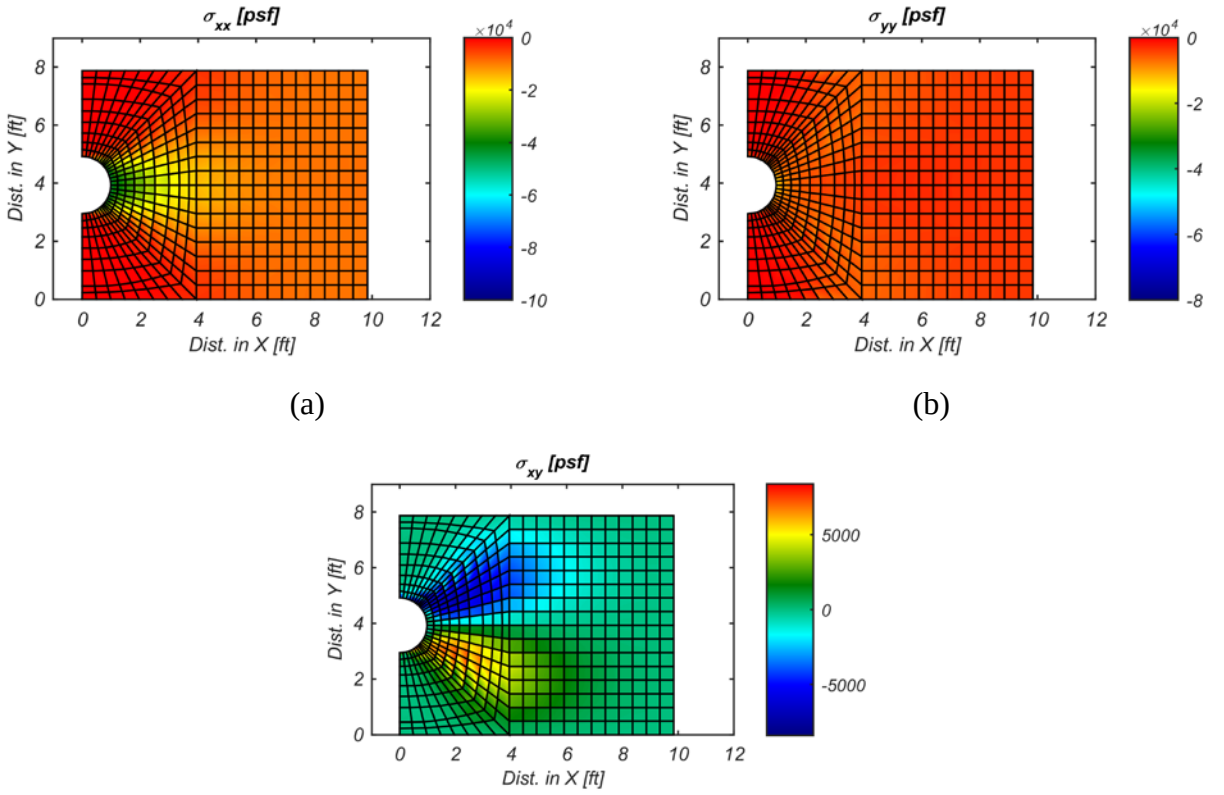

(a) (b)

(c)

Figure 4-5: Plan model for medium-dense sand with s = 4*d*: (a) stresses in X-direction; (b) stresses in Y-direction; (c) stresses in XY direction.

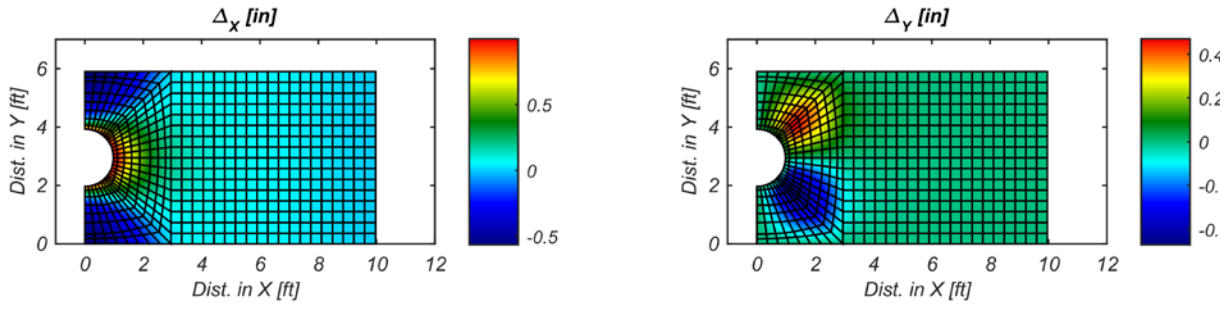

(a) (b)

Figure 4-6: Plan model for medium-stiff clay with s = 3*d*: (a) displacements in X-direction; (b) displacements in Y-direction.

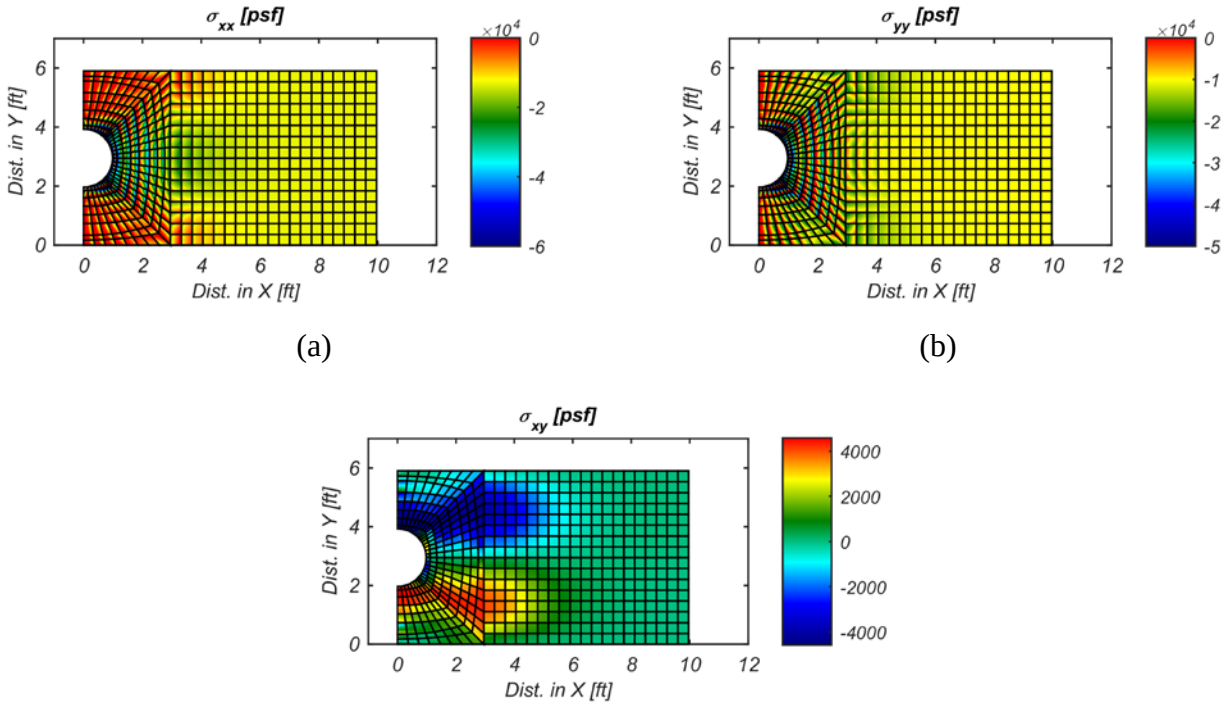

(a) (b)

(c)

Figure 4-7: Plan model for medium-stiff clay with s = 3*d*: (a) stresses in X-direction; (b) stresses in Y-direction; (c) stresses in XY direction.

4.5 3-D MODEL RESULTS

4.5.1 Effect of load distribution and detachment effects

The load distribution along the pile plays a fundamental role in this study. Depending on how it is applied, the passive soil resistance may not be totally mobilized. Two different load distributions were considered: (1) a concentrated load applied at the pile head as represented in Figure 4-8a, based on a common experimental test set ups where a top displacement is imposed to the wall; and (2) a *triangular load* distributed along the whole pile shown in Figure 4-8b, which is based on the load distribution considered during the design.

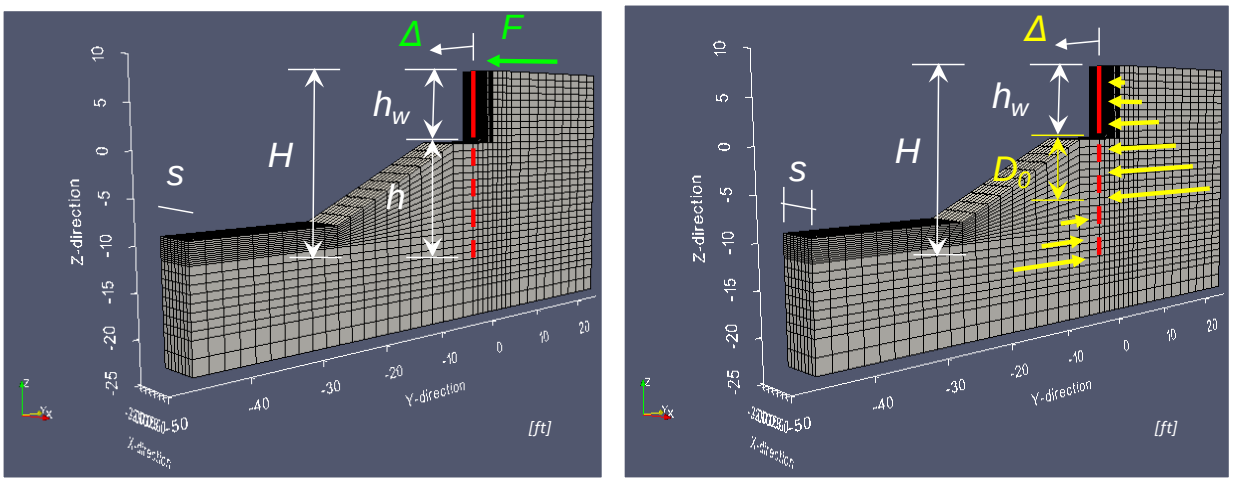

(a) (b)

Figure 4-8: Load distributions considered: (a) concentrated load; (b) triangular load.

Comparisons between both load distributions are herein shown in terms of system capacity and consequent arching factor evaluation for a case in which no slope in front of the pile is considered (flat case). Figure 4-9 shows the curves for medium-dense sands, for medium-sense clays shows the results for granular cohesive soils. In all cases, when applying the triangular load, the system shows about three times more capacity than when considering a concentrated load. This can explained due to the fact that with the load applied on the pile-head, the system is not able to develop full passive resistance.

The triangular load distribution is the selected hereforth for the subsequent analyses. Analyses with the concentrated load were also performed and results are shown in Appendix A. For medium-dense sand, Figure 4-9a shows that when applying a triangular load along the pile, the system capacity obtained is similar to the design values showing values of *n* reaching 1.0 for pile head displacements of about 2 inches. The same statement can be made for cohesive granular soils, shown in Figure 4-9b, where n=1 is reached at approximately 2 inches of top displacement.

For medium-stiff clay the system capacity is shown to three times more than expected when considering the triangular load, shown in Figure 4-9c, and considering the equal DOF assumption. The reason for this discrepancy can be related to the pile soil connection behind the pile assumed in the numerical model. In contrast to what happens with granular soils where the soil moves following the pile, for clays this does not happen, in which a gap behind the pile and consequent detachment of the pile relatively to the soil occurs, thus affecting the capacity of the whole system. Thus, the model of the pile-soil interface for the cohesive soils was improved by introducing gap elements to allow for the detachment of the wall.

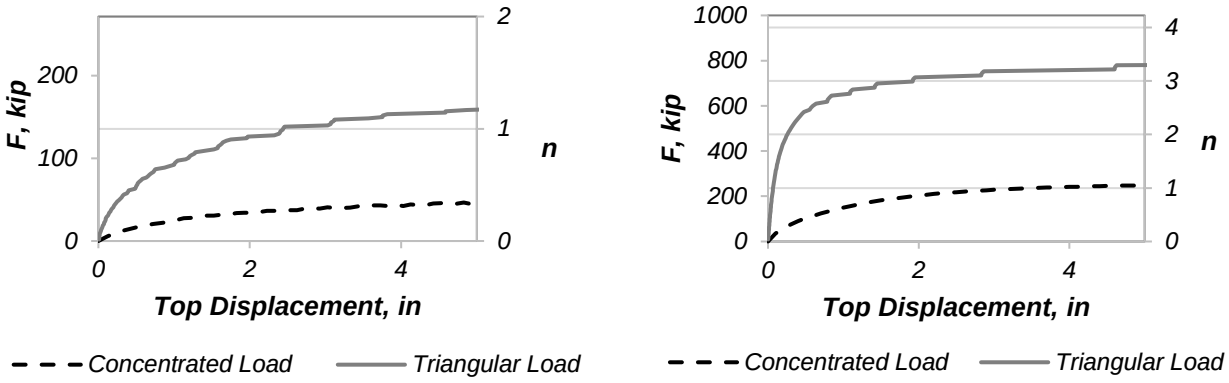

(a)

(b)

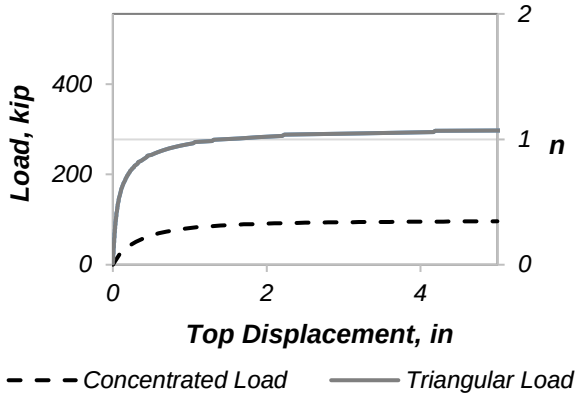

(c)

Figure 4-9: Comparison between capacity obtained with different load distribution: (a) medium-dense sand; (b) medium-stiff clay; (c) granular cohesive soil.

Figure 4-10 plots the capacity curve and consequent comparison with the expected capacity evaluated by *n,* considering occurrence of a gap and detachment of the pile on the medium-stiff clay for a flat case compared to the one when the detachment is not considered. With the improved model, both the expected capacity and the system capacity obtained through the numerical model are similar at large pile head displacements. Thus, for medium-stiff clays, this modeling assumption was considered in the analyses performed.

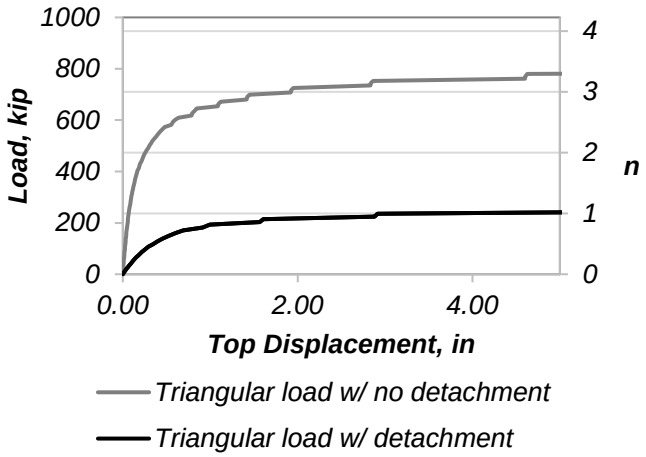

Figure 4-10: Capacity of medium-stiff clay considering gap behind the pile.

4.5.2 Validation of the 3-D Modeling Approach

In the absence of experimental results that could be used to validate the modeling approach for soldier pile retaining systems, in order to validate the modeling approach and analysis methodology used, two numerical models were developed in OpenSees to simulate full-scale tests performed at Oregon State University under the auspice of a Caltrans funded project (Nimityongsukul et al. 2012). The two tests simulated: (1) a single pile embedded in the soil with no slope, designated as the *Baseline* case; and (2) a pile embeded in the soil, but with a slope crest located four pile diameters in front of the pile, designated as the *4D Pile* case. The tests consisted of the application of an incremental horizontal load at a steel pipe pile head in both cases. The two simulated cases are described in detail in Nimityongsukul et al. (2012), in which the capacity of the single piles were evaluated through experimental testing and through analysis using *Plaxis 3D*.

Figure 4-11 shows the mesh of the finite element models developed in *Plaxis 3D* and Figure 4-12 shows mesh the finite element models developed in *OpenSees*. For both the *Baseline* and *4D Pile* cases, two numerical models in OpenSees are developed, differring in the way in which the interface between the soil elements and the pile was modeled. In the first model, the nodes of the pile were restrained to the soil nodes located at the same elevation, using a master-slave algorithm (*equalDOF* in *Open Sees*). In the second model, beam contact elements providing interaction between the beam element and the soil elements were defined using the formulation described in section 3.3.2.6. The parameters used in the *Open Sees* numerical models were defined based on the input parameters of the numerical model developed in *Plaxis 3D* by Nimityongskul et al. The assumed values are listed in Table 4-7 and Table 4-8 regarding to the soil and pile, respectively.

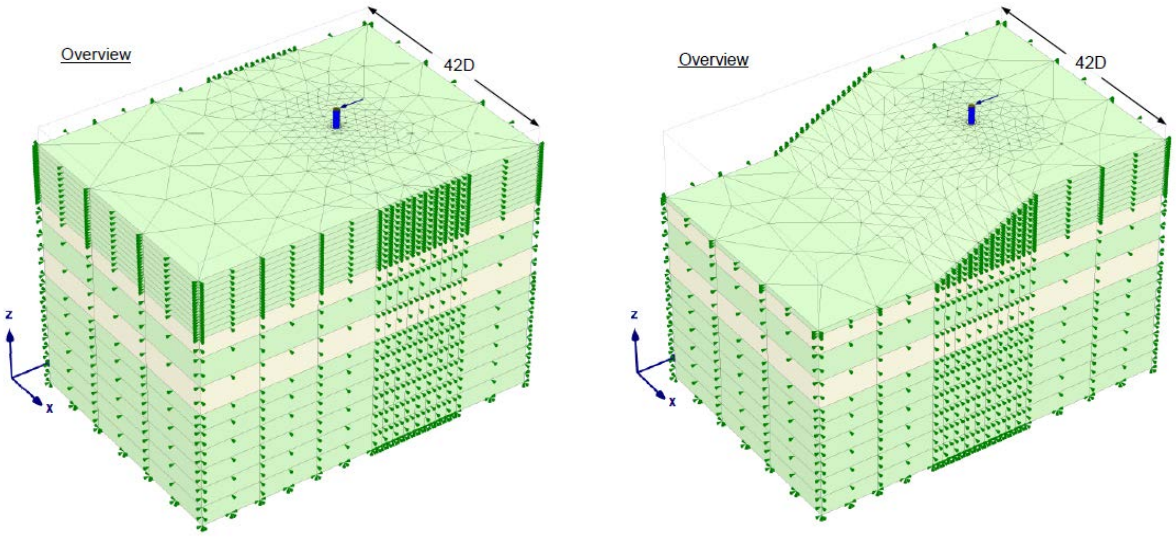

(a) (b)

Figure 4-11: Numerical models developed in Plaxis 3D by Nimityongsukul et al. (2012): (a) baseline model; (b) 4D pile model.

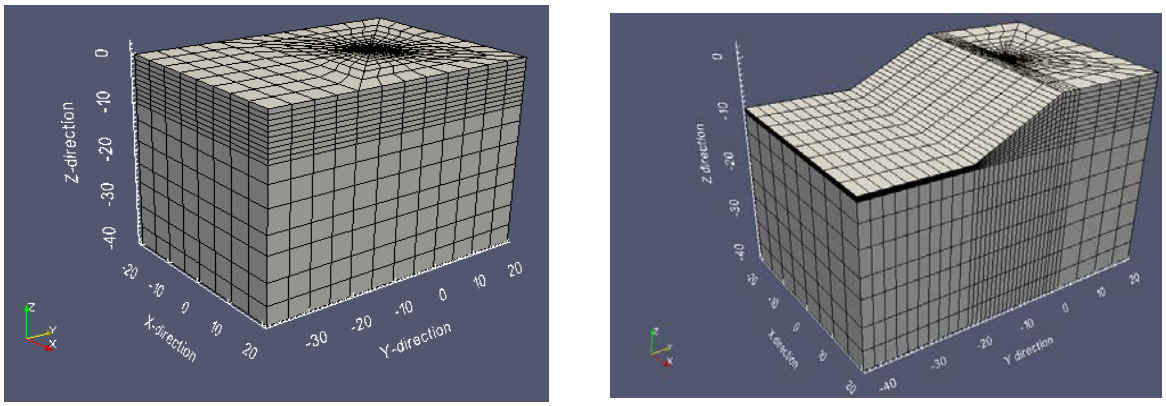

(a) (b)

Figure 4-12: Numerical models in OpenSees: (a) baseline model; (b) 4D pile model.

Table 4-7: Soil parameters

Soil Layer	Soil Unit Weight pcf	Cohesion puff	Young's Modulus ksf	Poisson's Ratio	Friction Angle degrees
(1) Upper Cohesive	115	2400	158	0.495	-
(2) Upper Sand	130	-	600	0.35	40
(3) Lower Cohesive	115	2400	158	0.495	-
(4) Lower Sand	130	-	600	0.35	45
(5) Blue Gray Clay	110	3500	158	0.495	-

Table 4-8: Pile parameters

Material Parameter	Density lb/in^3	Thickness in	Young's Modulus ksf	Poisson's Ratio
Steel Pipe Pile	0.289	0.375	$4.1x10^7$	0.1

Figure 4-13 shows the results measured in the field, results obtained for the numerical model developed in *Plaxis 3D*, and the results obtained considering the two cases modeled in *OpenSees*. Two curves are shown for the OpenSees results. The first curve shows results when the model considers *master-slave* (*equalDOF*) constraints between pile nodes and auxiliary pile nodes at the soil interface. In this case, the soil element nodes are connected with zero-length compression only gap in the case of the clayey soils and rigid links when in sandy soils. The compression only gap elements allow for detachment of the pile with respect included. The second curve corresponds to the case when friction contact interface elements are modeled in the interface.

Results in Figure 4-13 show a close match between the results obtained in *OpenSees* and the experimental results for the model that uses the equalDOF elements. In contrast, the *OpenSees* model in which friction contact elements are used provides relatively low stiffness and strength values. In addition, the model using friction contact elements had significant convergence issues

and computational times were greatly increased due to the increased number of iterations and reduced displacement increments needed to achieve convergence. Hence, based on these validation results, the model with the *equalDOFs* and detachment gap elements is considered to be the most adequate moving forward.

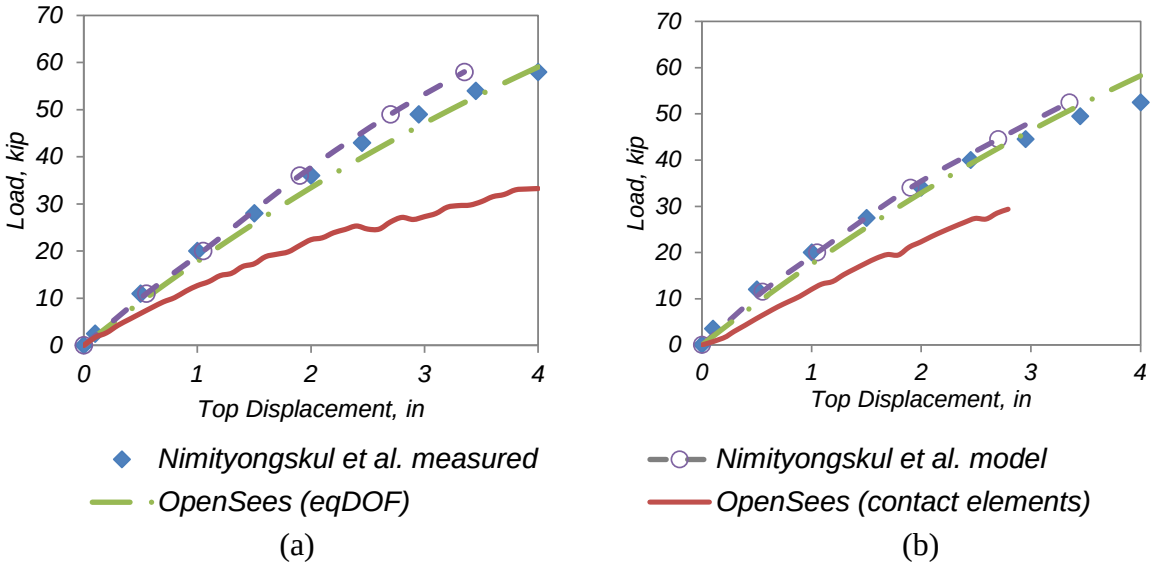

(a) (b)

Figure 4-13: Comparison of capacity curves between the values measured, values obtained in *Plaxis 3D* and values obtained in *Open Sees*: (a) baseline model; (b) 4D pile model.

Figure 4-14 shows pile deflections and rotations at different elevations obtained from field measurements and the OpenSees analyses. It can be seen that the deflections match extremely well, while the rotations show a reasonable match. Note, however, the finite element model estimates larger rotations than those observed in the field. For reference, Figure 4-15 shows an overlay of the deformed shapes obtained from the numerical analysis with the stresses in Y-direction.

In summary, the results displayed in terms of force-pile head displacement, rotation, and deflection obtained with the numerical model in Open Sees show a good approximation with the experimental tests for the two cases studied. Therefore, the modeling approach that considers equalDOF constraints and detachment effects for clays is considered to be adequate to achieve the main objectives of this study.

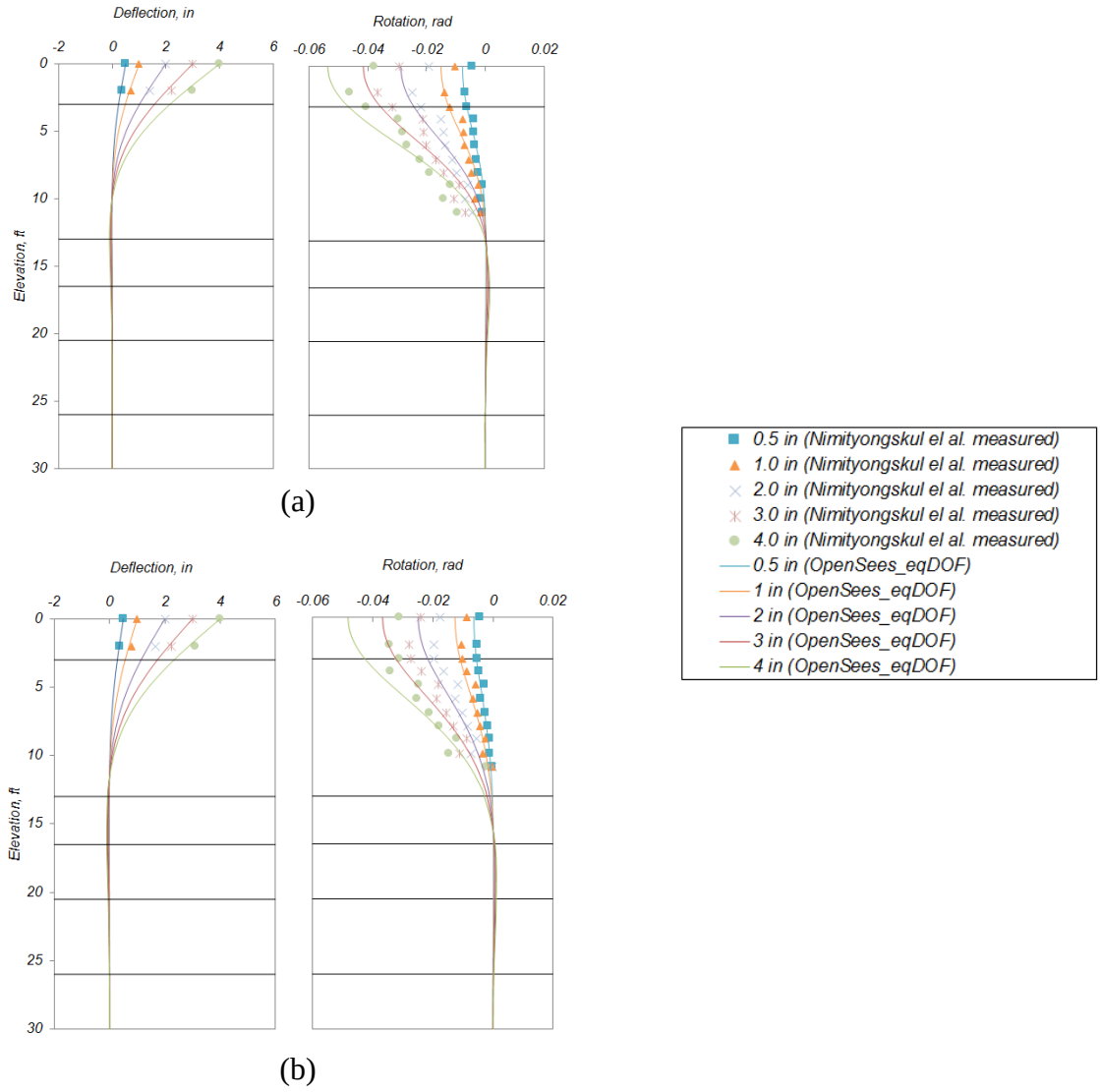

Figure 4-14: Deflection and rotation measured in the field (markers) and obtained from the *OpenSees* models (continuous lines): (a) baseline model; (b) 4D pile model.

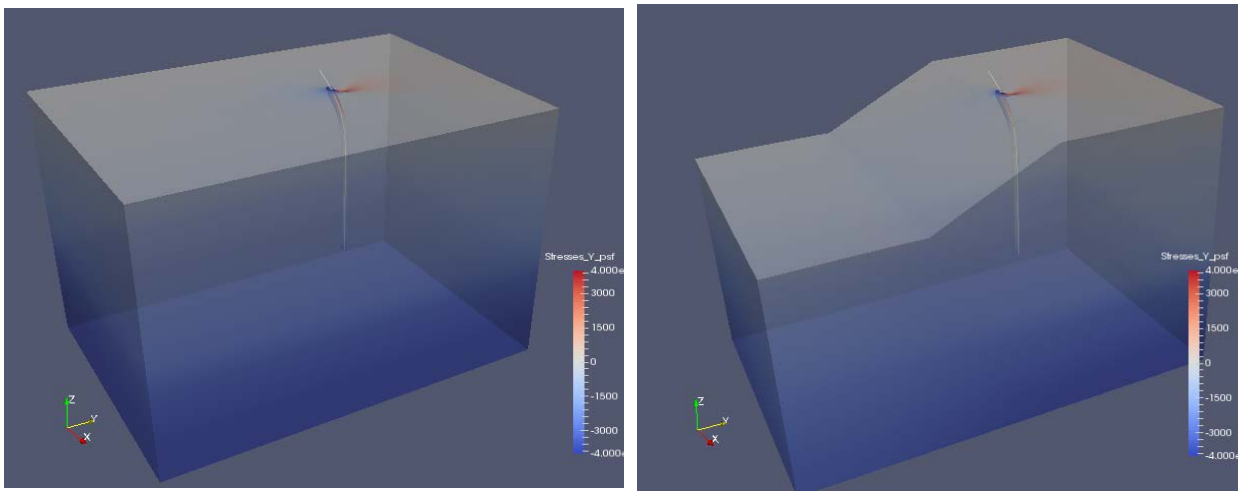

(a) (b)

Figure 4-15: Stresses in Y direction obtained with the *Open Sees* model: (a) baseline model; (b) 4D pile model.

4.5.3 Nonlinear Static Pushover Analysis Results

This section presents the results obtained for 3-D analyses. Results are summarized below by soil-type and considering the triangular load distribution for the pushover analyses. For the medium-dense sand a total of 28 analyses were performed, for the medium-stiff clay a total of 20 analyses were performed, and for the granular cohesive soil 27 analyses were performed.

4.5.3.1 Medium-dense sand

In the following figures and discussions presented for this soil type, a soldier pile wall height of 10 feet and spacing between piles of 4d was considered to illustrate the effect of the main parameters considered in the analysis.

Figure 4-16 shows the capacity of the system for a flat dredge line (no slope) and different embedment depths, which are 12 feet (slno) and 30 feet (slno_eqh), the latter being the design depth for the case with a 3:2 slope. It can be seen from this figure that increasing the embedment depth increases significantly the lateral capacity of the system.

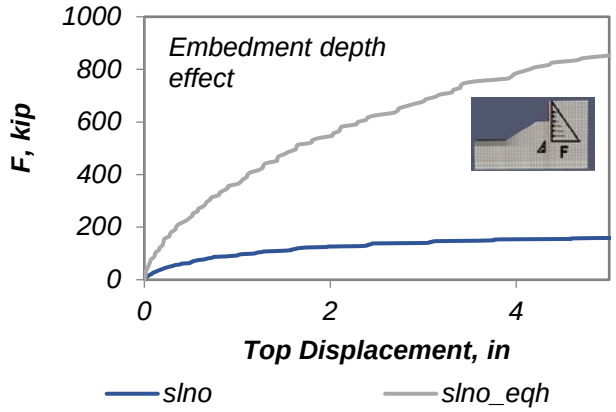

Figure 4-16: Effect of embedment depth on capacity curves for a soldier pile retaining wall with h_w = 10 ft and s = 4d. Soil type is medium-dense sand.

Figure 4-17 shows the effect of a slope in front of the soldier pile and the effect of the slope angle. It can be seen that for the same embedment depth and the same bench width (4d), the slope angle has only a negligible effect.

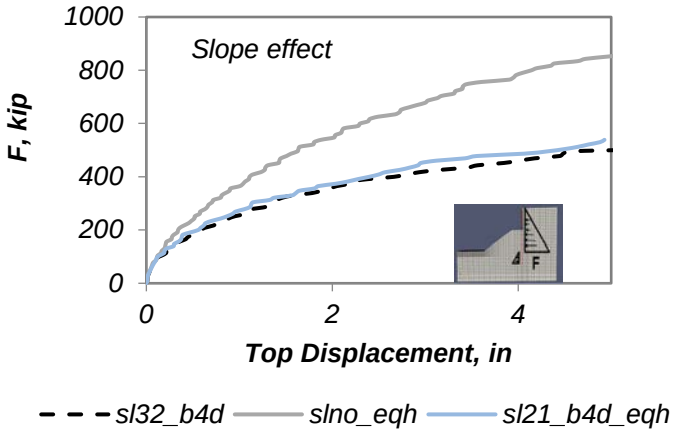

Figure 4-17: Effect of slope on capacity curves for a soldier pile retaining wall with h_w = 10 ft and s = 4d. Soil type is medium-dense sand.

Figure 4-18 shows the bench width effect on the system capacity. Clearly there is a noticeable increase in the system capacity as the bench width increases.

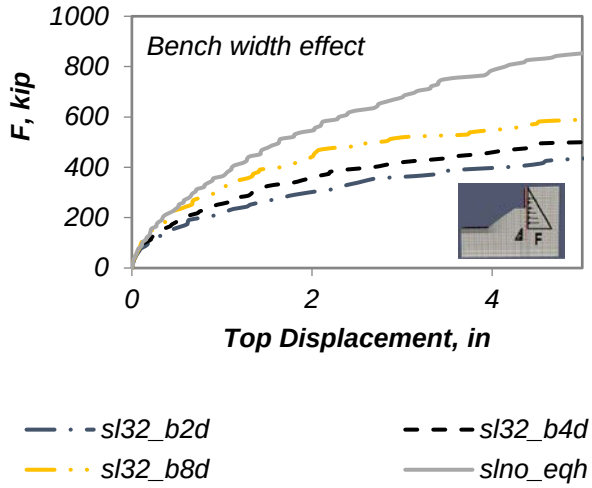

Figure 4-18: Effect of bench width on capacity curves for a soldier pile retaining wall with h_w = 10 ft and s = 4d. Soil type is medium-dense sand.

Figure 4-19 to Figure 4-22 show the deformed shapes overlaid with stresses for the flat dredge line. It can be seen that the model captures the soil heaving in front of the wall, while the backfill drops due to the lateral deformation of the wall. With respect to the stresses, from Figure 4-19 one can see that there is no tensile stresses, which means that the soil follows the pile and lagging without any resistance. This is expected since the medium-dense sand modeled does not have any cohesion. The arching effect in front of the pile is visible through stresses σ_{yy} shown in the plan view figures (Figure 4-20). In Figure 4-21, the stresses in the principal direction I, σ_I show a distribution of stresses that is consistent with the load distribution applied on the pile. The failure surface is not clearly identified in the σ_{xy} shown in Figure 4-22, although the formation of the active state starting at the toe and propagating towards the top on the backfill side indicate the initiation of the formation of the failure surface.

Other deformed shapes and stresses for cases in which the slope is considered are shown in Appendix B.

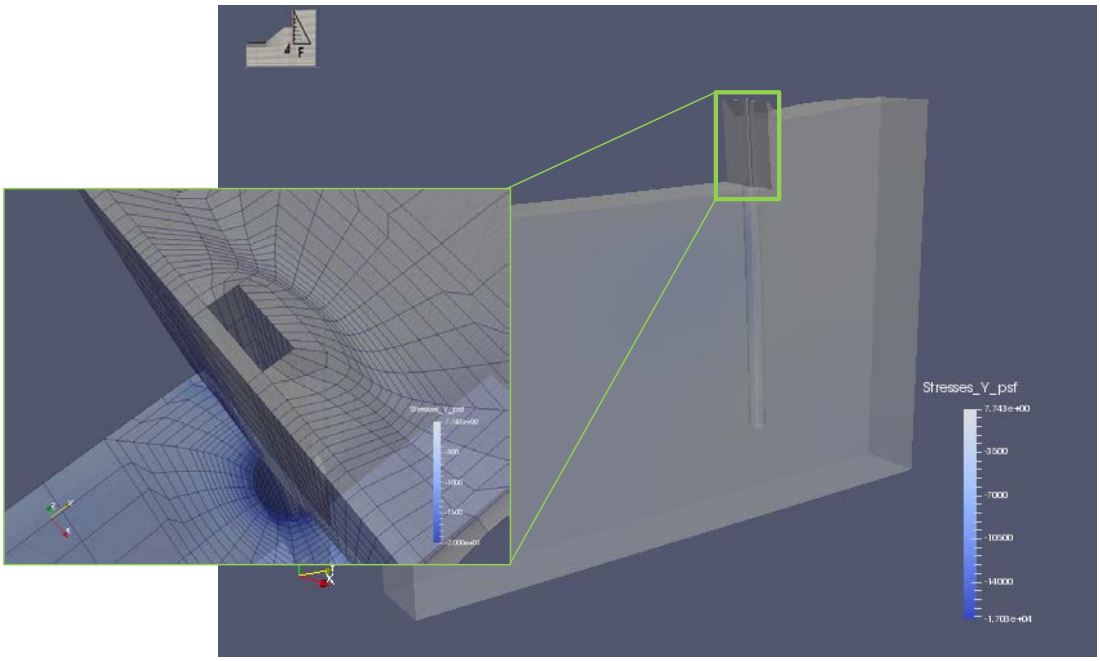

Figure 4-19: 3-D model – 3-D view of σ_{yy} stresses and deformed shape for a pile-head displacement = 2 in. Case: medium-dense sand, h_w=10 ft, s=4d, and no slope.

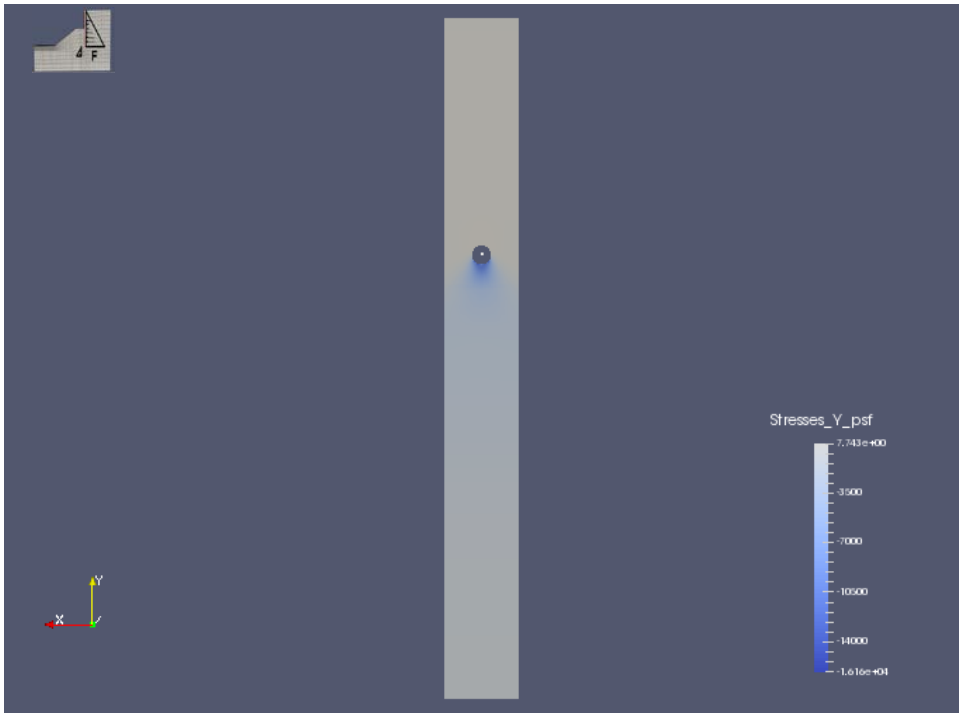

Figure 4-20: 3-D model – Plan view of σ_{yy} stresses at depth = -2d, for pile-head displacement = 2 in. Case: medium-dense sand, h_w=10 ft, s=4d, and no slope.

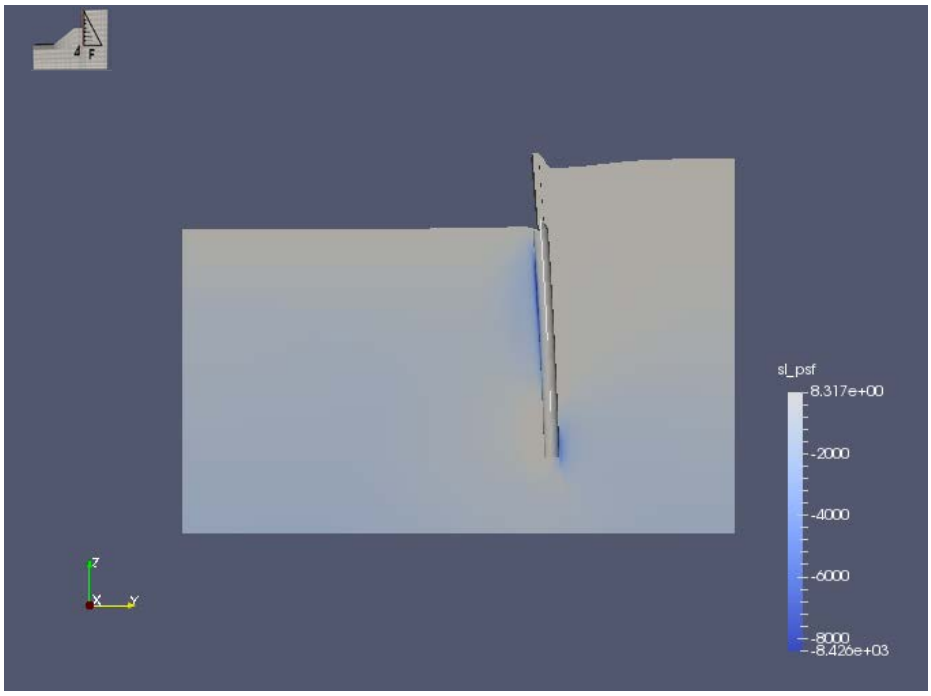

Figure 4-21: 3-D model – Elevation view of σ_I stresses for a pile-head displacement = 2 in. Case: medium-dense sand, h_w=10 ft, s=4d, and no slope.

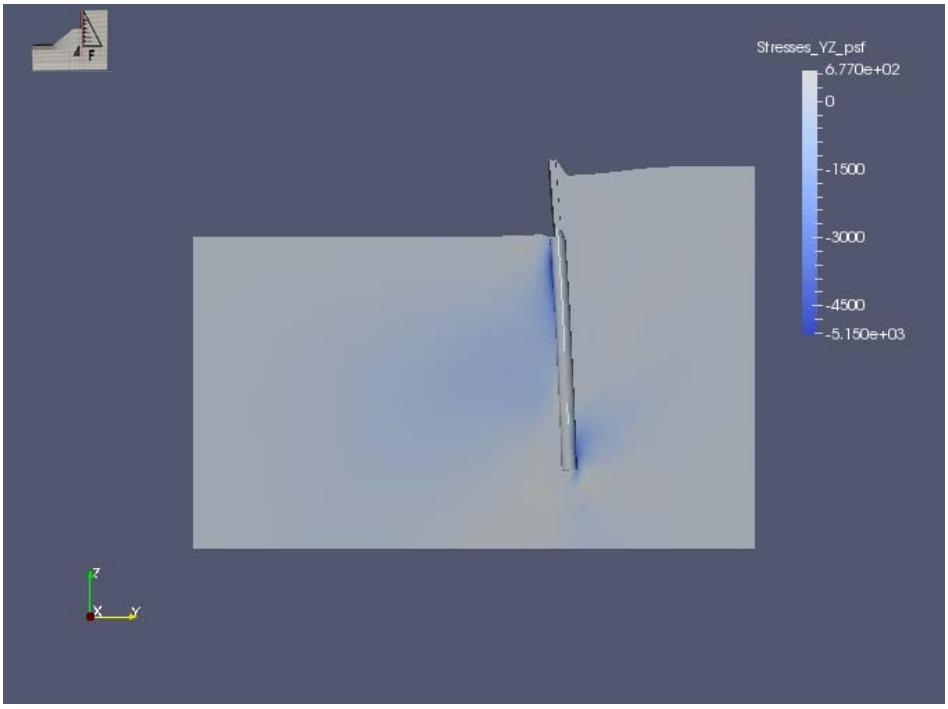

Figure 4-22: 3-D model – Elevation view of σ_{YZ} stresses in YZ direction and deformed shape for pile-head displacement = 2 in, Case: medium-dense sand, h_w=10 ft, s=4d, and no slope.

4.5.3.2 Medium-stiff clay

Figure 4-23 shows the capacity of the system for five different cases, including three different slope conditions and three bench widths. It can be seen from this figure for the medium-stiff clay, the different parameters have little effect on the capacity of the system. Results obtained with other soldier pile wall system geometries displayed in Appendix C show the same conclusions

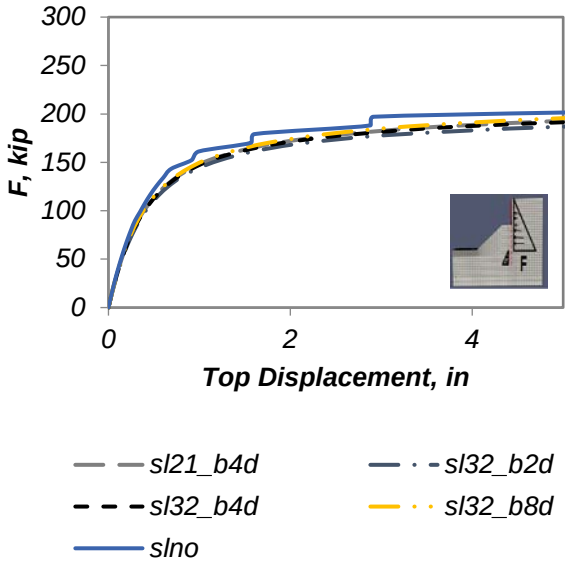

Figure 4-23: Capacity curves for soldier pile retaining wall system. Case: medium stiff clay, hw = 10 ft and s = 4d.

Figure 4-24 to Figure 4-26 show the deformed shapes and stresses of the soldier pile wall system for the cases. In Figure 4-24, the impact of considering the compression only gaps can be observed as the pile detaches from the backfill, which remains vertical due to the cohesion of the soil. The soil arching is pretty evident in Figure 4-25, which shows the .In the stresses obtained with medium-stiff clay the failure surface is even more evident in the XY stresses. As seen for medium-dense sands, the load distribution applied in the pile can be identified in Figure 4-26. Plots of analysis with slope are also shown in Appendix D.

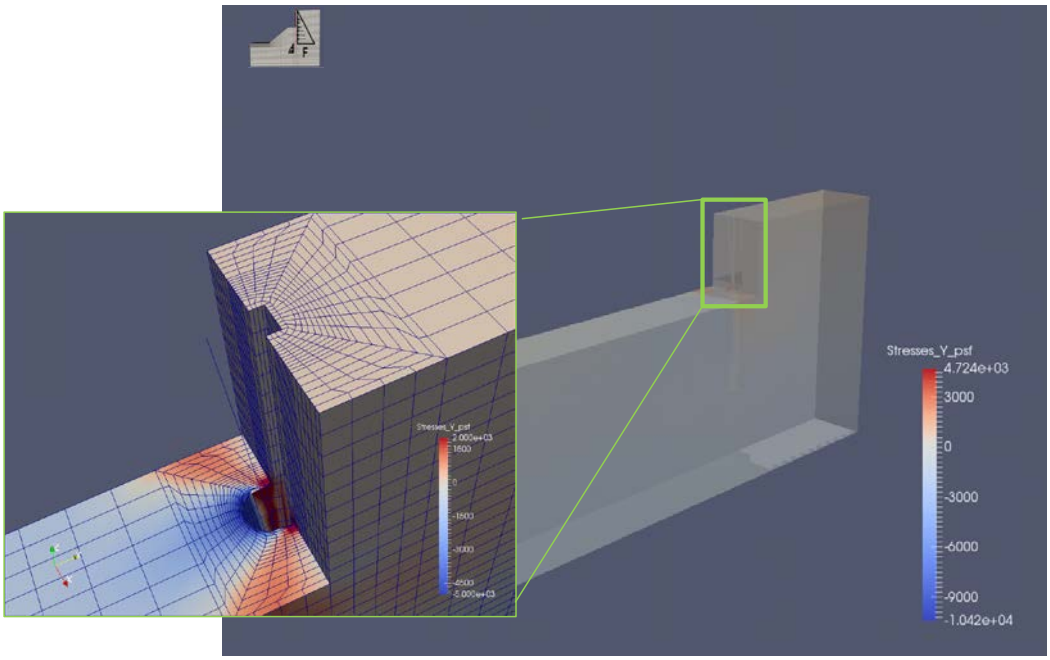

Figure 4-24: 3-D model – 3-D view of stresses in σ_{yy} for a pile-head displacement = 2 in. Case: medium-stiff clay, h_w = 10 ft, s = 4d, no slope.

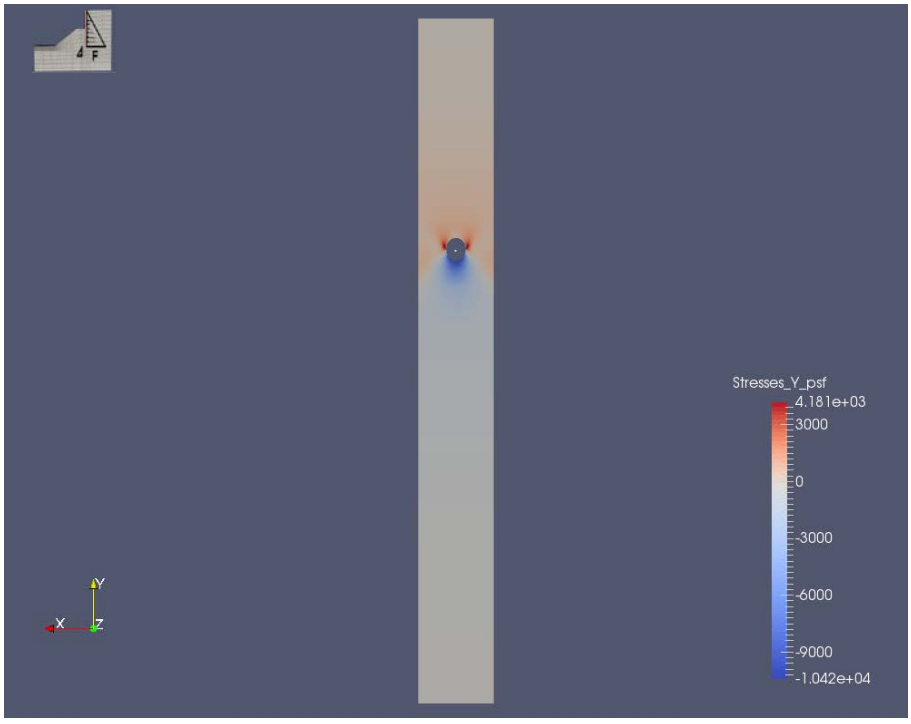

Figure 4-25: Plan view of stresses in σ_{yy} at z = - 2d, for a pile-head displacement = 2 in. Case: medium-stiff clay, h_w = 10 ft, s = 4d, no slope.

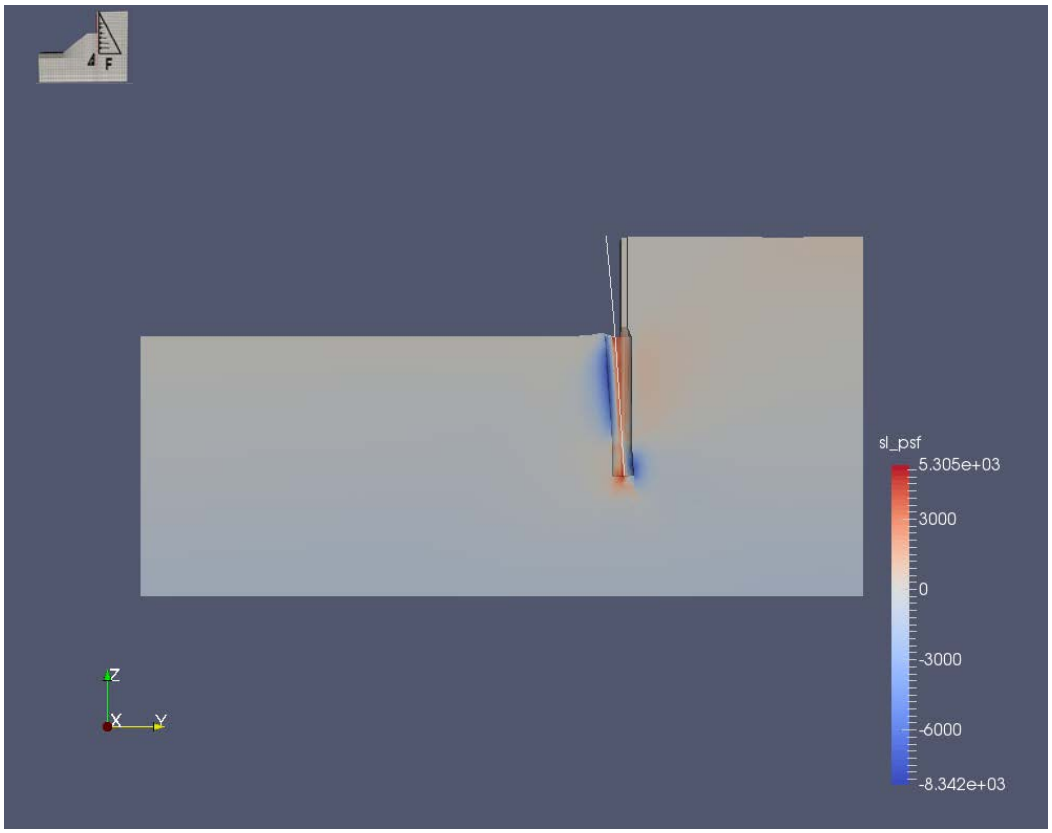

Figure 4-26: Elevation view of σ_1 stresses for a pile-head displacement = 2 in. Case: medium-stiff clay, h_w = 10 ft, s = 4d, no slope.

4.5.3.3 Granular Cohesive Soil

The figures in this subsection show, for the granular cohesive soil case, plots for a soldier pile system with a wall height of 10 ft and spacing between piles of 4*d*. Figure 4-27 shows the capacity of the system, considering a 2:1 slope with different embedment depth considered. The effect of the embedment depth is discernible, just as was the case for the medium-dense sand.

Figure 4-28 shows that the system capacity is only marginally affected by slope effects, when the soldier pile wall height is 10 ft. However, similarly to what was observed for the medium-dense sands, little effect is observed when considering the 10 ft wall case. However, the effects of slope in granular cohesive soils are noticeable for wall height of 15 ft (see in Appendix D).

Figure 4-29 illustrates the effect of the bench width on the system capacity on granular cohesive soils. From inspection of the figure, it can be seen that there are slight differences for h_w = 10 ft. These effects tend to be greater when h_w = 15 ft (see Appendix D), as the capacity increases as bench width increases.

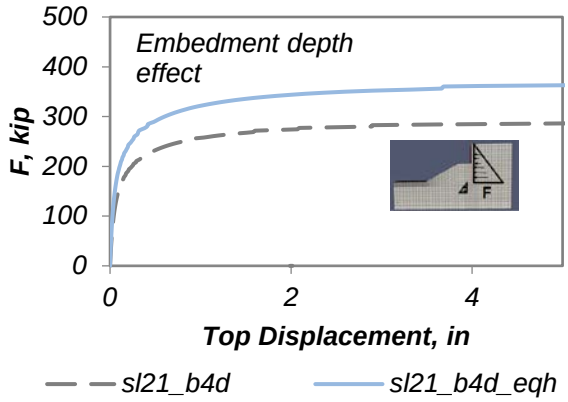

Figure 4-27: Capacity curves different embedment depths.
Case: granular cohesive soil, h_w = 10 ft and s = 4d.

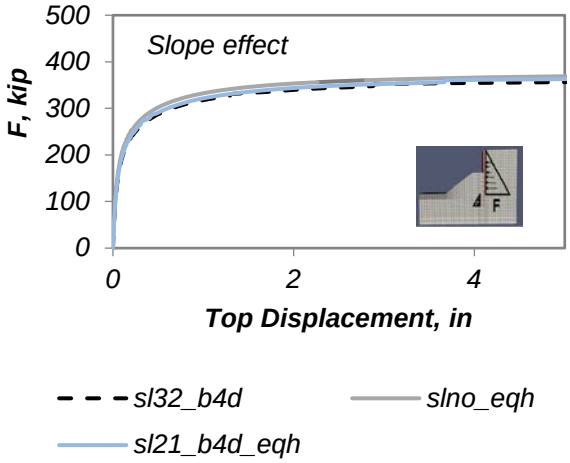

Figure 4-28: Capacity curves for different slope conditions.
Case: granular cohesive soil, h_w=10 ft and s=4d.

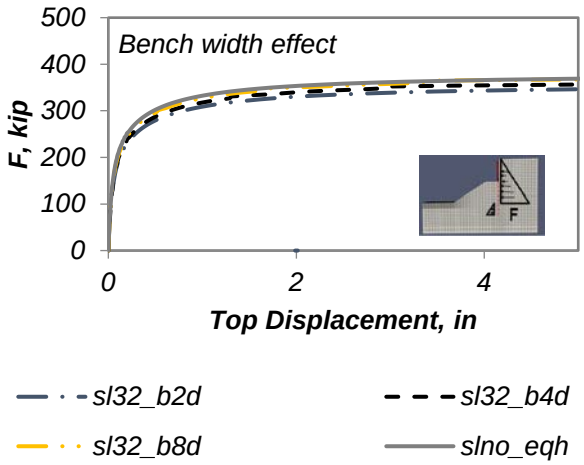

Figure 4-29: Capacity curves for different bench widths.
Case: granular cohesive soil, h_w=10 ft and s=4d.

Figure 4-30 shows an overlay of the deformed shape and stresses in the soil of the soldier pile retaining system for the granular cohesive soil when the pile head moved 2 inches in the Y-direction. The stresses represented are the σ_{yy}. From the observation of the deformed shape in this figure, it can be seen that the movement of the soil towards the load direction of the pile movement is not as pronounced as in case of the medium-dense sand, due to the cohesion of the soil model. Therefore, some tensile stresses are developed in the soil domain.

Figure 4-31 illustrates a plan view at a depth of 2d below the dredge line for the same deformation state represented in Figure 4-30. In terms of the values of the stresses developed for this example, it can be seen that the granular cohesive soil shows similar response patterns when compared with medium-stiff clay, but with smaller values.

Similarly to the other soil type cases modeled, plots containing stresses and deformed shapes of a case with slope are shown in Appendix D.

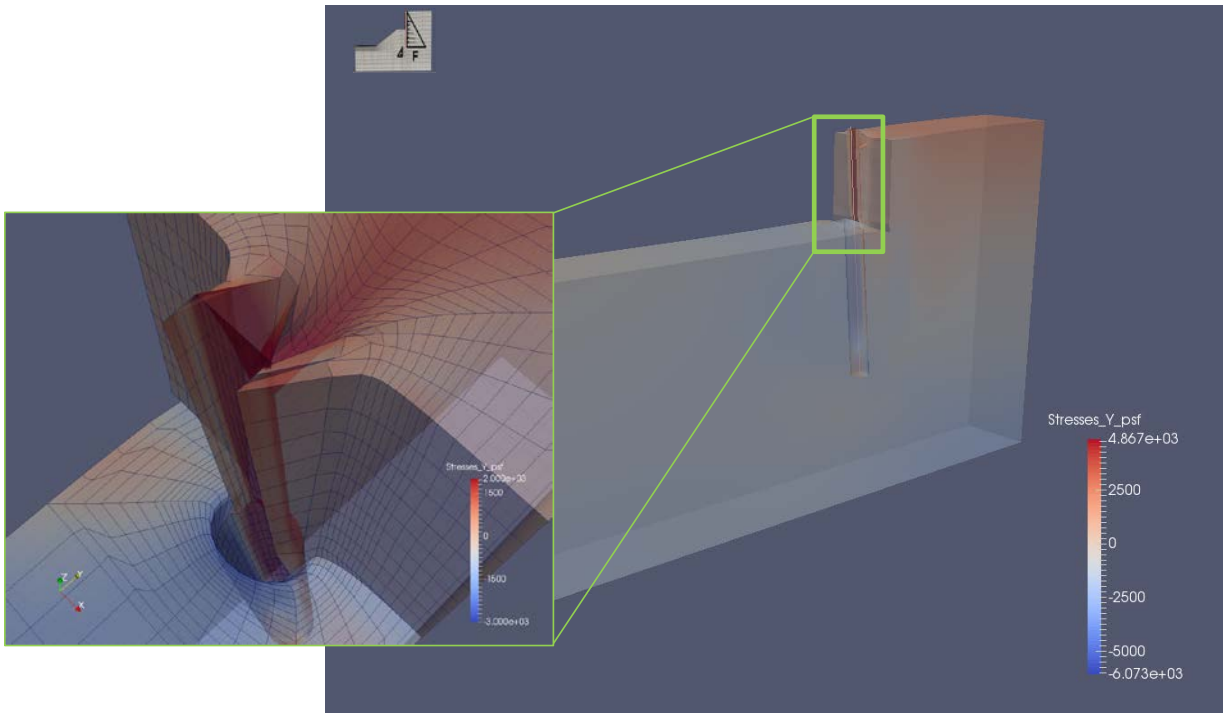

Figure 4-30: 3-D view of σ_{yy} stresses for a pile-head displacement = 2 in. Case: granular cohesive soil, h_w = 10 ft, s = 4d, no slope.

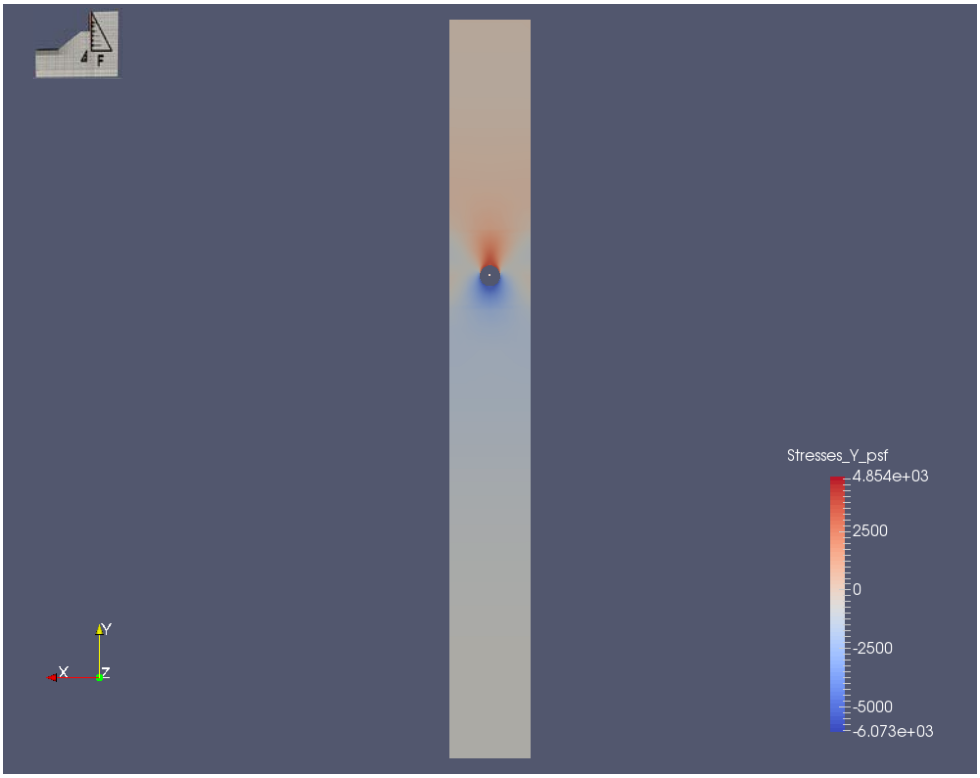

Figure 4-31: Plan view of σ_{yy} stresses for a pile-head displacement = 2 in at z = -2d. Case: granular cohesive soil, h_w = 10 ft, s = 4d, no slope.

5 ARCHING CAPABILITY FACTOR ASSESSMENT

5.1 Overview

The main objective of this work is to make inferences on the arching capability factor. In the subsequent analysis of the results presented in this subsection, the *n* factor is used to compare the values of the arching capability factor used in the design and the one is estimated based on the finite element model results and the procedures described in section 3.3.5 on Assessment of the Arching Capability Factor. The *n* factor used herein is given by equation (3-23). Note that when the *n* factor is equal to one (1), the estimated passive resistance from the finite element model results in the passive resistance estimated in the design (using equation (3-22)), which makes use of the arching capability factor as obtained using the Caltrans (2011) procedures.

5.2 Effect of Bench Width

Figure 5-1 shows the *n* factor obtained for the case in which the soil modeled is the medium-dense sand. The results displayed in this figure show that the arching capability factor is adequate when no slope is considered in front of the soldier pile wall, with *n* approaching values larger than 1 for displacements in excess of 2 inches. In turn, when the presence of slope is considered, the *n* factor is always larger than 1, even for relatively small displacements, indicating that the *f* factor in conjunction with the procedure used to estimate the lateral resisting capacity of the soldier pile system is too conservative. These results can be justified due to the fact that the bench width was not considered in the design. Even though the impact of choosing analytical methods for estimating the passive resistance could be analyzed in the future, these results clearly indicate that the bench width should be a parameter considered in design.

Figure 5-2 shows the *n* factor obtained for the case in which the soil modeled is the medium-stiff clay. This figure shows that the arching capability factor is adequate for all cases, since *n*

approaches 1.0 for large displacements. Neither slope nor bench width affects the capability arching factor for medium-stiff clays as aforementioned. Thus the adjustment capability factor seems adequate for all cases analyzed.

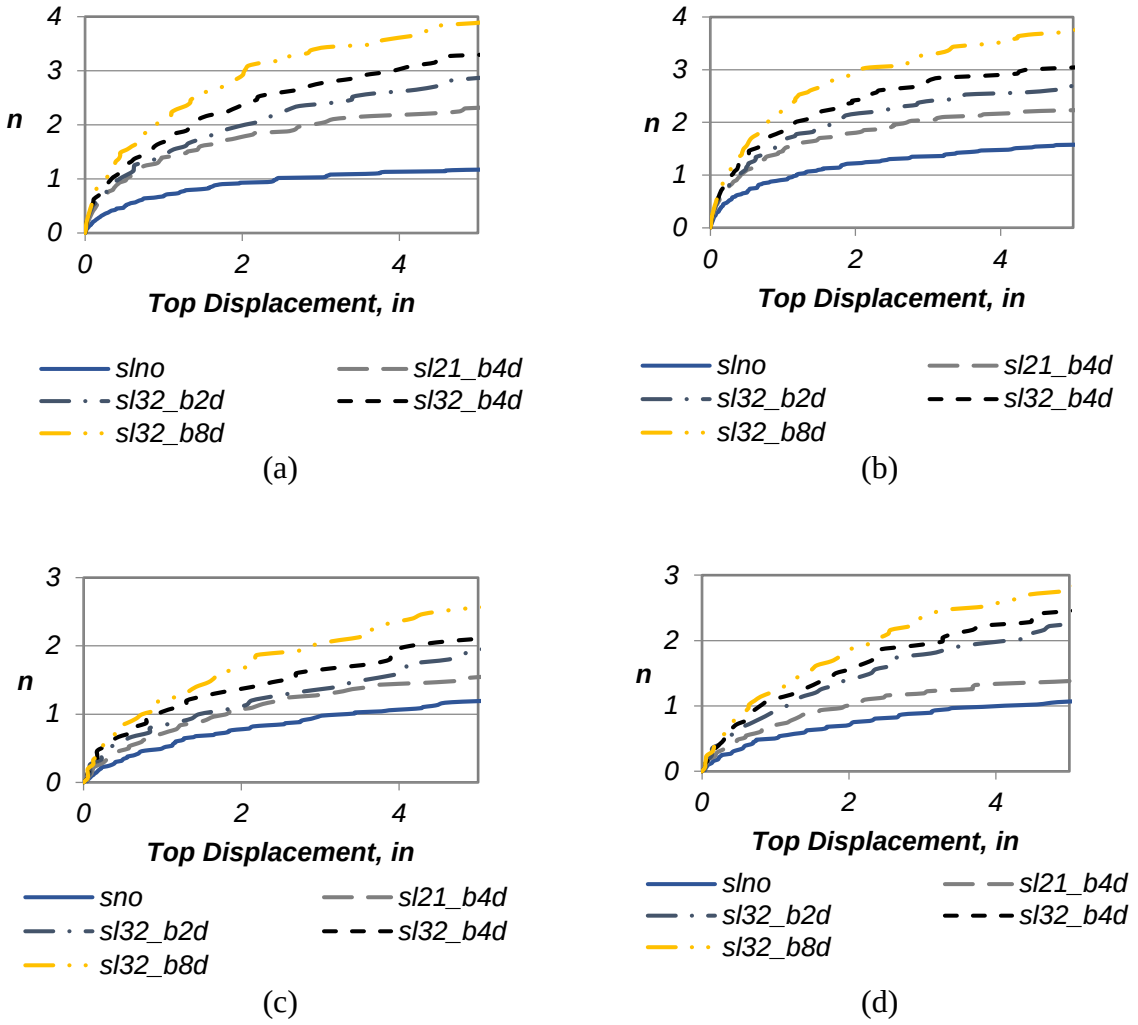

Figure 5-1: Arching capability factor assessment for medium-dense sand: (a) h_w = 10 ft and s = 4d; (b) h_w = 10 ft and s = 3d; (c) h_w = 15 ft and s = 4d; (d) h_w = 15 ft and s = 3d.

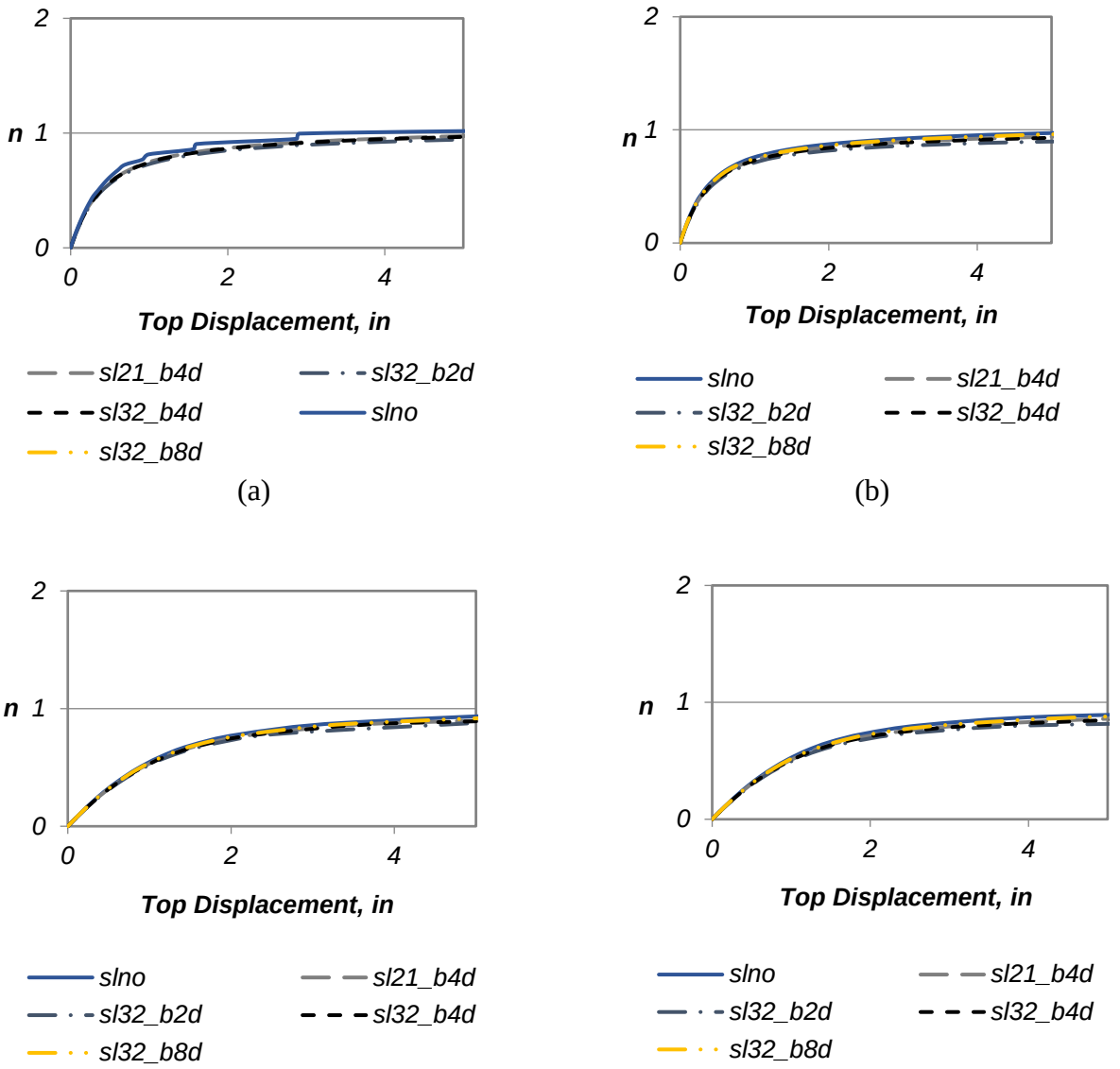

Figure 5-2: Arching capability factor assessment for medium-stiff clay: (a) h_w = 10 ft and s = 4d; (b) h_w = 10 ft and s = 3d; (c) h_w = 15 ft and s = 4d; (d) h_w = 15 ft and s = 3d.

Figure 5-3 shows the *n* factor obtained for the case in which the soil modeled is the granular cohesive soil. The observations from this figure yield statements similar to the ones made for the medium-dense sand results, mainly: (1) the arching capability factor is adequate for the case with no slope; (2) when a slope is present, the design becomes conservative when using the procedure

used in this report for the design of the walls; (3) the bench width plays an important role in the capacity of the system.

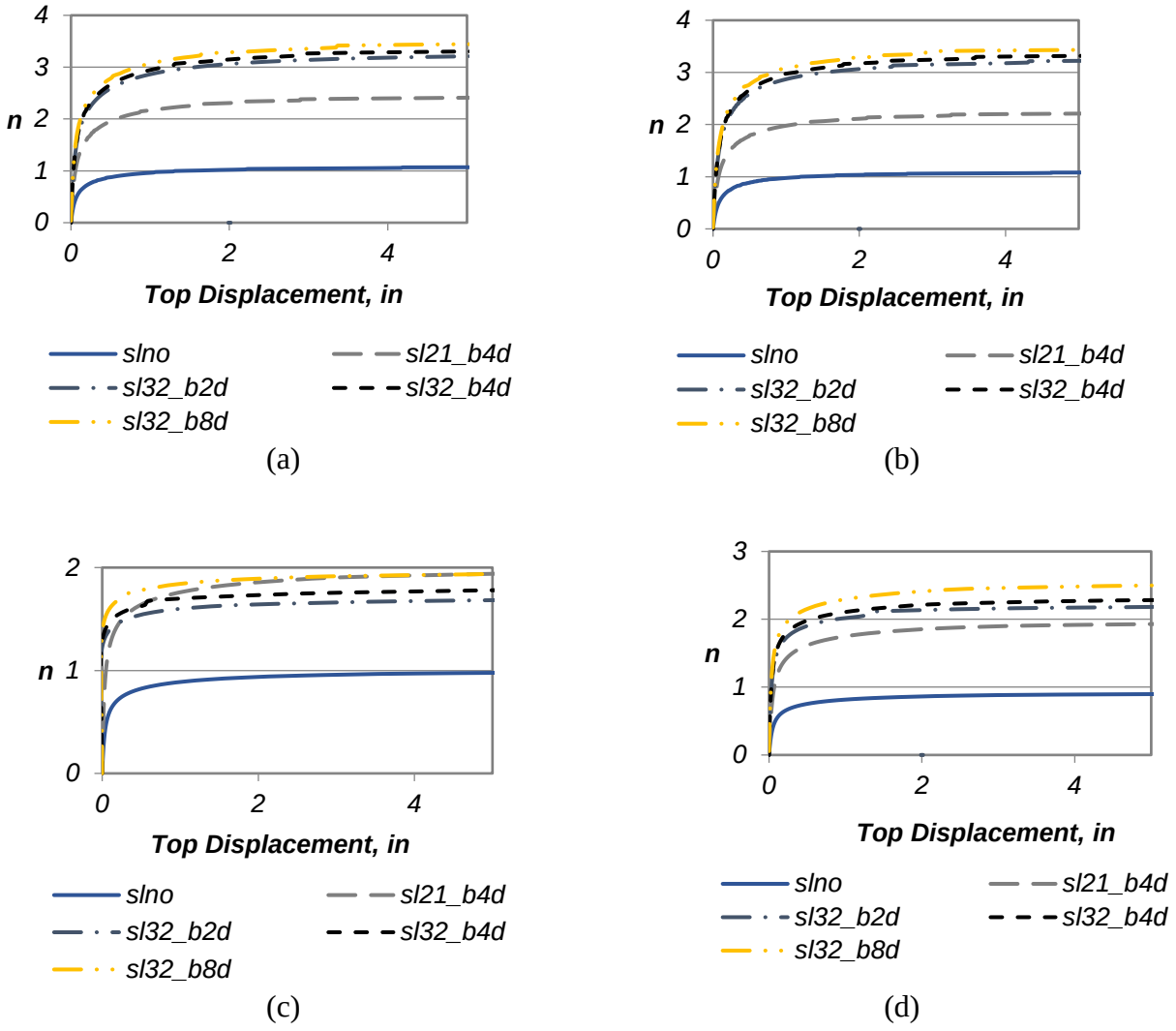

Figure 5-3: Arching capability factor assessment for medium-stiff clay: (a) h_w = 10 ft and s = 4d; (b) h_w = 10 ft and s = 3d; (c) h_w = 15 ft and s = 4d; (d) h_w = 15 ft and s = 3d.

5.3 Effect of Soldier Pile Retaining Wall Geometry: Wall height and pile spacing

After a general view of the arching capability factor assessment, parameters involved in this study as the height of the wall or the spacing between piles are also assessed in order to evaluate their influence in the results presented obtained.

Figure 5-4, Figure 5-5, and Figure 5-6 illustrate the effect of the wall height on the arching capability factor. The results obtained for h_w = 15 ft show smaller *n* for higher top displacements, meaning that the resistance obtained is generally closer to the theoretical resistance than when considering h_w= 10 ft, being the results more conservative when dealing with walls with smaller height.

Figure 5-7, Figure 5-8 and Figure 5-9 show the comparison between different spacing between piles. Regarding to the comparison between different space between piles for many cases considered it is worth noting that only Figure 5-7 shows that for s = 3d yields more conservative results. In other words, as seen in Figure 5-7a, for example, it can be seen that a larger displacement is needed to mobilize the passive resistance for the s = 4d than the s = 3d case. For all other cases, the pile spacing does not play a role on this parametrization of the *n* factor.

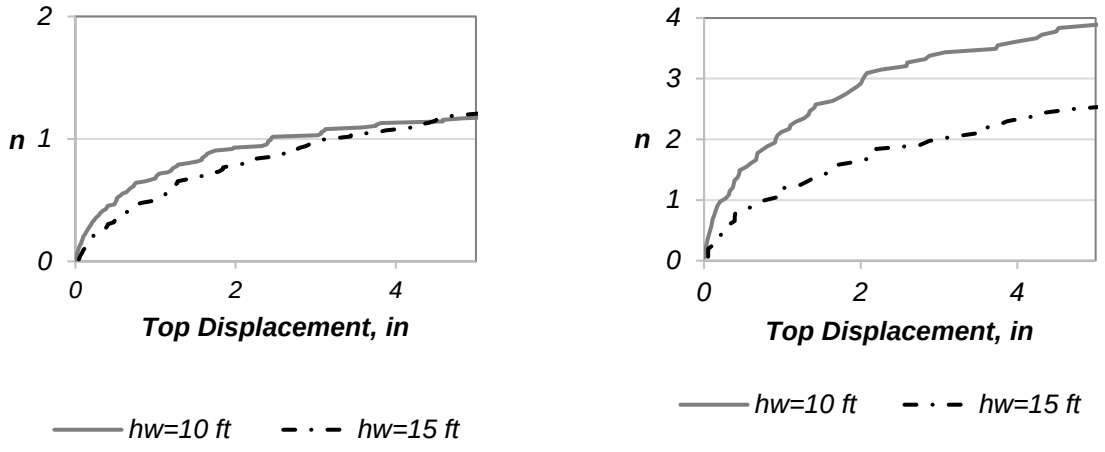

(a) (b)

Figure 5-4: Effect of wall height on arching capability factor for medium-dense sand case: (a) s = 4d, with no slope; (b) s = 4d, 3:2 slope, and bench width = 8d.

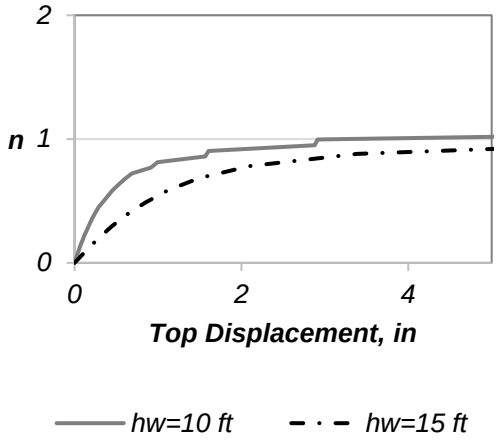

Figure 5-5: Effect of wall height on arching capability factor for medium-stiff clay soil case: s = 4d, no slope.

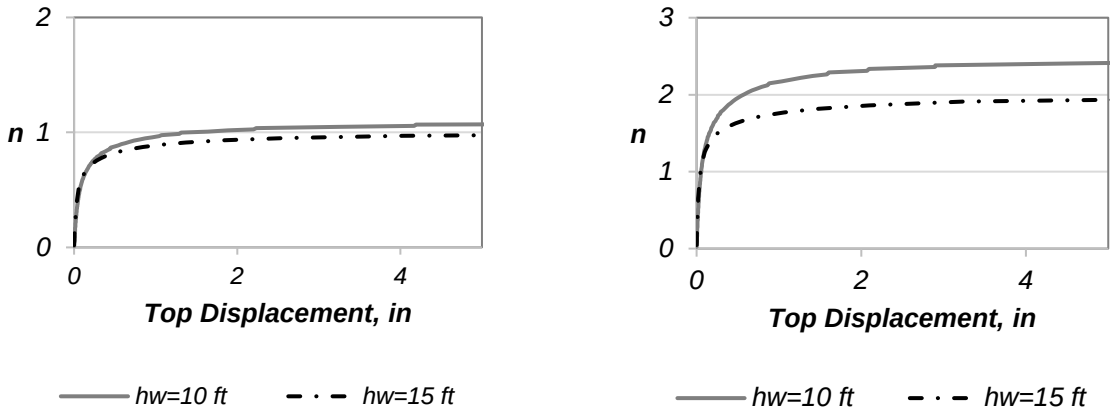

(a) (b)

Figure 5-6: Effect of wall height on arching capability factor for granular cohesive soil case: (a) s = 4d, no slope; (b) s = 4d, 2:1 slope, and 4d bench width.

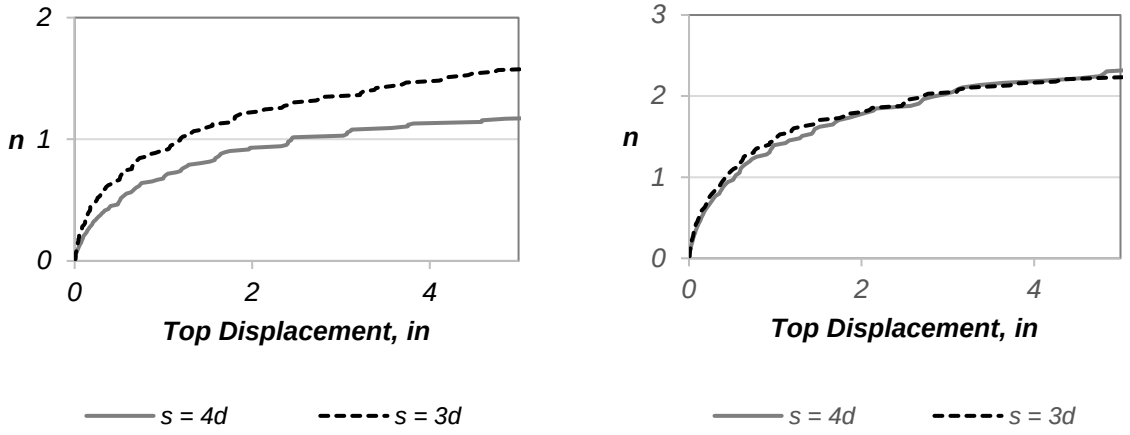

(a) (b)

Figure 5-7: Effect of pile spacing on arching capability factor for medium-dense sand case: (a) h_w=10 ft, no slope; (b) h_w=10 ft, 2:1 slope, and 4d bench width.

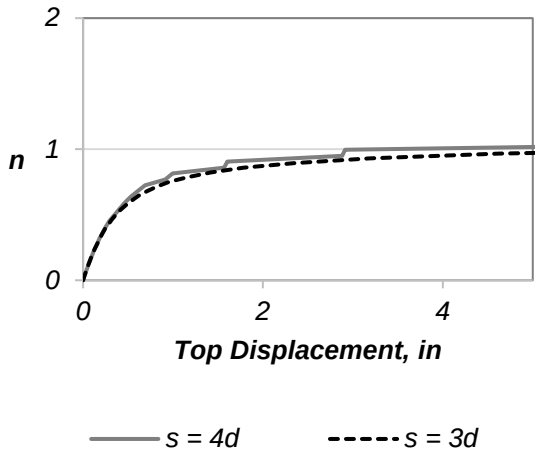

Figure 5-8: Effect of pile spacing on arching capability factor for medium-stiff clay case: h_w=10 ft, no slope.

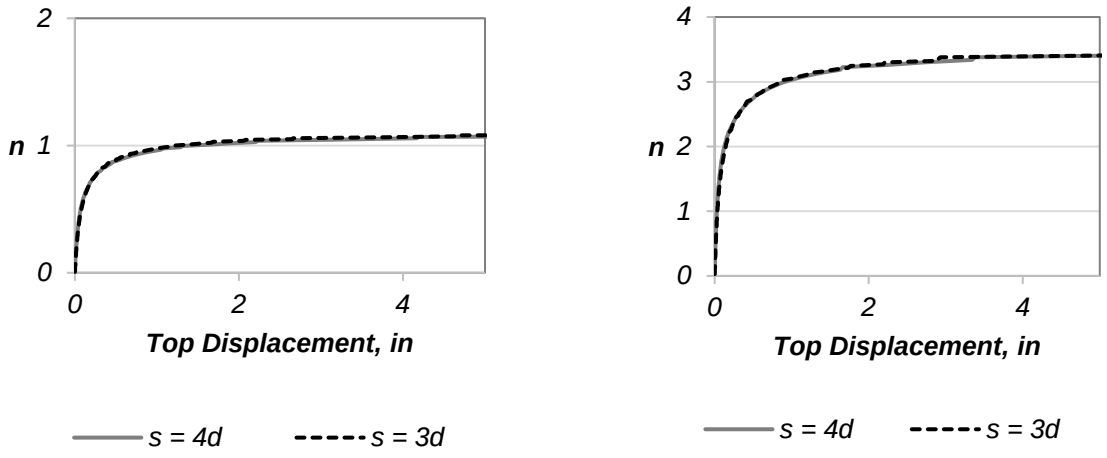

(a) (b)

Figure 5-9: Effect of pile spacing on arching capability factor for granular cohesive soil case: (a) h_w=10 ft, no slope; (b) h_w=10 ft, 3:2 slope, and 8d bench.

5.4 Effect of Analysis Dimensionality: 2-D versus 3-D analysis

Due to the computational complexity and time taken to perform and summarize responses from 3-D analysis, often designers resort to 2-D analyses. It is therefore important to understand, what the differences in the results are when 2-D nonlinear analyses are done instead of the 3-D analyses. The following figures serve to illustrate the difference in terms of results obtained when performing 2-D and 3-D results in terms of system capacity and the n factor. Note that all 2-D finite element models were modeled with a thickness of the adjusted pile width. Other modeling assumption are similar across models, except that the 2-D case is assumed in plane-strain condition.

Comparing the results from 2-D and 3-D analyses, by inspection of Figure 5-10, Figure 5-11, and Figure 5-12, one can say the results from 2-D analyses match the results from 3-D analysis until a pile head displacement of approximately 1 inch. For larger levels of displacement, the 2-D analyses yield higher system capacity than 3-D analyses, for all soil types. These results thus indicate that for pile head displacements greater than 1 inch, 2-D analyses tend to be

unconservative when compared to the 3-D analysis counterparts. Other results are shown in Appendix E.

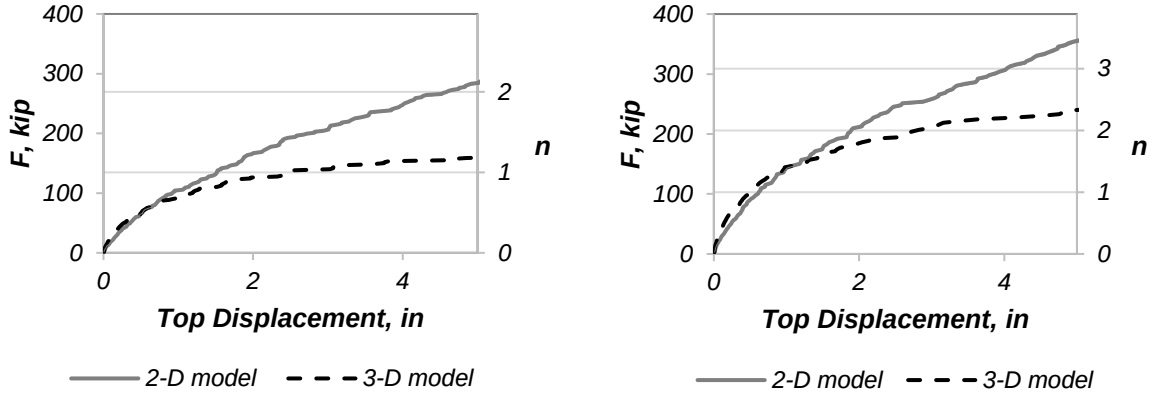

(a) (b)

Figure 5-10: Effect of analysis dimensionality on system capacity and arching capability factor for medium-dense sand: (a) h_w = 10 ft, s = 4d, no slope; (b) h_w = 10 ft, s = 4d, 2:1 slope, and 4d bench width.

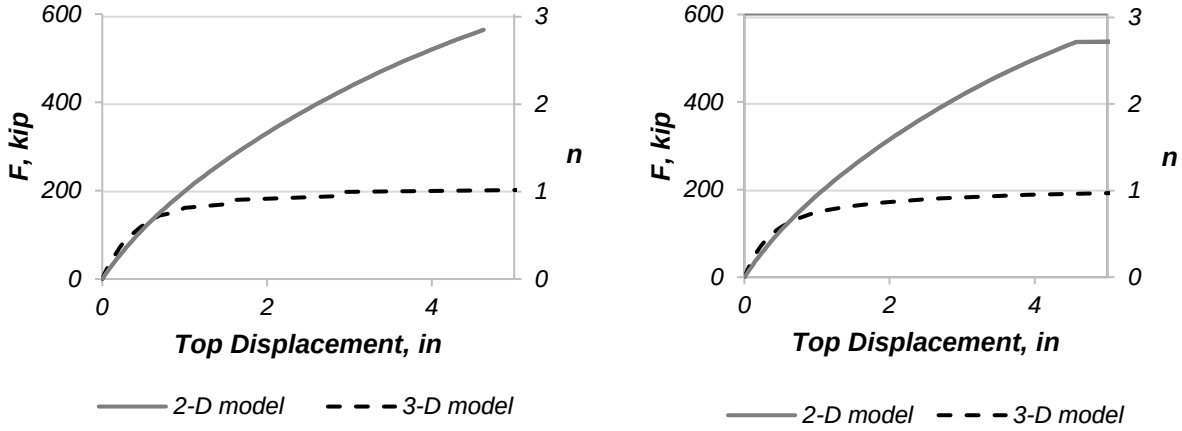

a) b)

Figure 5-11: Effect of analysis dimensionality on system capacity and arching capability factor for medium-stiff clay: (a) h_w = 10 ft, s = 4d, no slope; (b) h_w = 10 ft, s = 4d, 2:1 slope, and 4d bench width.

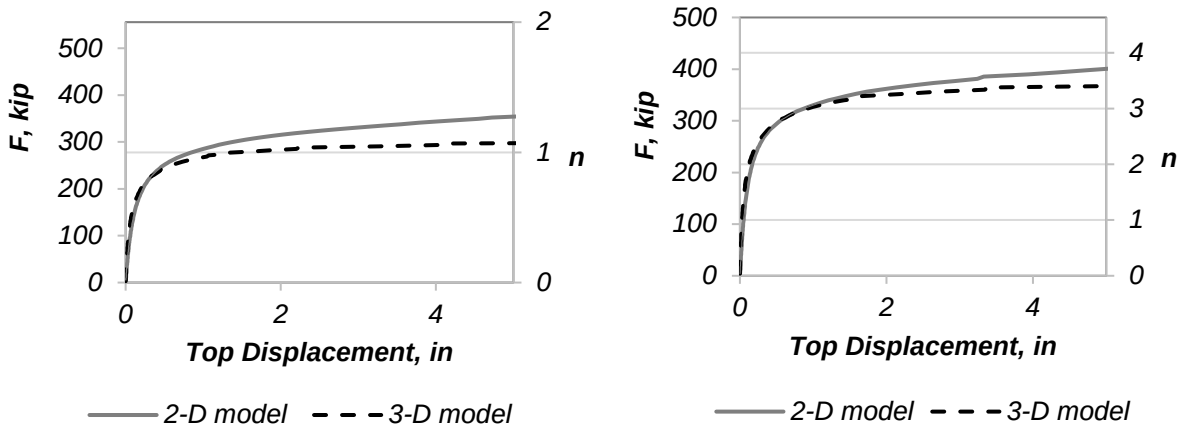

(a) (b)

Figure 5-12: Effect of analysis dimensionality on system capacity and arching capability factor for granular cohesive soil: (a) h_w = 10 ft, s = 4d, no slope; (b) h_w = 10 ft, s = 4d, 3:2 slope, 8d bench width.

6 PROPOSED REVISIONS TO THE PASSIVE RESISTANCE EQUATION

Based on the numerical results shown in this report and referring to the design procedure adopted in this study, which makes use of classical theories for passive pressure estimation, including logspiral and Rankine theories, a new adjustment factor is proposed herein to account for the bench width and a methodology for its computation is also proposed.

In general, the calculation of the passive pressures can be divided in two different components, the frictional component and the cohesion component. Thus, the passive pressure can be given by:

$$P_p = P_{p_cohesion} + P_{p_friction} \tag{6-1}$$

where

$$P_{p_cohesion} = 2c\sqrt{K_p}h \tag{6-2}$$

$$P_{p_friction} = \frac{1}{2}\gamma_{soil}K_p h^2 \tag{6-3}$$

Thus the total passive resistance for a soldier pile system can be given by (Caltrans 2011):

$$R_p = \frac{1}{2}\gamma_{soil}K_p h^2 \cdot f \cdot d + 2c\sqrt{K_p}h \cdot f \cdot d \tag{6-4}$$

As shown in the finite element analyses results, the bench width affected primarily the granular soils, therefore the cohesion component need not be affected, while the friction component should be affected by a new factor. Thus, the adjusted equation for the passive resistance is given by:

$$R_p = \frac{1}{2}\gamma_{soil}K_p h^2 \cdot f \cdot d \cdot \boldsymbol{f_B} + 2c\sqrt{K_p}h \cdot f \cdot d \tag{6-5}$$

where f_B is a bench width adjustment factor.

To obtain f_B, an auxiliary factor, f_b, needs to be derived first. The auxiliary factor can be obtained from experimental data, when available, or from results of high-fidelity nonlinear finite element models. Based on the analyses developed herein, in which the bench width was only varied for the 3:2 slope conditions, the auxiliary factor determines the increase in capacity with the increase of the bench width, which could be given by:

$$f_b = \frac{n_{sl32,i}}{n_{sl32,2d}}; i = \{2d, 4d, 8d\} \tag{6-6}$$

where $n_{sl32,i}$ is the n factor for the slope case considered (sl32) and i corresponds to the bench widths considered, which are 2d, 4d, and 8d. In this study, a minimum bench width of $2d$ was considered as reference. This assumption is conservative since the design approach followed herein used the Caquot & Kerisel (1948) graphs which considers no bench width at all.

Recalling that only the frictional component in the system capacity is affected by the bench width, the capacity obtained from analysis can be inferred by the following equation (6-7).

$$F \cdot f_b = F_{friction} \cdot f_B + F_{cohesion} \tag{6-7}$$

which can be simplified to:

$$f_B = \frac{\left(f_b - \frac{F_{cohesion}}{F} \right)}{\frac{F_{friction}}{F}} \tag{6-8}$$

For cohesionless soils, $F_{cohesion} = 0$, therefore $f_B = f_b$, and for frictionless soils f_B is not valid.

Figure 6-1 shows the values to be used for f_B obtained for medium-dense sand and granular cohesive soil cases and for a bench widths equal 2d, 4d, and 8d. In this graph, f_B is plotted versus

the design value D_0 and the pile diameter d. By fitting a power law to the points, the following general expression can be obtained:

$$f_B = 1.22\left(\frac{b_w}{D_0 \cdot d}\right)^{0.133} \tag{6-9}$$

Note that the main objective of this section was to illustrate how this factor could be estimated. However, based on the lack of experimental data on the topic, and due to the limited number of numerical analyses for different values of the slopes, soil characteristics, and bench widths available in the literature it is still premature to propose a general equation for f_B.

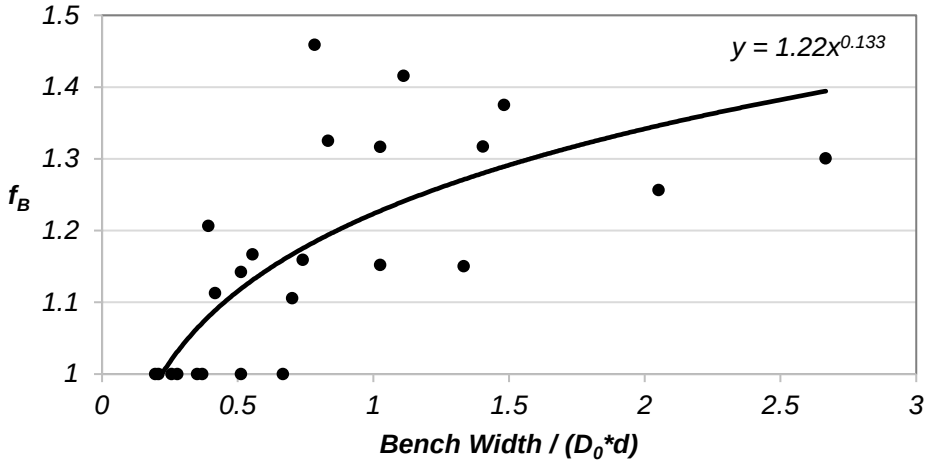

Figure 6-1: Plot to determine bench width effect factor, f_B.

7 SIMULATION OF A PROPOSED EXPERIMENTAL PROGRAM

7.1 OVERVIEW

This chapter corresponds to the last task proposed in this project. The main objective here is to perform an assessment of an analytical model able to predict the performance of eventual large scale tests.

7.2 PROPOSED EXPERIMENTAL PROGRAM

Figure 7-1 shows a plan view of the proposed experimental plan. In the design of the full-scale testing program to study the effect of bench width and soil slope, several factors (e.g., pile properties, testing method, and soil properties) must be controlled for consistency of the test results. Most of these factors can be controlled within the limits of the experimental planning and design.

The experimental program should include at least three different bench widths (0d, 4d, and 8d), two different wall heights, and two different soil types, and two different slopes. These could be developed by pre-installing piles in one site containing cohesionless soils and another one containing cohesive soils. This series of 6 to 8 full-scale tests for each soil type will utilize the existing native cohesive soils on site as shown in Nimityongsukul et al. (2012). These tests will include a series of single soldier pile tests driven to various depths, as well as two 3-pile system tests. All tests will use a central reaction mass. These test results are complemented by the eight full-scale driven pile tests conducted in the same material at the site in 2009. It is expected that the prototype for our model testing is a soldier pile and lagging retaining structure, with a foundation consisting of HP14x89 piles set in 24-inch diameter drilled holes with the annulus filled with concrete (typically a “four-sack mix”). Figure 7-1 and Figure 7-2 illustrate the main features of the proposed test set-up for combined single pile and system tests.

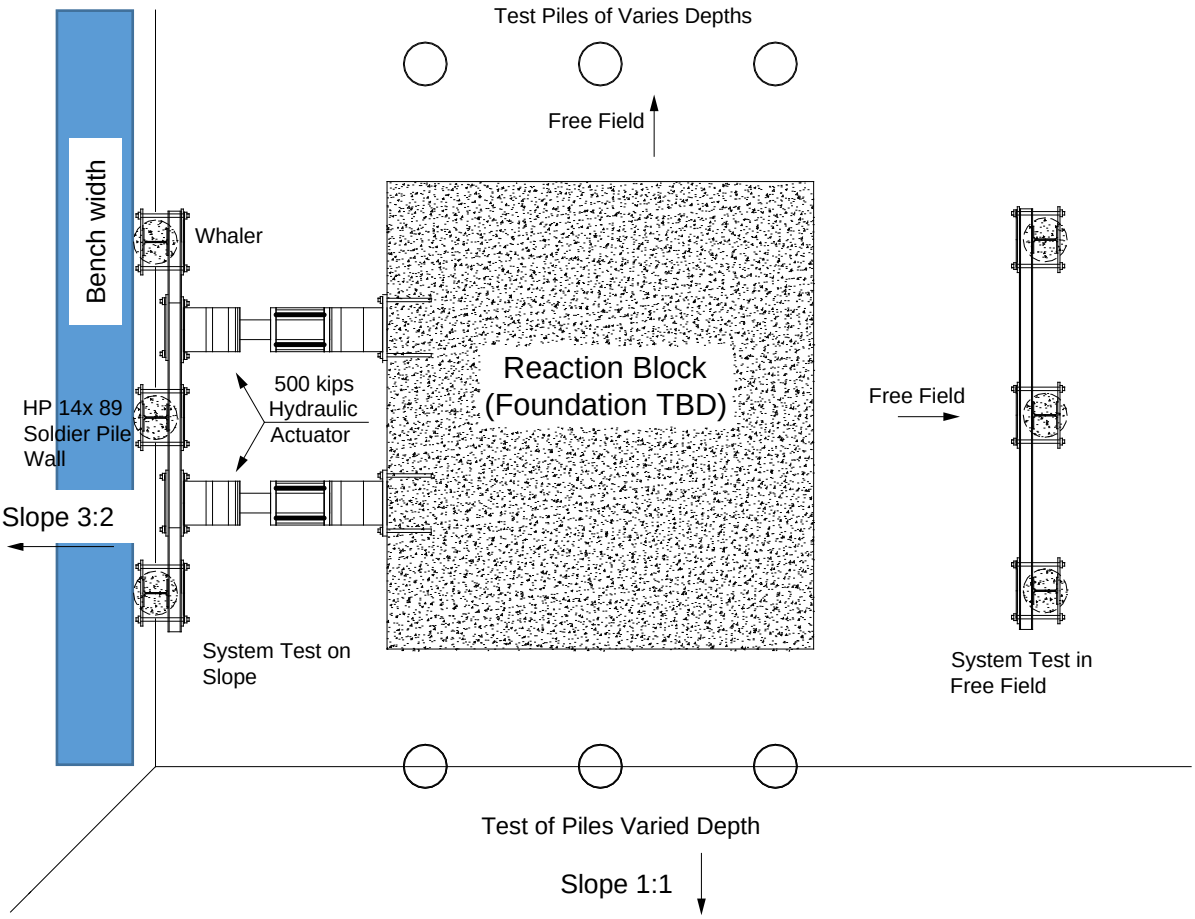

Figure 7-1: Plan view of the proposed test set-up for combined single pile and system tests.

7.3 SIMULATION OF AN EXAMPLE OF A PROPOSED EXPERIMENT

In the absence of the final selection of a possible testing site, three numerical models, one representing three possible type of soils were developed. The model of the experimental test is shown in Figure 7-3. The modeling assumptions described in Chapter 3 were employed in this analysis also. In these models, the height of the pile above the ground is 10 ft, and the spacing between piles is 4*d*. The slope modeled corresponds to the 3:2 condition shown in Figure 7-2.

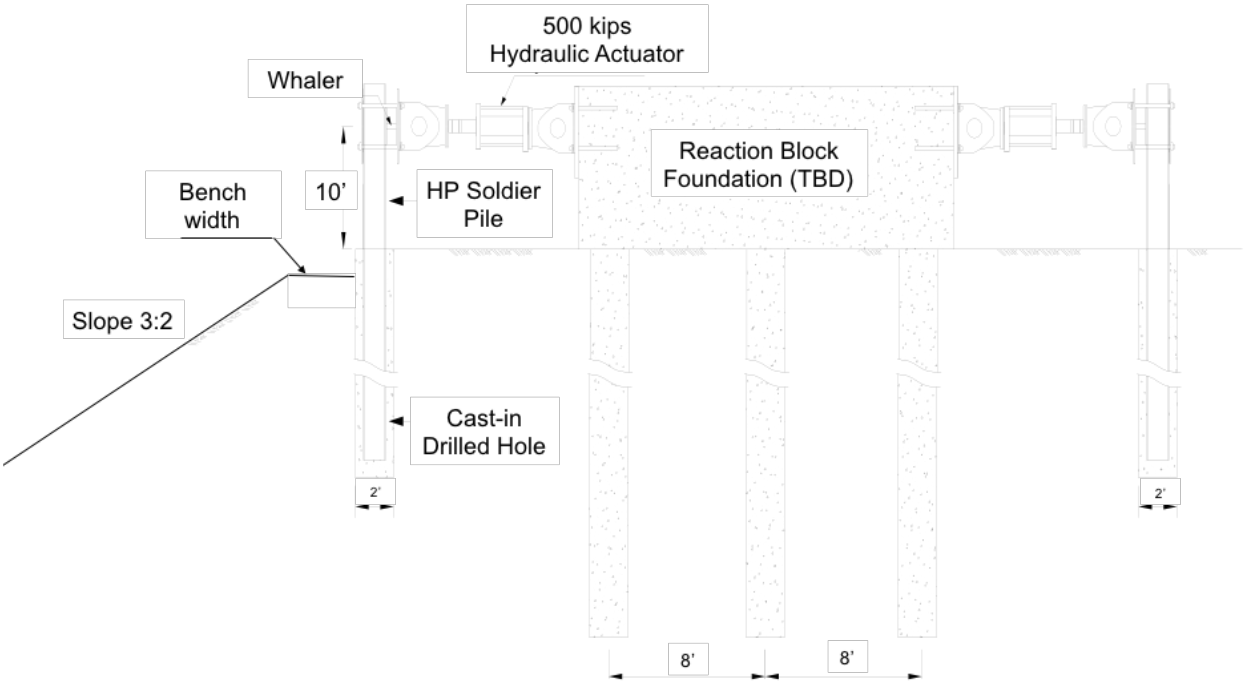

Figure 7-2: Profile view of proposed test set-up for combined single pile and system tests.

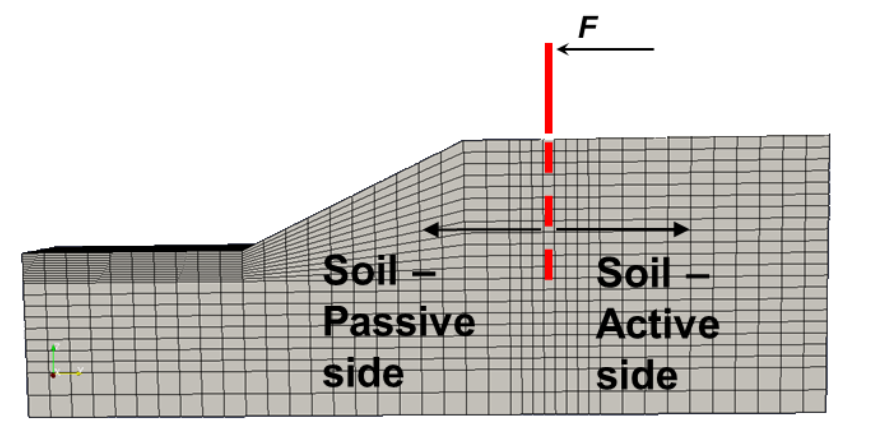

Figure 7-3: Schematic representation of the experimental simulation.

Figure 7-4 shows the system capacity of the experiment simulation. It can be seen that in the cohesionless soil (medium dense sand case), the effect of the bench width is noticeable as there is a drop of 30-40% from the 8d bench width case to the case with a bench width of 2d (see Figure 7-4a). This effect is not as noticeable in the granular cohesive soil case shown in Figure 7-4b. The total capacity in the simulation of the experiments is about 150 kips, which is well below the

capacity of the actuator of 550 kips. In addition, the stroke capacity of the actuator is +/- 24 inches, which is well within the limit of the expected deformation capacity of the system.

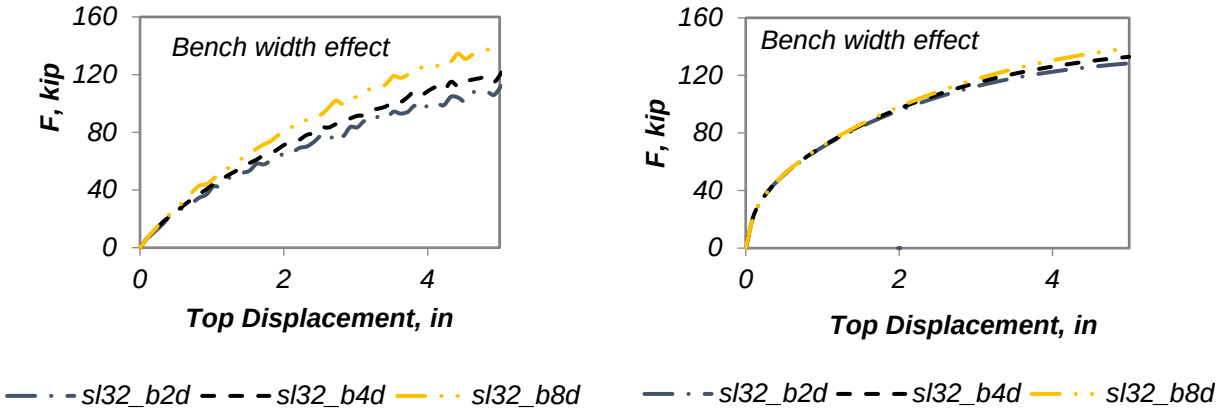

(a) Medium-dense sand case (b) Granular cohesive soil case

Figure 7-4: Capacity curves obtained from the experiment simulation, hw = 10 ft, s = 4d.

7.4 EFFECT OF LOAD DISTRIBUTION

It is worth noting that the testing program proposed includes the use of a concentrated load applied at the pile tip. However, as discussed in this report, the loading distribution affects the passive resistance that can be mobilized. Thus, the testing proposed would be used to validate numerical models that could be then used to assess the effect of different load distributions.

8 SUMMARY, CONCLUSIONS, AND SUGGESTIONS FOR FURTHER RESEARCH

In this work, an assessment of the current design procedures for soldier pile wall systems was performed to gain a fundamental understanding of the effects of several parameters on the arching capability factor used in Caltrans (2011). The 3-D effects for soil arching were extensively studied as well as the influence of a sloping ground in front of the soldier pile walls through nonlinear static analyses where incremental loads were applied to the soldier pile in order to develop the passive resistance of the system.

The nonlinear finite element modeling approach and modeling assumptions were validated using experimental results available from a testing program recently performed at Oregon State University. The correlation between experimental results and analytical results obtained using the OpenSees models developed was very good. The first modeling assumption that plays an important contribution to the response is the load distribution. Significantly different capacities were obtained when loads are applied on the pile head only, or when loads are distributed along the height of the wall. It was found that depending on how the load is applied the total passive resistance might not be mobilized. Thus, in the interest of the main objective of this study, the earth pressure distribution considered in design was applied to the soldier pile retaining system analyses. Nonetheless, it was shown that the modeling performed could capture the differences in the results and mobilized passive resistance. The second modeling assumption was related to the way the soil was connected with the pile in the numerical model. For clays, it was found that compression only gaps needed to be placed connecting the pile and the soil elements, leading to a model that could capture the effect of the pile detaching from the wall. While this is clearly not an active state of stress in clay soils, the passive resistance was modeled more realistically this way. This modeling option was not needed when modeling cohesionless soils.

Based on the parametric analyses performed, the analyses results indicated that:

(1) For granular soils:

a) The presence of slope in front of the pile affects the system capacity for granular soils. If a slope is present, in contrast to a flat dredge line, a decay in passive resistance is observed.

b) When results for slopes with different angles (3:2 and 2:1 slopes) are compared, small differences in capacity can be observed. However, the *n* factor values obtained were higher for steeper slopes. This difference in capacity cannot be well explained by the Caquot and Kerisel graphs, which do not account for pile spacing, and the arching capability factor does not seem to also capture those effects.

c) The bench width plays a significant role in the passive resistance of the system for granular soils. This effect is typically not considered explicitly in design when using classical soil theories, such as logspiral and Rankine. Gathering all results for the granular soils, an exponential relationship was proposed to take into account the bench width effects in the determination of the passive resistance of granular soils. This exponential relationship is a first step to address the issue, but results are very preliminary and these need to be confirmed with further numerical and experimental studies.

d) When slope is present in front of the soldier pile, the arching capability factor seems conservative being related with the aforementioned considerations in design.

(2) For medium-stiff clays:

a) The existence of slope in front of a soldier pile wall did not significantly affect the capacity of the system.

b) Results indicate that the arching capability factors defined in CALTRANS (2011) are adequate when the slope in front of the pile is not present. The *n* factor obtained tended to 1.0 for large displacements (nearing 5 inches).

In terms of geometry of the soldier pile system, some conclusions can also be drawn:

(1) In general, the values of the arching capability factor seemed to better estimate capacity when considering larger wall heights (15 foot versus 10 foot); (2) the *n* factor increases with increasing space between piles, indicating that the arching capability factor is more conservative for larger pile spacing.

(2) Comparing results from 3-D and 2-D analyses, the 2-D analyses capture adequately the initial stiffness of the system for all soil types, and results between the 3-D and 2-D analyses match well for pile head displacements up to approximately 1 inch. For larger pile head displacements, the capacity of the 2-D numerical models typically is considerably greater than that of the corresponding 3-D numerical model. Thus, after a pile head displacement greater than 1 inch, 2-D analyses might be unconservative for all types of soil. These results indicate that another factor may be warranted when designing soldier pile retaining systems, where 3-D effects are important.

(3) A preliminary experimental program was developed and results of the simulation of the experimental program indicate that the bench width effects and slope effects will be well captured with the experimental program proposed. In addition, the current capabilities at OSU allow for these tests to be executed successfully.

9 REFERENCES

AASHTO, 2012. LFRD Bridge Design Specifications. 6th ed. s.l.:Customary U.S. Units.

Adachi, T., Kimura, M. & Tada, S., 1989. Analysis on the preventive mechanism of landslide stabilizing piles. Numerical models in geomechanics, Numog III, Elsevier, pp. 691-698.

Arduino, P., Petek, K. A. & Mackenzie-Helnwein, P., 2007. Three-Dimensional beam-solid contact element formulation for analysis of pile interaction. Cordoba, Argentina, Asociacion Argentina de mecanica Computacional, pp. 2909-2916.

Atkinson, J. H. & Potts, D. M., 1977. Stability of a shallow circular tunnel in cohesionless soil. Geotechnique, 27(2), pp. 203-215.

Bishop, A. W., 1955. The use of the slip circle in the stability analysis of slopes. Geotechnique, Volume 5, pp. 7-17.

Bolton, M., 1979. A guide to Soil Mechanics. London: Macmillan Press, Ltd.

Bosscher, P. J. & Gray, D. H., 1986. Soil arching in sandy slopes. Journal of Geotechnical Engineering, ASCE, 112(6), pp. 626-644.

Boufia, A. & Bouguerra, A., 1996. Centrifuge testing on the behavior of a horizontally loaded flexible pile near to a slope. International Journal of Rock Mechanics and Mining Sciences and Geomechanics, 33(3).

Brown, D. A. & Shie, C. F., 1991. Some numerical experiments with a three-dimensional finite element model of a laterally loaded pile. Computers and Geotechnics, Volume 12, pp. 149-162.

CALTRANS, 2000. Trenching and Shoring Manual. s.l.:s.n., Sacramento, California

CALTRANS, 2011. Trenching and Shoring Manual. s.l.:s.n., Sacramento, California

Caquot, A. & Kerisel, J., 1948. Tables for the calculation of passive pressure, active pressure and bearing capacity of foundations. Paris: Gauthier-Villais, Imprimeur-Libraire.

Chae, K. S., Ugai, K. & Wakai, A., 2004. Lateral resistance of short single piles and pile groups located near slopes. International Journal of Geomechanics, 4(2), pp. 93-103.

Chelapati, C. V., 1964. Arching in soils due to the deflection of a rigid horizontal strip. Proceedings of the Symposium on Soil-Structure Interaction. Tucson, Arizona, pp. 356-377.

Chen, L. T., Poulos, H. G. & Hull, T., 1997. Model tests on pile groups subjected to lateral soil movement. Soils and Foundations, 37(1), pp. 1-12.

Cuthill, E. & McKee, J., 1969. Reducing the bandwidth of sparse symmetric matrices. ACM '69 Proceedings of the 24th national conference, pp. 157-172, New York, NY, USA.

Dafalias, Y. & Manzari, M. T., 2004. Simple plasticity sand model accounting for fabric change effects. Journal of Engineering Mechanics, Volume 130, pp. 622-634.

Drucker, D. C. & Prager, W., 1952. Soil mechanics and plastic analysis for limit design. Quarterly of Applied Mathematics, 10(2), pp. 157-165.

Duncan, J. M., Byrne, P., Wong, K. & Mabry, P., 1980. Strength, stress-strain and bulk modulus parameters for finite element analysis of stresses and movements in soil masses, University of California, Berkeley: Geotechnical Engineering Department of Civil Engineering.

Elgamal, A., Yang, Z. & Parra, E., 2002. Computational modeling of cyclic mobility and post-liquefaction site response. Soil Dynamics and Earthquake Engineering, 22(4), pp. 259-271.

Elgamal, A. & Yang, Z. P. E. R. A., 2003. Modeling of cyclic mobility in saturated cohesionless soils. International Journal of Plasticity, 19(6), pp. 883-905.

Finn, W. D. L., 1963. Boundary value problems of soil mechanics. Journal of the Soil mechanics and Foundations Division, ASCE, Volume 89, pp. 39-72.

Georgiadis & Georgiadis, 2010. Undrained lateral pile response in sloping ground. Journal of Geotechnical and Geoenvironmental Engineering, ASCE.

Ito, T. & Matsui, T., 1978. Methods to estimate lateral force acting on stabilizing piles. Soils and Foundations (Japan), 18(2), pp. 41-44.

Janbu, N., Bjerrum, L. & Kjaernsli, B., 1956. Soil-mechanics applied to some engineering problems. Norwegian Geotechnical Institute, Volume 16.

Kahyaoglu, M., Imancli, G., Ozturk, A. U. & Kayalar, A. S., 2009. Computational 3-D finite element analyses of model passive piles. Computational Materials Science, 46(1), pp. 193-202.

Kourkoulis, R., Gelagoti, F., Anastasopoulos, I. & Gazetas, G., 2011. Slope stabilizing piles and pile-groups: paramatric study and design insights. Journal of Geotechnical and Geoenvironmental Engineering, ASCE, 137(7), pp. 663-677.

Kourkoulis, R., Gelagoti, F., Anastasopoulos, I. & Gazetas, G., 2012. Hybrid method for analysis and design of slope stabilizing piles. Journal of Geotechnical and Geoenvironmental Engineering, ASCE, 138(1), pp. 1-14.

Kulhawy, F. H. & Mayne, P., 1990. Manual on estimating soil properties for foundation design, Cornell University, Ithaca, NY: EPRI.

Liang, R. Y., Al Bodour, W., Yamin, M. & Joorabchi, A. E., 2010a. Analysis method for drilled shaft-stabilized slopes using arching concept. Washington DC, Trans. Res. Rec. 10-3582, pp. 38-46.

Liang, R. Y. & Yamin, M., 2010b. Three-dimensional finite element study of arching behavior in slope/drilled shafts system. International Journal for numerical and analytical methods in Geomechanics, 34(11), pp. 1157-1168.

Liang, R. Y. & Zeng, S., 2002. Numerical dtudy of soil arching mechanism in drilled shafts for slope stabilization. Soils and Foundations, 42(2), pp. 83-92.

Liu, Q. & Zhang, J., 2010. Numerical analysis of soil arching effects of anti-slide pile. Taiyuan, China, s.n.

Low, B., Tang, S. K. & Choa, V., 1994. Arching in piled embankments. Journal of Geotechnical Engineering, 120(11), pp. 1917-1938.

Lu, J., Elgamal, A. & Yang, Z., 2011. OpenSeesPL: 3D lateral pile-ground interaction- User Manual. San Diego: Department of Structural Engineering, University of California.

Mazzoni, S., MckKenna, Scott, M. H. & Fenves, G. L., 2009. The OpenSees command language manual, Version 2.0. University of California, Berkeley: Pacific Earthquake Engineering Research Center.

Mezazigh, S. & Levacher, D., 1998. Laterally loaded piles in sand: slope effect on p-y reaction curves. Canadian Geotechnical Journal, 35(3), pp. 433-441.

NAVFAC, 1986. Design Manual DM-7.02 Foundations and Earth Structures, 82nd Edition, US Government Printing Office (GPO)

Nimityongsukul, N., Barker, P. & Ashford, S. A., 2012. Effects of soil slope on lateral capacity of piles in cohesive and cohesionless soils: The Kiewit Center for infrastructure and Transportation, Oregon State University.

Ogata, N. & Gose, S., 1995. Sloping rock layer foundation of bridge structure. Proc. Rock Foundation, R. Yoshinaka and R. Kikuchi, eds., Balkema, Rotterdam, The Amsterdam, 285–292.

Parra, E., 1996. Numerical modeling of liquefaction and lateral ground deformation including cyclic mobility and dilatation response in soil systems, Troy, NY: Department of Civil Engineering, Rensselaer Polytechnic Institute.

Petek, K. A., 2006. Development and application of mixed beam-solid models for analysis of soil-pile interaction problems, Ph.D. Dissertation, University of Washington.

Popovics, S., 1973. A numerical approach to the complete stress strain curve for concrete. Cement and Concrete research, 3(5), pp. 583-599.

Poulos, H. G., 1976. Behavior of laterally loaded piles near a cut or slope. Australian Geomechanics Journal, 6(1), pp. 6-12.

Scott, M. H. & Fenves, G. L., 2010. A Krylov subspace accelerated Newton algorithm: application to dynamic progressive collapse simulation of frames. Journal of Structural Engineering, 136(5).

Spencer, E., 1967. A method of analysis of the stability of embankments assuming parallel inter-slice forces. Geotechnique, Volume 17, pp. 11-26.

Terashi, M., Kitazume, M. M. A. & Yamamoto, Y., 1991. Lateral resistance of a long pile in or near the slope. Rotterdam, Netherlands, s.n., pp. 245-252.

Terzaghi, K., 1936. Stress distribution in dry and saturated sand above a yielding trap door. Intl Conf On Soil Mechanics Proc, Vol 1, pp. 307-311.

Terzaghi, K., 1943. Theoretical Soil Mechanics. New York: John Wiley and Sons, Inc.

Wair, B. R., DeJong, J. T. & Shantz, T., 2012. Guidelines for estimation of shear wave velocity profiles, Report 2012/08: Pacific Earthquake Engineering Research Center.

Wang, S. T. & Reese, L. C., 1986. Study of design method for vertical drilled shaft retaining walls, University of Texas: Department of Transportation Federal Highway Administration.

Wang, W. L. & Liang, J., 1979. Unsheathed excavation in soils. Journal of the Geotechnical Division, ASCE, 105(GT9), pp. 1117-1121.

Wang, W. L. & Salmassian, K., 1978. Unsheathed excavation in cohesive soils. Journal of the Geotechnical Division, ASCE, 104(GT4), pp. 493-496.

Wang, W. L. & Yen, B. C., 1974. Soil arching in slopes. Journal of Geotechnical Division, ASCE, 100(GT1), pp. 61-78.

Wriggers, P., 2006. Computational Contact Mechanics. Springer-Verlag Berlin Heidelberg, ISBN: 978-3-540-32608-3 (Originally published by John Wiley & Sons Ltd., 2002.)

Yang, Z., 2000. Numerical modeling of earthquake site response including dilatation and liquefaction, Ph.D. Dissertation, Department of Civil Engineering and Engineering Mechanics, Columbia University, New York, NY.

Yang, Z., Elagamal, A. & Parra, E., 2003. Computational model for cyclic mobility ans associated shear deformation. Geotechnical and Geoenvironmental Engineering, ASCE, 129(12), pp. 1119-1127.

Yang, Z. & Elgamal, A., 2002. Influence of permeability on liquefaction-induced shear deformation. Journal of Engineering Mechanics, ASCE, 128(7), pp. 720-729.

Yue, G., Feng, F. & Hui, J., 2011. Numerical simulation of soil arching effect in deep foundation pit with different influencing factors. International Conference on Electrical and Control Engineering (ICECE), Yichang, China.

TABLE OF CONTENTS

TABLE OF FIGURES **2**

A. NONLINEAR STATIC PUSHOVER ANALYSIS RESULTS CONSIDERING A CONCENTRATED LOAD AT THE PILE HEAD **8**

A.1 Medium-dense sand **8**

A.1.1 Capacity Curves 8

A.1.2 Deformed Shapes and Stresses 10

A.2 Medium-stiff clay **13**

A.2.1 Capacity Curves 13

A.2.2 Deformed Shape and Stresses 15

A.3 Granular cohesive soil **18**

A.3.1 Capacity Curves 18

A.3.2 Deformed Shape and Stresses 20

B. DEFORMED SHAPES AND STRESSES FOR CASES WITH SLOPE IN FRONT OF THE PILE **23**

C. RESULTS FOR MEDIUM-STIFF CLAYS, WITHOUT INTERFACE GAP ELEMENTS **32**

C.1.1 Capacity Curves 32

C.1.2 Deformed Shape and Stresses 34

C.1.3 Arching Capability Factor Assessment 38

D. NONLINEAR STATIC PUSHOVER ANALYSIS RESULTS WITH TRIANGULAR PUSHOVER LOAD **39**

D.1 Medium-dense sand **39**

D.1.1 Capacity Curves 39

D.2 Medium-stiff clay **42**

D.2.1 Capacity Curves 42

D.3 Granular cohesive soil **45**

D.3.1 Capacity Curves 45

E. PUSHOVER RESULTS FOR 2-D ANALYSES WITH TRIANGULAR LOAD DISTRIBUTION **49**

E.1 Medium-dense sand **49**

E.1.1 Capacity Curves 49

E.1.2 Deformed Shape and Stresses 51

E.1.3 Arching Capability Factor Assessment 54

E.2 Medium-stiff clay **55**

E.2.1 Capacity Curves 55

E.2.2 Deformed Shape and Stresses 56

E.2.3 Arching Capability Factor Assessment 59

E.3 Granular cohesive soil **60**

E.3.1 Capacity Curves 60

E.3.2 Deformed Shape and Stresses 62

E.3.3 Arching Capability Factor Assessment 65

TABLE OF FIGURES

Figure A-1: Capacity curves for medium-dense sand, h_w = 10 feet and s = 4d: (a) Effect of slope angle; (b) Effect of bench width 8

Figure A-2: Capacity curves for medium-dense sand, h_w = 10 feet and s = 3d: (a) Effect of slope angle; (b) Effect of bench width 8

Figure A-3: Capacity curves for medium-dense sand, h_w = 15 feet and s = 4d: (a) Effect of slope angle; (b) Effect of bench width 9

Figure A-4: Capacity curves for medium-dense sand, h_w = 15 feet and s = 3d: (a) Effect of slope angle; (b) Effect of bench width 9

Figure A-5: Applied pushover load: concentrated load at the pile head – Plan view of σ_{YY} for a pile-head displacement = 2 in. Case: medium-dense sand, h_w = 10 feet, s = 4d, no slope 10

Figure A-6: Applied pushover load: concentrated load at the pile head – Elevation view of σ_{YZ} for a pile-head displacement = 2 in Case: medium-dense sand, h_w = 10 feet, s = 4d, no slope.... 11

Figure A-7: Applied pushover load: concentrated load at the pile head – Elevation view of σ_I for a pile-head displacement = 2 in,. Case: medium-dense sand, h_w = 10 feet, s = 4d, no slope 12

Figure A-8: Capacity curves for medium-stiff clay for h_w = 10 feet and s = 4d 13

Figure A-9: Capacity curves for medium-stiff clay for h_w = 10 feet and s = 3d 13

Figure A-10: Capacity curves for medium-stiff clay for h_w = 15 feet and s = 4d 14

Figure A-11: Capacity curves for medium-stiff clay for h_w = 15 feet and s = 3d 14

Figure A-12: Applied pushover load: concentrated load at the pile head – Plan view of σ_{YY} for a pile-head displacement = 2 in. Case: medium-stiff clay, h_w = 10 feet, s = 4d, no slope 15

Figure A-13: Applied pushover load: concentrated load at the pile head – Elevation view of σ_{YZ} for a pile-head displacement = 2 in. Case: medium-stiff clay, h_w = 10 feet, s = 4d, no slope..... 16

Figure A-14: Applied pushover load: concentrated load at the pile head – Elevation view of σ_I for a pile-head displacement = 2 in. Case: medium-stiff clay, h_w = 10 feet, s = 4d, no slope..... 17

Figure A-15: Capacity curves for granular cohesive soil for h_w = 10 feet and s = 4d: (a) Effect of slope angle; (b) Effect of bench width..... 18

Figure A-16: Capacity curves for granular cohesive soil for h_w = 10 feet and s = 3d: (a) Effect of slope angle; (b) Effect of bench width 18

Figure A-17: Capacity curves for granular cohesive soil for h_w = 15 feet and s = 4d: (a) Effect of slope angle; (b) Effect of bench width 19

Figure A-18: Capacity curves for granular cohesive soil for h_w = 15 feet and s = 3d: a) Effect of slope angle; b) Effect of bench width 19

Figure A-19: Applied pushover load: concentrated load at the pile head – Plan view of σ_{YY} for a pile-head displacement = 2 in, for granular cohesive soil, h_w = 10 feet, s = 4d, no slope 20

Figure A-20: Applied pushover load: concentrated load at the pile head – Elevation view of σ_{YZ} and deformed shape for a pile-head displacement = 2 in, for granular cohesive soil, h_w = 10 feet, s = 4d, no slope 21

Figure A-21: Applied pushover load: concentrated load at the pile head – Elevation view of σ_I and deformed shape for a pile-head displacement = 2 in, for granular cohesive soil, h_w = 10 feet, s = 4d, no slope 22

Figure B-1: 3-D model – Plan view of σ_{YY} at depth = -2d, for a pile-head displacement = 2 in, for medium-dense sand, h_w = 10 feet and s = 4d with 3:2 slope and 4d bench 23

Figure B-2: 3-D model – Elevation view of σ_I and deformed shape for a pile-head displacement = 2 in, for medium-dense sand, h_w = 10 feet and s = 4d with 3:2 slope and 4d bench 24

Figure B-3: 3-D model – Elevation view of σ_{YY} and deformed shape for a pile-head displacement = 2 in, for medium-dense sand, h_w = 10 feet and s = 4d with 3:2 slope and 4d bench 25

Figure B-4: 3-D model – Plan view of σ_{YY} at depth = -2d for a pile-head displacement = 2 in. Case: medium-stiff clay, h_w = 10 feet and s = 4d with 3:2 slope and 4d bench 26

Figure B-5: 3-D model – Elevation view of σ_{YZ} and deformed shape for a pile-head displacement = 2 in. Case: medium-stiff clay, h_w = 10 feet and s = 4d with 3:2 slope and 4d bench 27

Figure B-6: 3-D model – Elevation view of σ_I and deformed shape for a pile-head displacement = 2 in. Case: medium-stiff clay, h_w = 10 feet and s = 4d with 3:2 slope and 4d bench 28

Figure B-7: 3-D model – Plan view of σ_{YY} at depth = -2d for a pile-head displacement = 2 in, for granular cohesive soil, h_w = 10 feet and s = 4d with 3:2 slope and 4d bench 29

Figure B-8: 3-D model – Elevation view of σ_{YZ} and deformed shape for a pile-head displacement = 2 in, for granular cohesive soil, h_w = 10 feet and s = 4d with 3:2 slope and 4d bench 30

Figure B-9: 3-D model – Elevation view of σ_I and deformed shape for a pile-head displacement = 2 in, for granular cohesive soil, h_w = 10 feet and s = 4d with 3:2 slope and 4d bench..... 31

Figure C-1: Capacity curves for medium-stiff clay for 3-D analyses not considering detachment: h_w = 10 feet and s = 4d..... 32

Figure C-2: Capacity curves for medium-stiff clay for 3-D analyses not considering detachment: h_w = 10 feet and s = 3d..... 32

Figure C-3: Capacity curves for medium-stiff clay for 3-D analyses not considering detachment: h_w = 15 feet and s = 4d..... 33

Figure C-4: Capacity curves for medium-stiff clay for 3-D analyses not considering detachment: h_w = 15 feet and s = 3d..... 33

Figure C-5: 3-D model not considering detachment – 3-D view of σ_{YY} and deformed shape for a pile-head displacement = 2 in. Case: medium-stiff clay: h_w = 10 feet, s = 4d, no slope 34

Figure C-6: 3-D model not considering detachment – Plan view of σ_{YY} for a pile-head displacement = 2 in. Case: medium-stiff clay, h_w = 10 feet, s = 4d, no slope 35

Figure C-7: 3-D model not considering detachment – Elevation view of σ_I and deformed shape for a pile-head displacement = 2 in. Case: medium-stiff clay, h_w = 10 feet, s = 4d, no slope..... 36

Figure C-8: 3-D model not considering detachment – Elevation view of σ_{YZ} and deformed shape for a pile-head displacement = 2 in. Case: medium-stiff clay, h_w = 10 feet, s = 4d, no slope..... 37

Figure C-9: Arching capability factor assessment for medium-stiff clay not considering detachment: (a) h_w = 10 feet and s = 4d; (b) h_w = 10 feet and s = 3d; (c) h_w = 15 feet and s = 4d; (d) h_w = 15 feet and s = 3d 38

Figure D-1: Effect of embedment depth on capacity curves for medium-dense sand in 3-D analyses: h_w = 10 feet and s = 4d 39

Figure D-2: Effect of slope angle on capacity curves for medium-dense sand in 3-D analyses: h_w = 10 feet and s = 4d..... 39

Figure D-3: Effect of bench width on capacity curves for medium-dense sand in 3-D analyses: h_w = 10 feet and s = 4d..... 40

Figure D-4: Capacity curves for medium-dense sand in 3-D analyses for h_w = 10 feet and s = 3d: (a) slope effect; (b) effect of bench width..... 40

Figure D-5: Capacity curves for medium-dense sand in 3-D analyses for h_w = 15 feet and s = 4d:(a) slope effect; (b) effect of bench width..... 41

Figure D-6: Capacity curves for medium-dense sand in 3-D analyses for h_w = 15 feet and s = 3d: (a) slope effect; (b) effect of bench width 41

Figure D-7: Effect of bench width for medium-stiff clay for 3-D analyses: h_w = 10 feet and s = 4d 42

Figure D-8: Effect of bench width for medium-stiff clay for 3-D analyses: h_w = 10 feet and s = 3d 43

Figure D-9: Effect of bench width for medium-stiff clay for 3-D analyses: h_w = 15 feet and s = 4d 44

Figure D-10: Effect of bench width for medium-stiff clay for 3-D analyses: h_w = 15 feet and s = 3d 45

Figure D-11: Effect of embedment depth on capacity curves for granular cohesive in 3-D analyses: h_w = 10 feet and s = 4d 46

Figure D-12: Effect of slope angle on capacity curves for granular cohesive in 3-D analyses: h_w = 10 feet and s = 4d 46

Figure D-13: Effect of bench width on capacity curves for granular cohesive in 3-D analyses: h_w = 10 feet and s = 4d 47

Figure D-14: Capacity curves for granular cohesive soil in 3-D analyses for h_w = 10 feet and s = 3d: (a) slope effect; (b) effect of bench width 47

Figure D-15: Capacity curves for granular cohesive soil in 3-D analyses for h_w = 15 feet and s = 4d: (a) slope effect; (b) effect of bench width 48

Figure D-16: Capacity curves for granular cohesive soil in 3-D analyses for h_w = 15 feet and s = 3d: (a) slope effect; (b) effect of bench width 48

Figure E-1: Capacity curves for medium-dense sand in 2-D analyses: (a) h_w = 10 feet and s = 4d; (b) h_w = 10 feet and s = 3d; (c) h_w = 15 feet and s = 3d; (d) h_w = 15 feet and s = 4d 49

Figure E-2: Effect of slope angle on capacity curves for medium-dense sand in 2-D analyses: h_w = 10 feet and s = 4d 50

Figure E-3: Effect of bench width on capacity curves for medium-dense sand in 2-D analyses: h_w = 10 feet and s = 4d 50

Figure E-4: Effect of embedment depth on capacity curves for medium-dense sand in 2-D analyses: h_w = 10 feet and s = 4d 51

Figure E-5: 2-D model - stresses σ_{YY} and deformed shape for a pile-head displacement = 2 in, for medium-dense sand, h_w = 10 feet, s = 4d, no slope 51

Figure E-6: 2-D model - σ_I at a pile-head displacement = 2 in, for medium-dense sand, h_w = 10 feet, s = 4d, no slope 52

Figure E-7: 2-D model - σ_{YZ} at a pile-head displacement = 2 in, for medium-dense sand, h_w = 10 feet and s = 4d with 3:2 slope and 4d bench 53

Figure E-8: Arching capability factor assessment for medium dense sand using 2-D analysis: (a) h_w = 10 feet and s = 4d; (b) h_w = 10 feet and s = 3d; (c) h_w = 15 feet and s = 3d; (d) h_w = 15 feet and s = 4d 54

Figure E-9: Capacity curves for medium-stiff clay for 2-D analyses: (a) h_w = 10 feet and s = 4d; (b) h_w = 10 feet and s = 3d; (c) h_w = 15 feet and s = 3d; (d) h_w = 15 feet and s = 4d 55

Figure E-10: 2-D model - σ_{XX} direction and deformed shape for a pile-head displacement = 2 in. Case: medium-stiff clay, h_w = 10 feet, s = 4d, no slope 56

Figure E-11: 2-D model - σ_I for a pile-head displacement = 2 in. Case: medium-stiff clay, h_w = 10 feet and s = 4d with 3:2 slope and 4d bench 57

Figure E-12: 2-D model - σ_{XY} and deformed shape for a pile-head displacement = 2 in. Case: medium-stiff clay, h_w = 10 feet and s = 4d with 3:2 slope and 4d bench 58

Figure E-13: Arching capability factor assessment for medium-stiff clay using 2-D analysis: (a) h_w = 10 feet and s = 4d; (b) h_w = 10 feet and s = 3d; (c) h_w = 15 feet and s = 3d; (d) h_w = 15 feet and s = 4d 59

Figure E-14: Capacity curves for granular cohesive soil for 2-D analyses: (a) h_w = 10 feet and s = 4d; (b) h_w = 10 feet and s = 3d; (c) h_w = 15 feet and s = 3d; (d) h_w = 15 feet and s = 4d 60

Figure E-15: Effect of slope angle on capacity curves for granular cohesive in 2-D analyses: h_w = 10 feet and s = 4d 61

Figure E-16: Effect of bench width on capacity curves for granular cohesive in 2-D analyses: h_w = 10 feet and s = 4d 61

Figure E-17: 2-D model - σ_{YY} at a pile-head displacement = 2 in, for granular cohesive soil, h_w = 10 feet, s = 4d, no slope 62

Figure E-18: σ_I at a pile-head displacement = 2 in, for granular cohesive soil, h_w = 10 feet, s = 4d, no slope 63

Figure E-19: σ_{YZ} at a pile-head displacement = 2 in, for granular cohesive soil, h_w = 10 feet and s = 4d with 3:2 slope and 4d bench 64

Figure E-20: Arching capability factor assessment for granular cohesive soil using 2-D analysis: (a) h_w = 10 feet and s = 4d; (b) h_w = 10 feet and s = 3d; (c) h_w = 15 feet and s = 4d; (d) h_w = 15 feet and s = 3d 65

A. NONLINEAR STATIC PUSHOVER ANALYSIS RESULTS CONSIDERING A CONCENTRATED LOAD AT THE PILE HEAD

A.1 Medium-dense sand

A.1.1 Capacity Curves

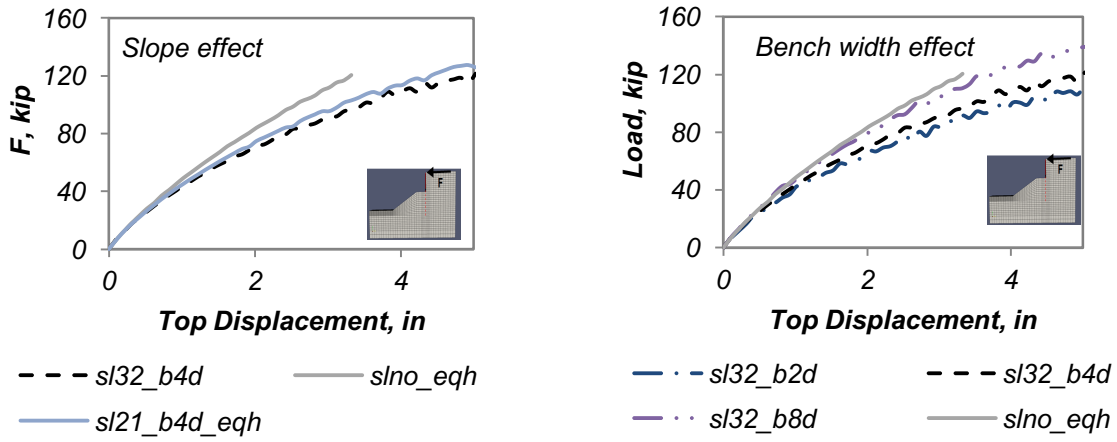

(a) (b)

Figure A-1: Capacity curves for medium-dense sand, h_w = 10 feet and s = 4d: (a) Effect of slope angle; (b) Effect of bench width

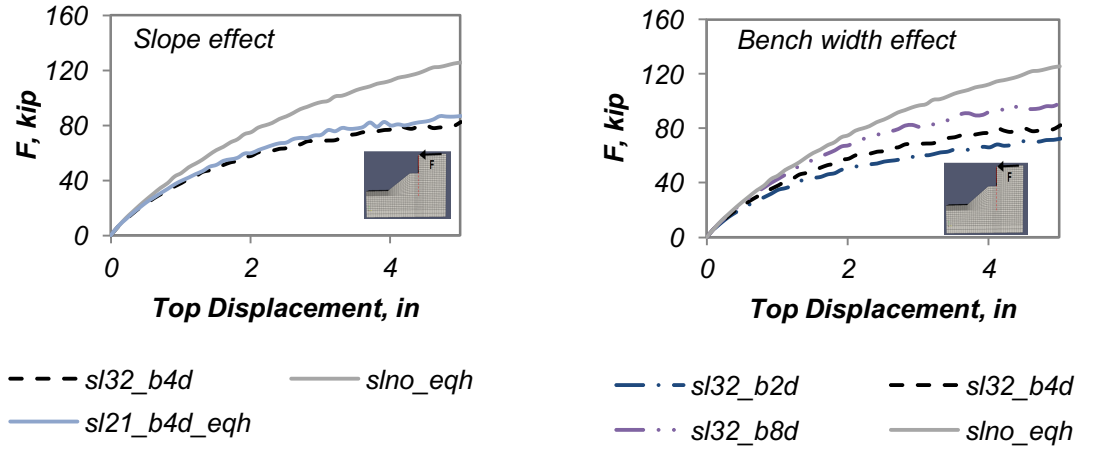

(a) (b)

Figure A-2: Capacity curves for medium-dense sand, h_w = 10 feet and s = 3d: (a) Effect of slope angle; (b) Effect of bench width

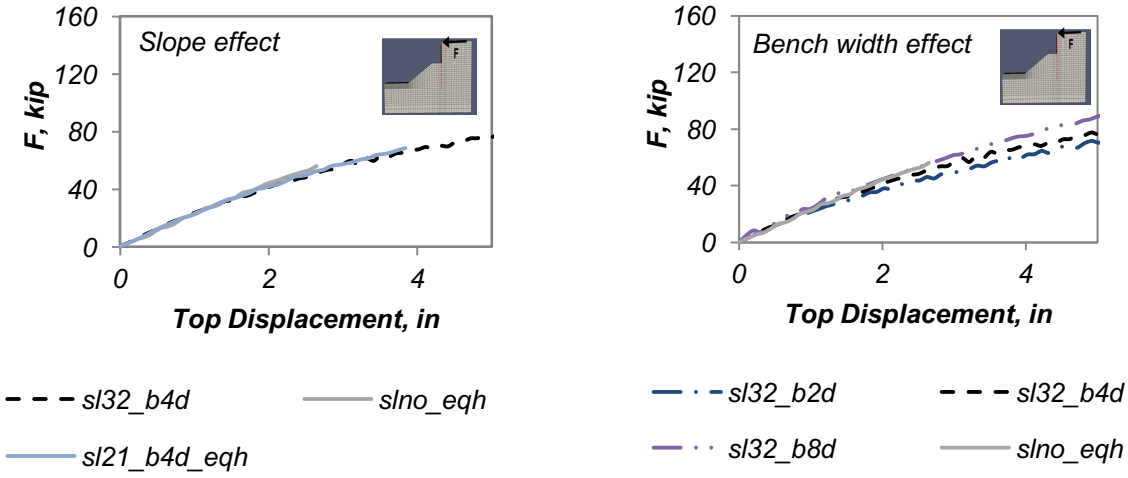

(a) (b)

Figure A-3: Capacity curves for medium-dense sand, h_w = 15 feet and s = 4d: (a) Effect of slope angle; (b) Effect of bench width

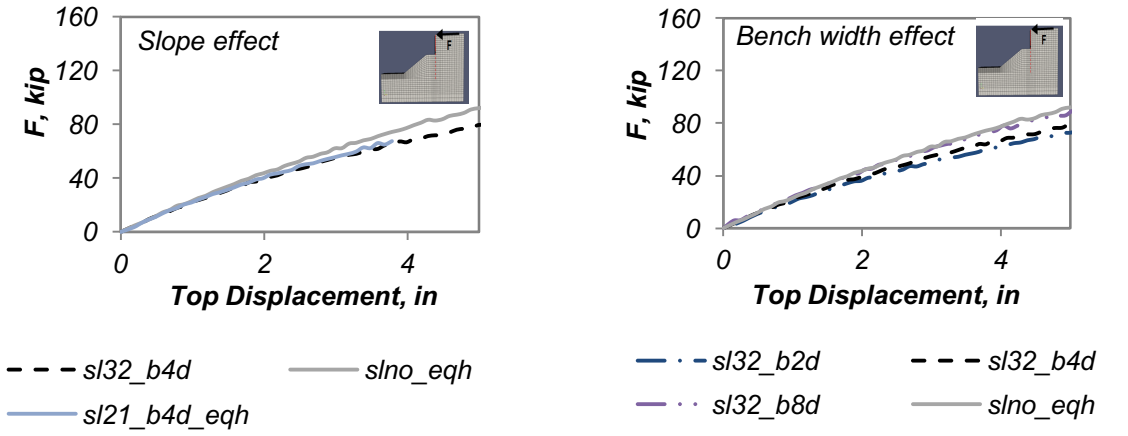

(a) (b)

Figure A-4: Capacity curves for medium-dense sand, h_w = 15 feet and s = 3d: (a) Effect of slope angle; (b) Effect of bench width

A.1.2 Deformed Shapes and Stresses

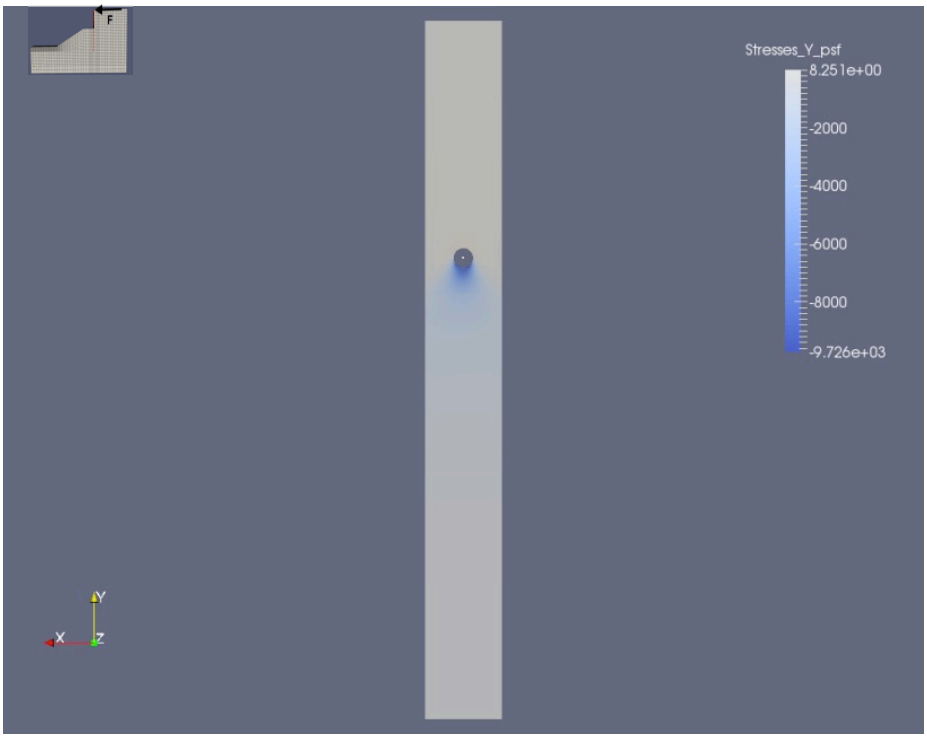

Figure A-5: Applied pushover load: concentrated load at the pile head – Plan view of σ_{YY} for a pile-head displacement = 2 in. Case: medium-dense sand, h_w = 10 feet, s = 4d, no slope

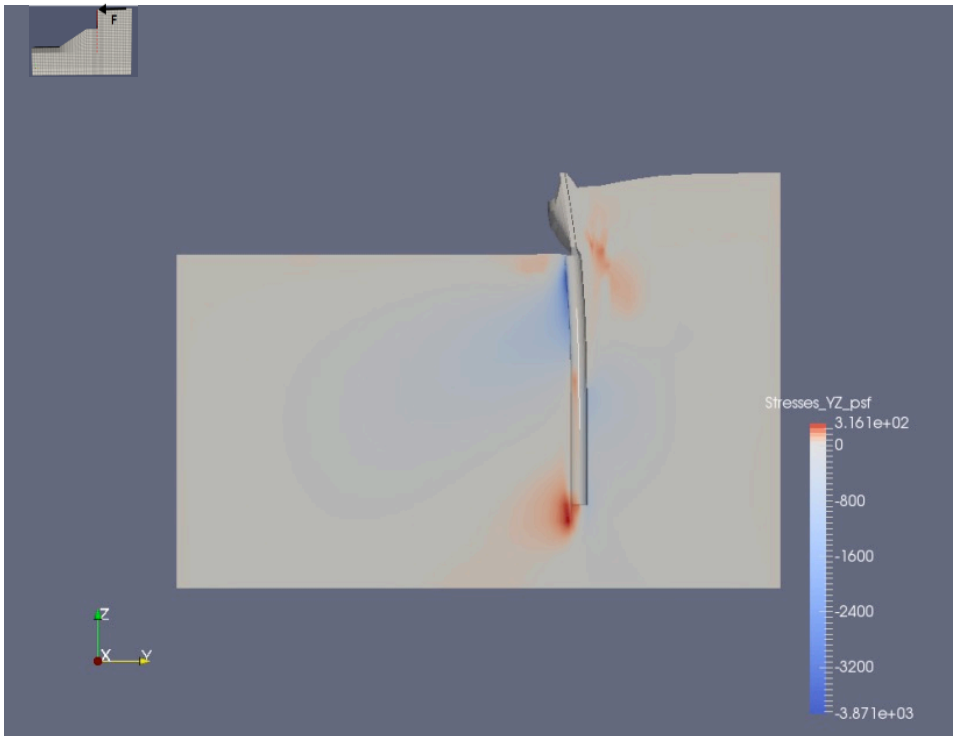

Figure A-6: Applied pushover load: concentrated load at the pile head – Elevation view of σ_{YZ} for a pile-head displacement = 2 in Case: medium-dense sand, h_w = 10 feet, s = 4d, no slope

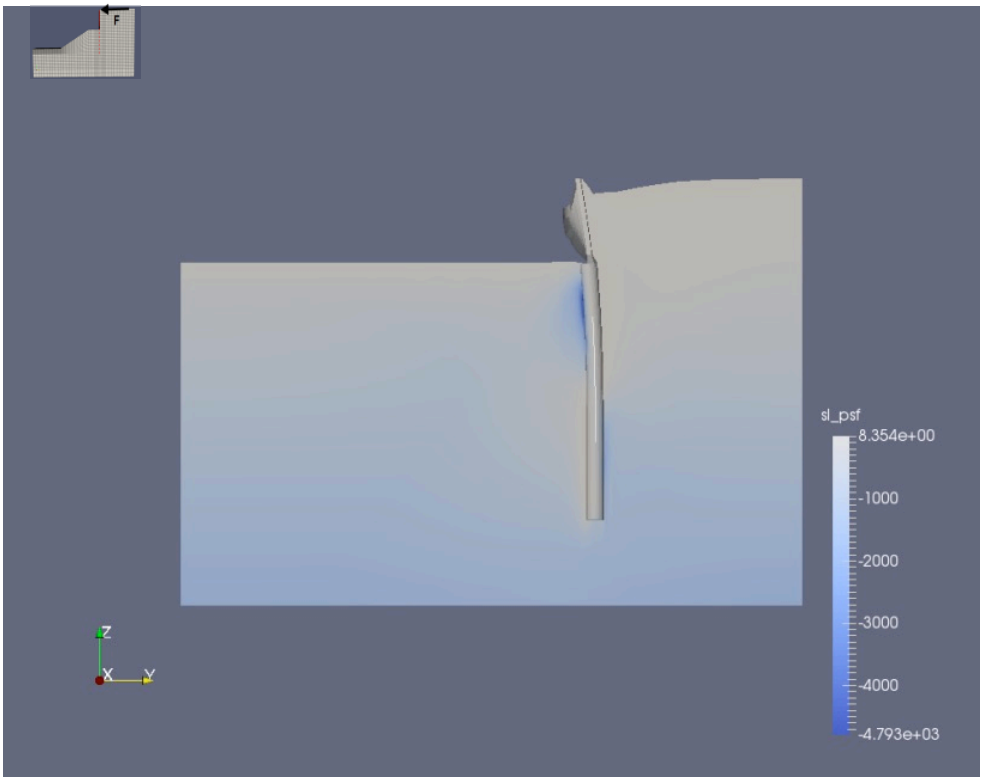

Figure A-7: Applied pushover load: concentrated load at the pile head – Elevation view of σ_1 for a pile-head displacement = 2 in,. Case: medium-dense sand, h_w = 10 feet, s = 4d, no slope

A.2 Medium-stiff clay

A.2.1 Capacity Curves

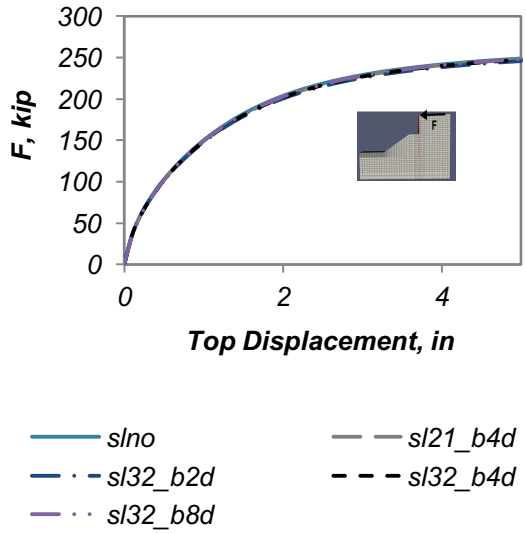

Figure A-8: Capacity curves for medium-stiff clay for h_w = 10 feet and s = 4d

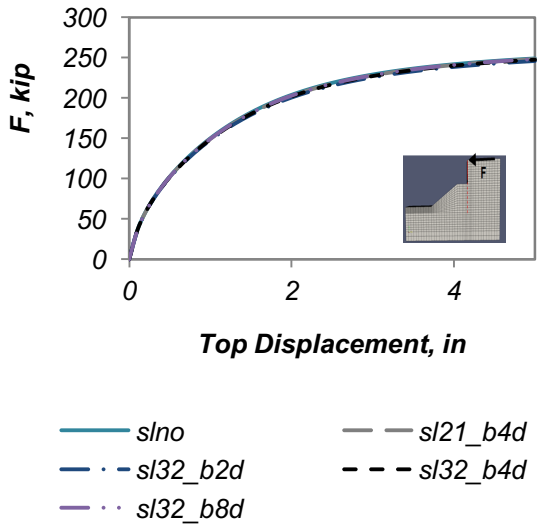

Figure A-9: Capacity curves for medium-stiff clay for h_w = 10 feet and s = 3d

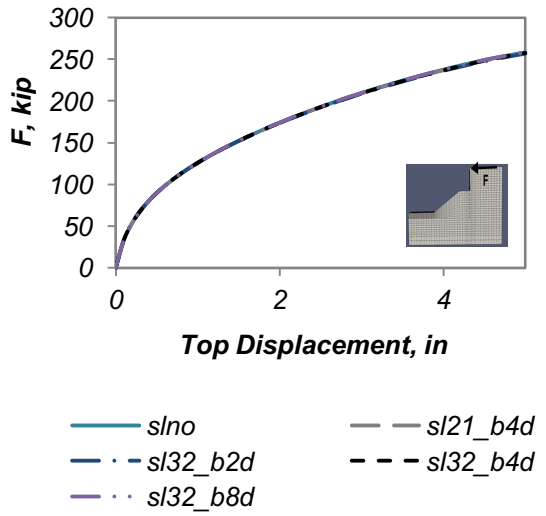

Figure A-10: Capacity curves for medium-stiff clay for h_w = 15 feet and s = 4d

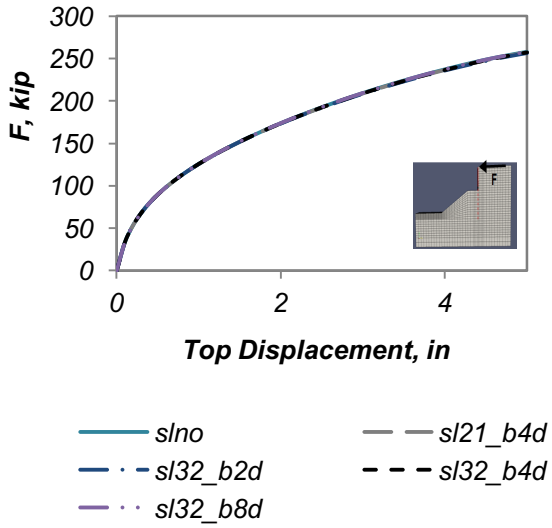

Figure A-11: Capacity curves for medium-stiff clay for h_w = 15 feet and s = 3d

A.2.2 Deformed Shape and Stresses

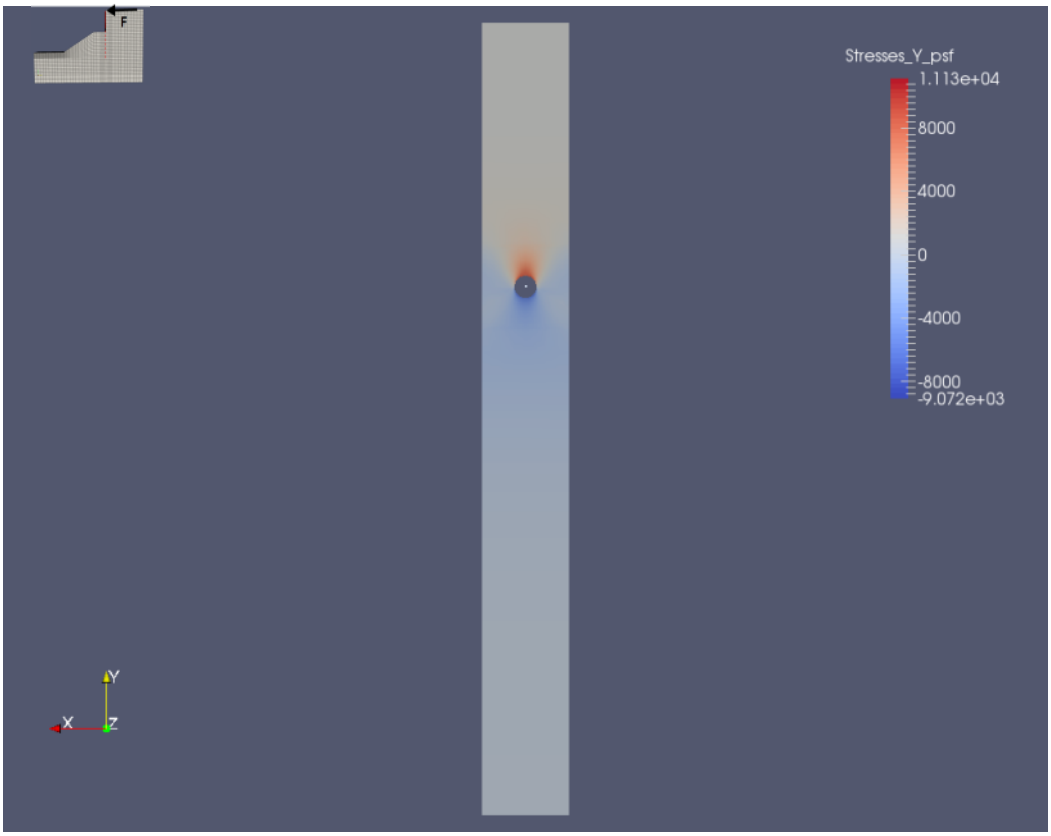

Figure A-12: Applied pushover load: concentrated load at the pile head – Plan view of σ_{YY} for a pile-head displacement = 2 in. Case: medium-stiff clay, h_w = 10 feet, s = 4d, no slope

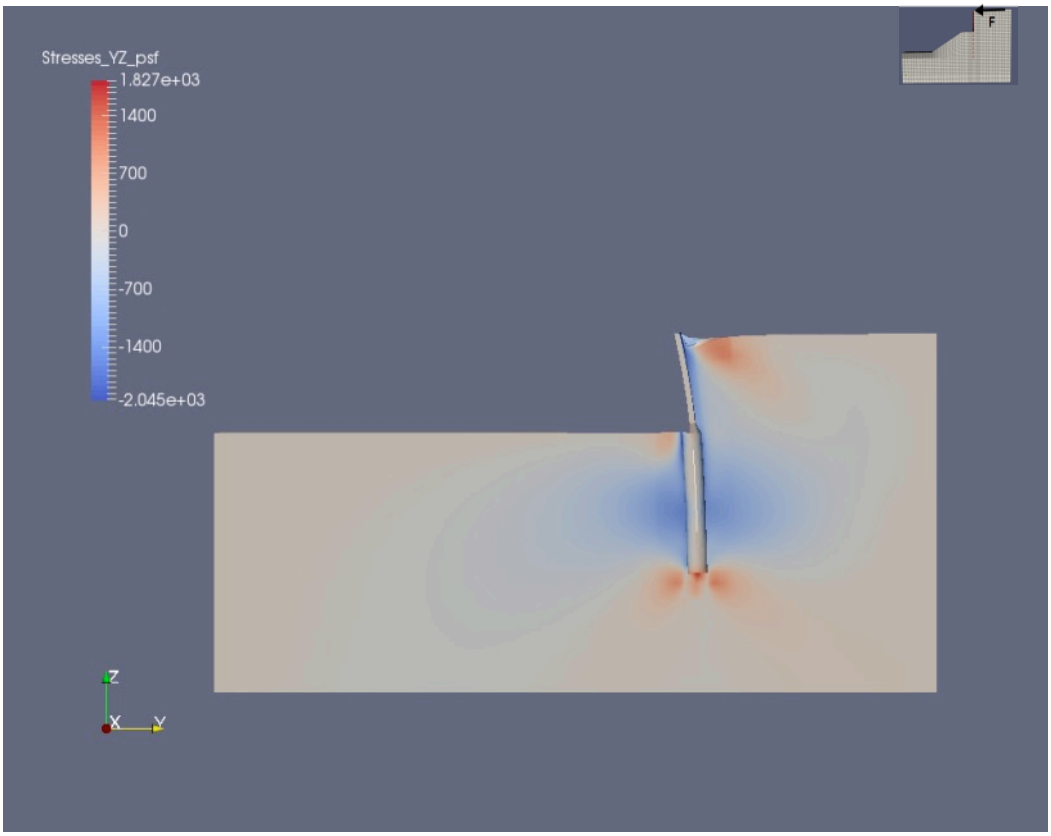

Figure A-13: Applied pushover load: concentrated load at the pile head – Elevation view of σ_{YZ} for a pile-head displacement = 2 in. Case: medium-stiff clay, h_w = 10 feet, s = 4d, no slope

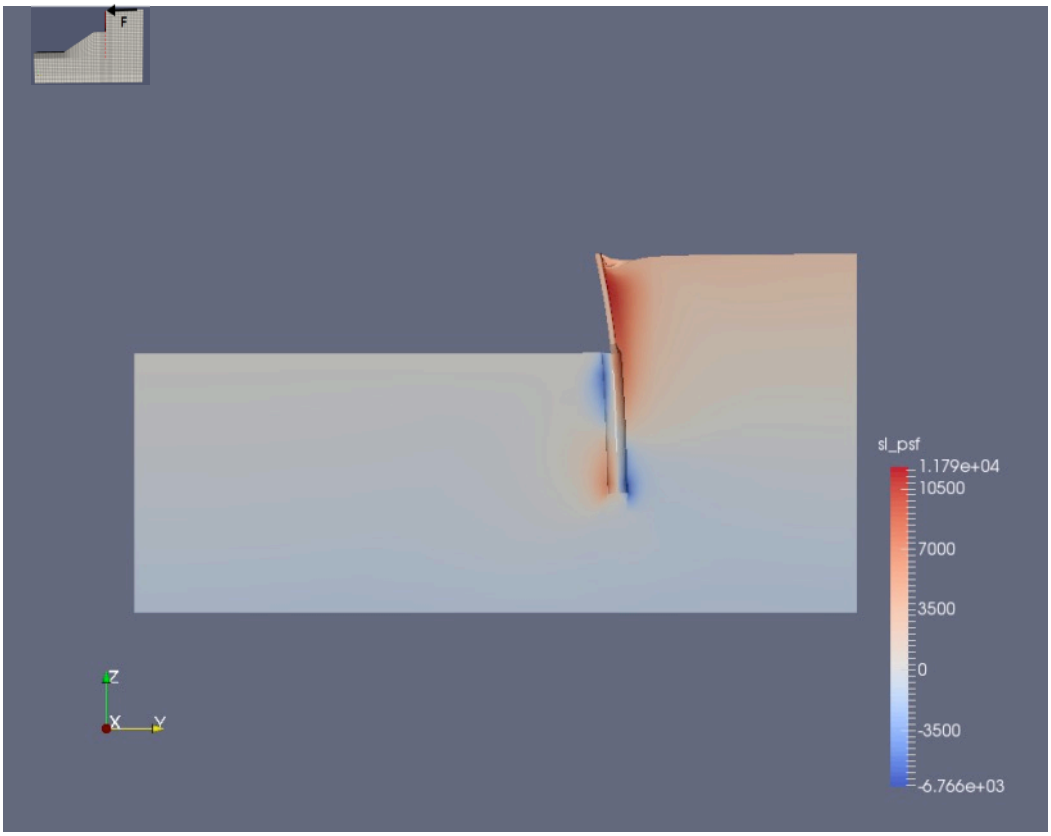

Figure A-14: Applied pushover load: concentrated load at the pile head – Elevation view of σ_I for a pile-head displacement = 2 in. Case: medium-stiff clay, h_w = 10 feet, s = 4d, no slope

A.3 Granular cohesive soil

A.3.1 Capacity Curves

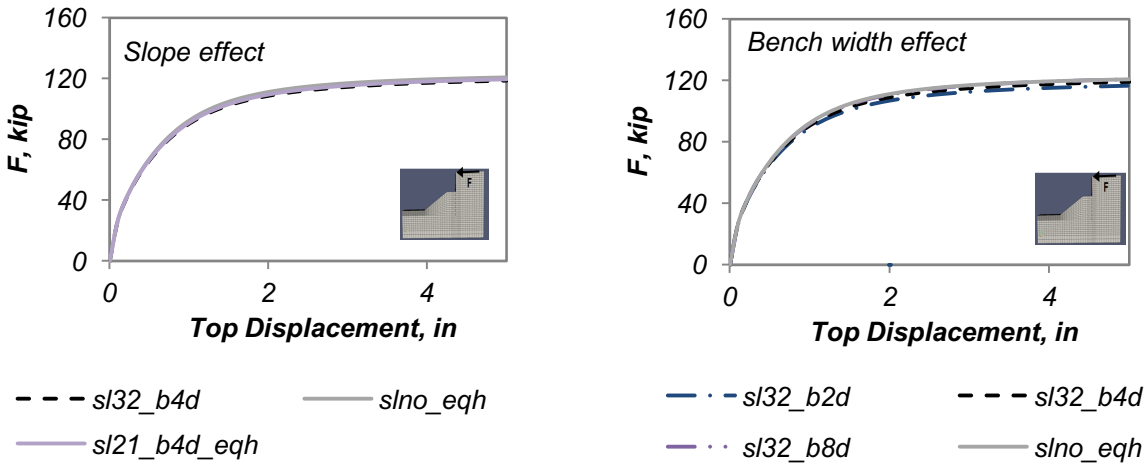

(a) (b)

Figure A-15: Capacity curves for granular cohesive soil for h_w = 10 feet and s = 4d: (a) Effect of slope angle; (b) Effect of bench width

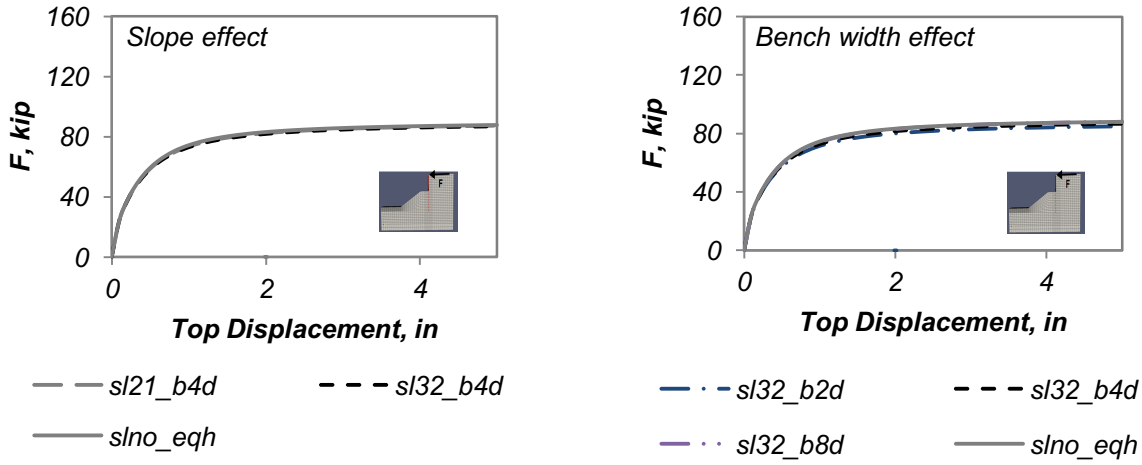

(a) (b)

Figure A-16: Capacity curves for granular cohesive soil for h_w = 10 feet and s = 3d: (a) Effect of slope angle; (b) Effect of bench width

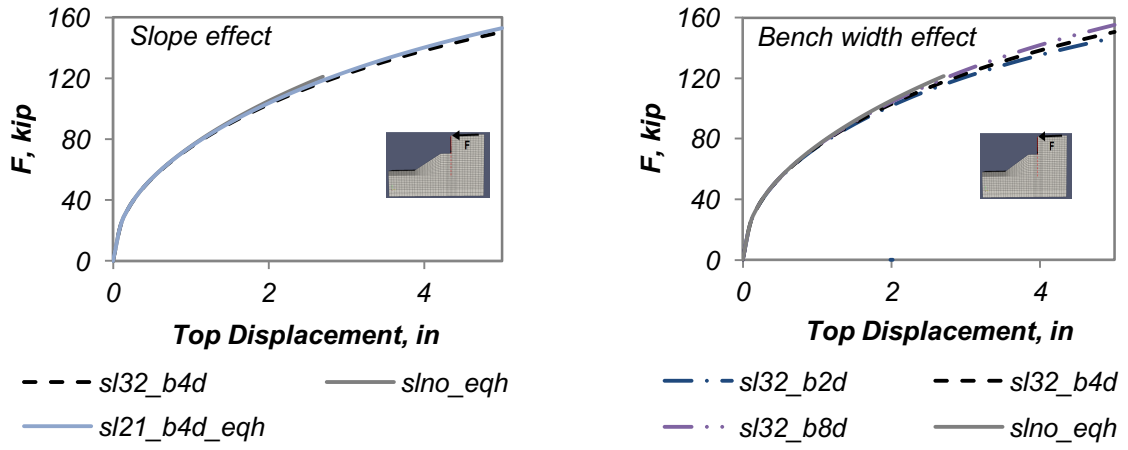

(a) (b)

Figure A-17: Capacity curves for granular cohesive soil for h_w = 15 feet and s = 4d: (a) Effect of slope angle; (b) Effect of bench width

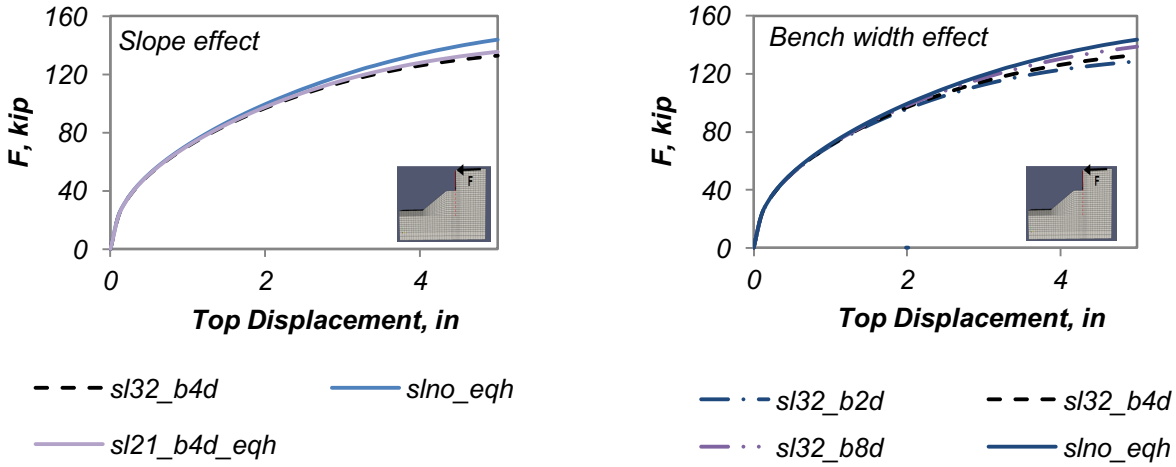

(a) (b)

Figure A-18: Capacity curves for granular cohesive soil for h_w = 15 feet and s = 3d: a) Effect of slope angle; b) Effect of bench width

A.3.2 Deformed Shape and Stresses

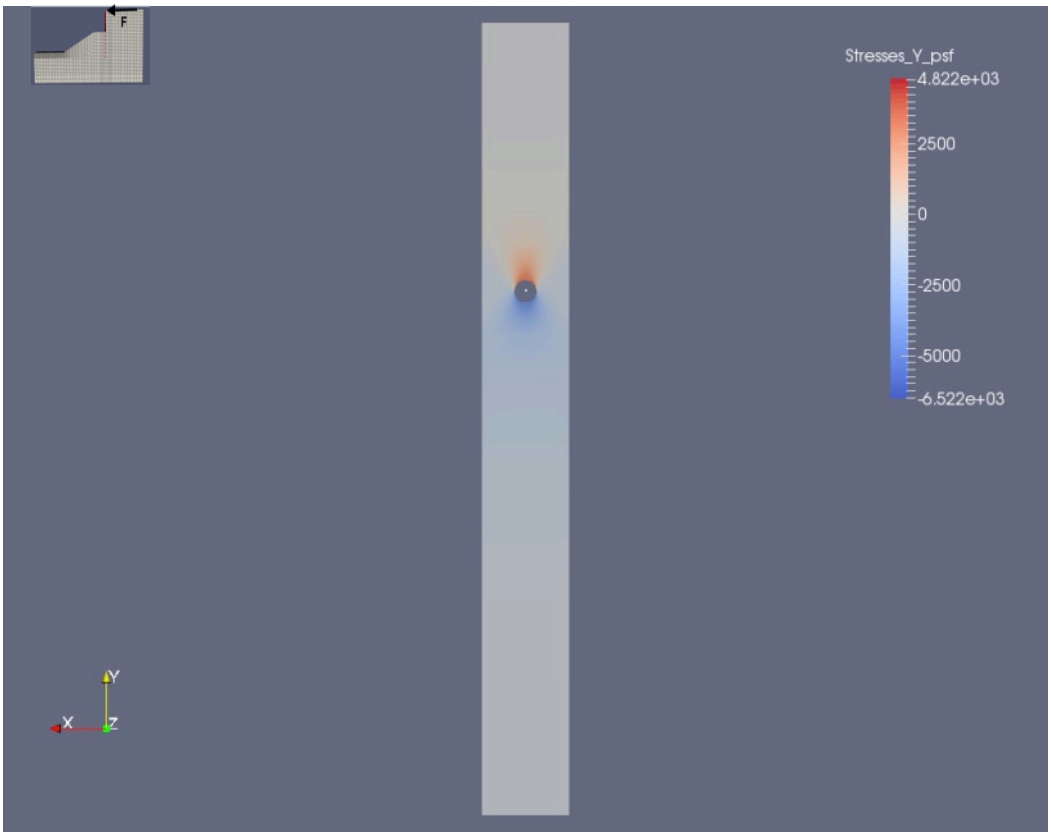

Figure A-19: Applied pushover load: concentrated load at the pile head – Plan view of σ_{YY} for a pile-head displacement = 2 in, for granular cohesive soil, h_w = 10 feet, s = 4d, no slope

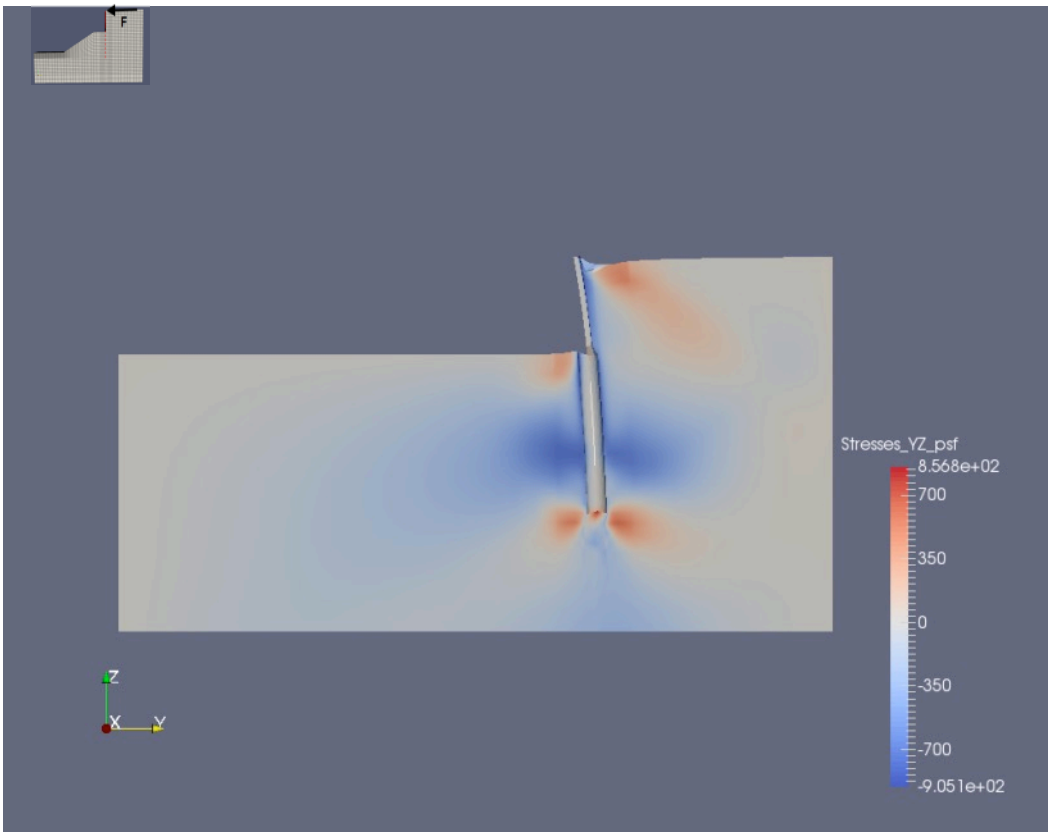

Figure A-20: Applied pushover load: concentrated load at the pile head – Elevation view of σ_{YZ} and deformed shape for a pile-head displacement = 2 in, for granular cohesive soil, h_w = 10 feet, s = 4d, no slope

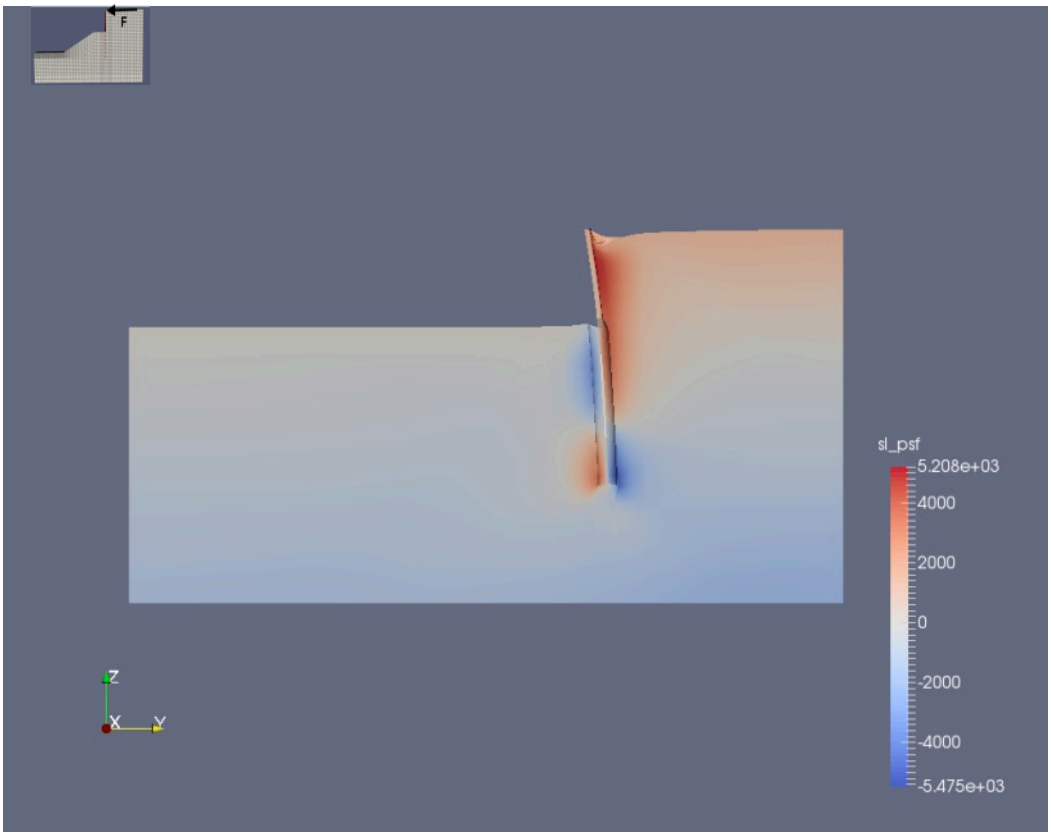

Figure A-21: Applied pushover load: concentrated load at the pile head – Elevation view of σ_I and deformed shape for a pile-head displacement = 2 in, for granular cohesive soil, h_w = 10 feet, s = 4d, no slope

B. DEFORMED SHAPES AND STRESSES FOR CASES WITH SLOPE IN FRONT OF THE PILE

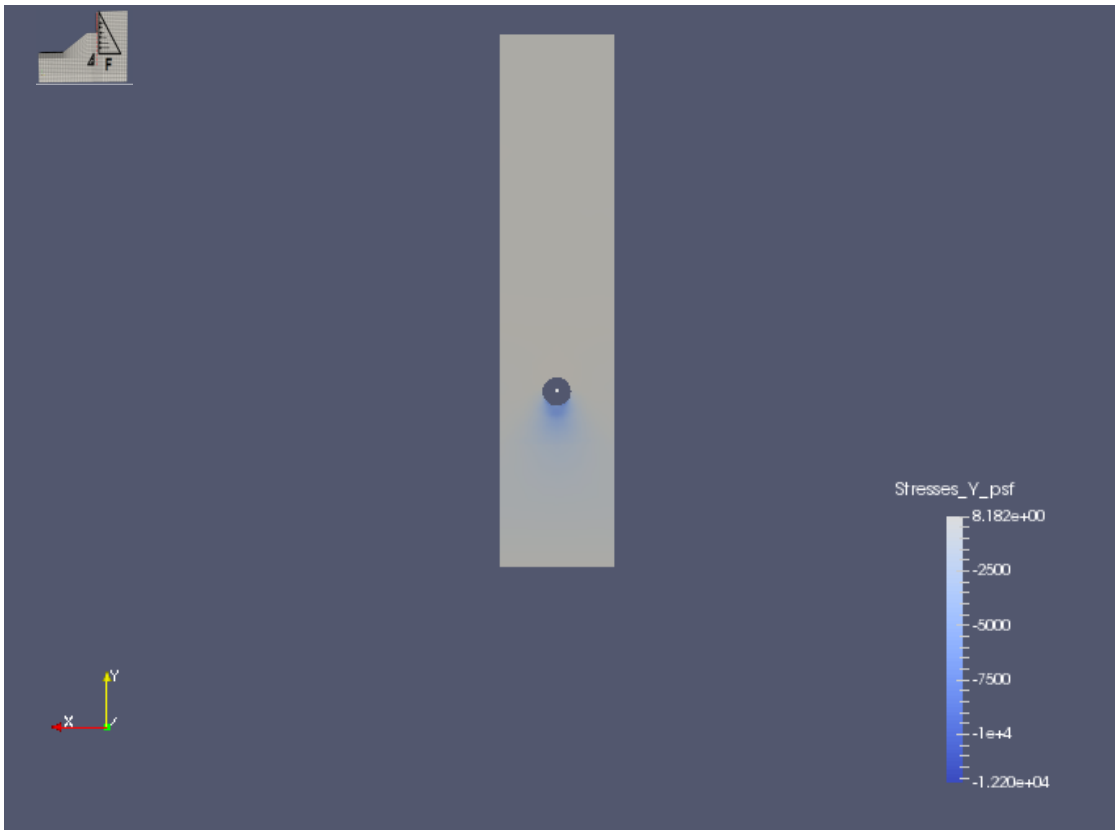

Figure B-1: 3-D model – Plan view of σ_{YY} at depth = -2d, for a pile-head displacement = 2 in, for medium-dense sand, h_w = 10 feet and s = 4d with 3:2 slope and 4d bench

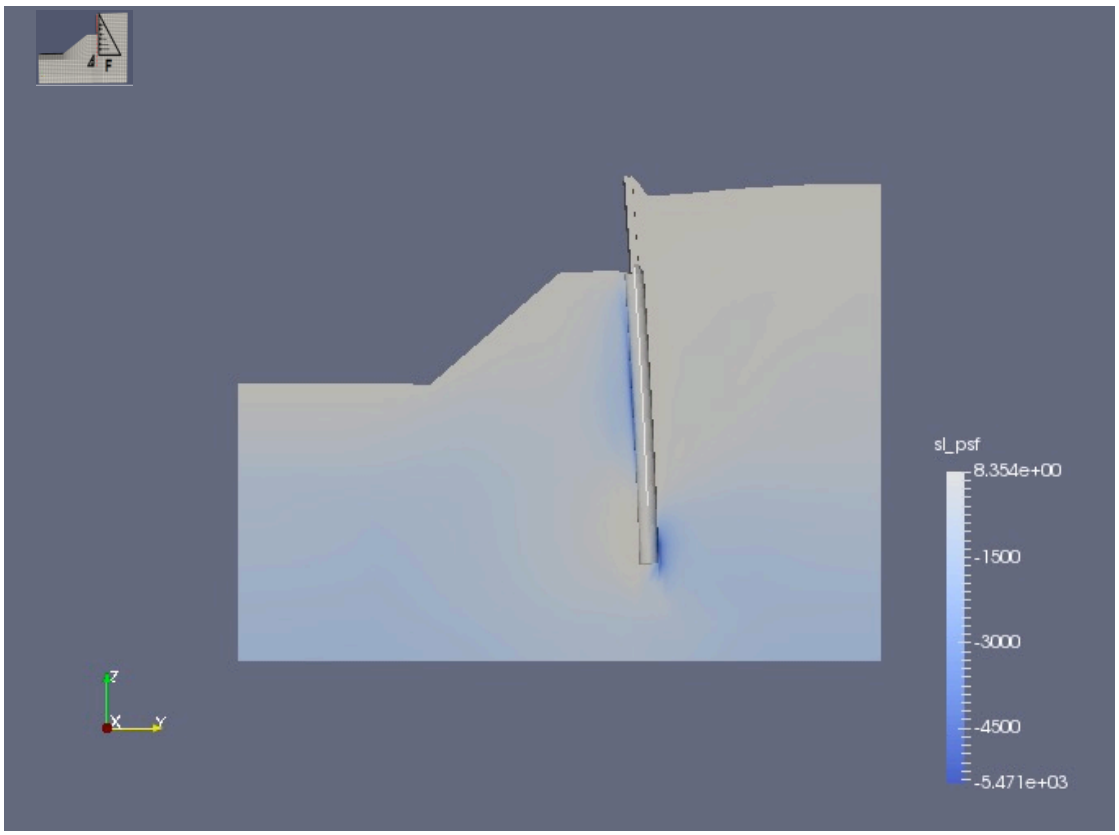

Figure B-2: 3-D model – Elevation view of σ_I and deformed shape for a pile-head displacement = 2 in, for medium-dense sand, h_w = 10 feet and s = 4d with 3:2 slope and 4d bench

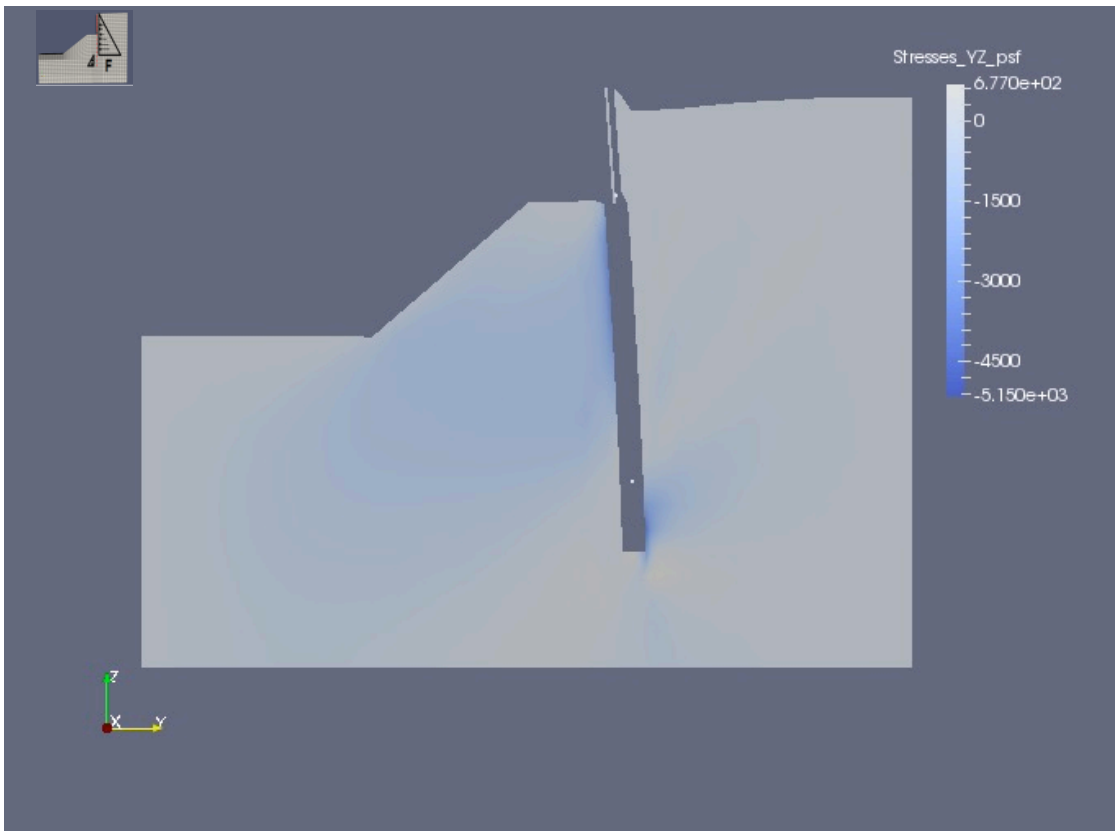

Figure B-3: 3-D model – Elevation view of σ_{YY} and deformed shape for a pile-head displacement = 2 in, for medium-dense sand, h_w = 10 feet and s = 4d with 3:2 slope and 4d bench

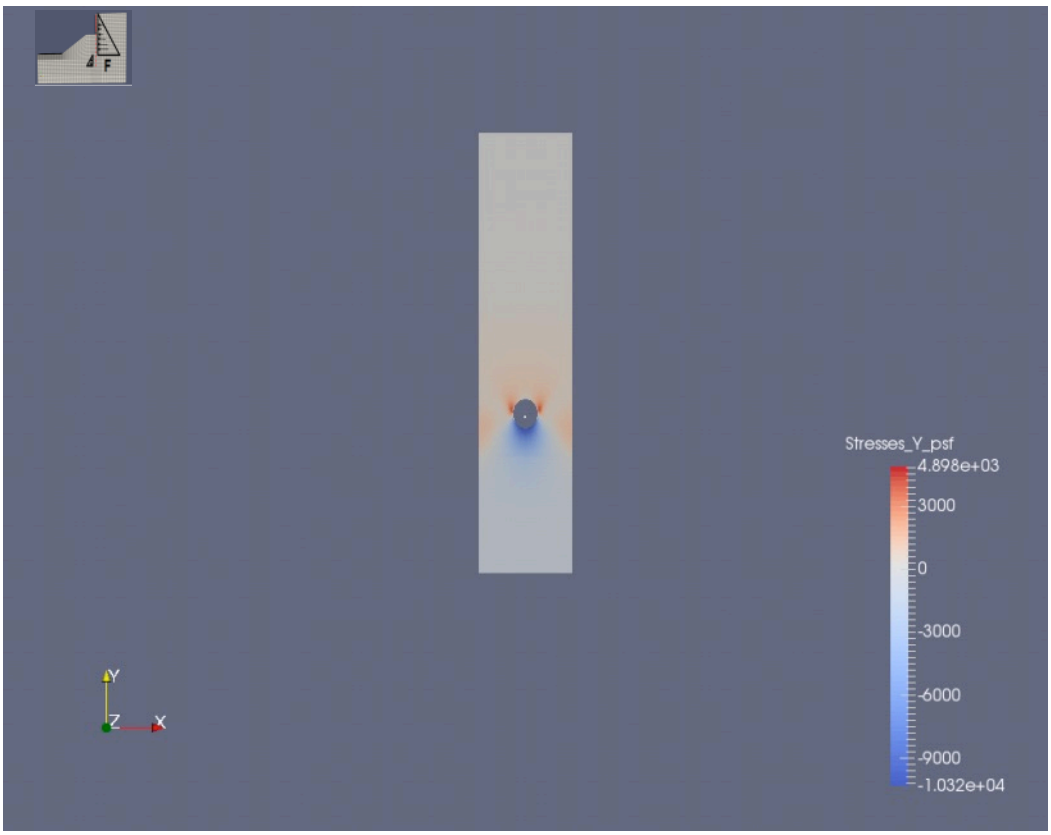

Figure B-4: 3-D model – Plan view of σ_{YY} at depth = -2d for a pile-head displacement = 2 in.
Case: medium-stiff clay, h_w = 10 feet and s = 4d with 3:2 slope and 4d bench

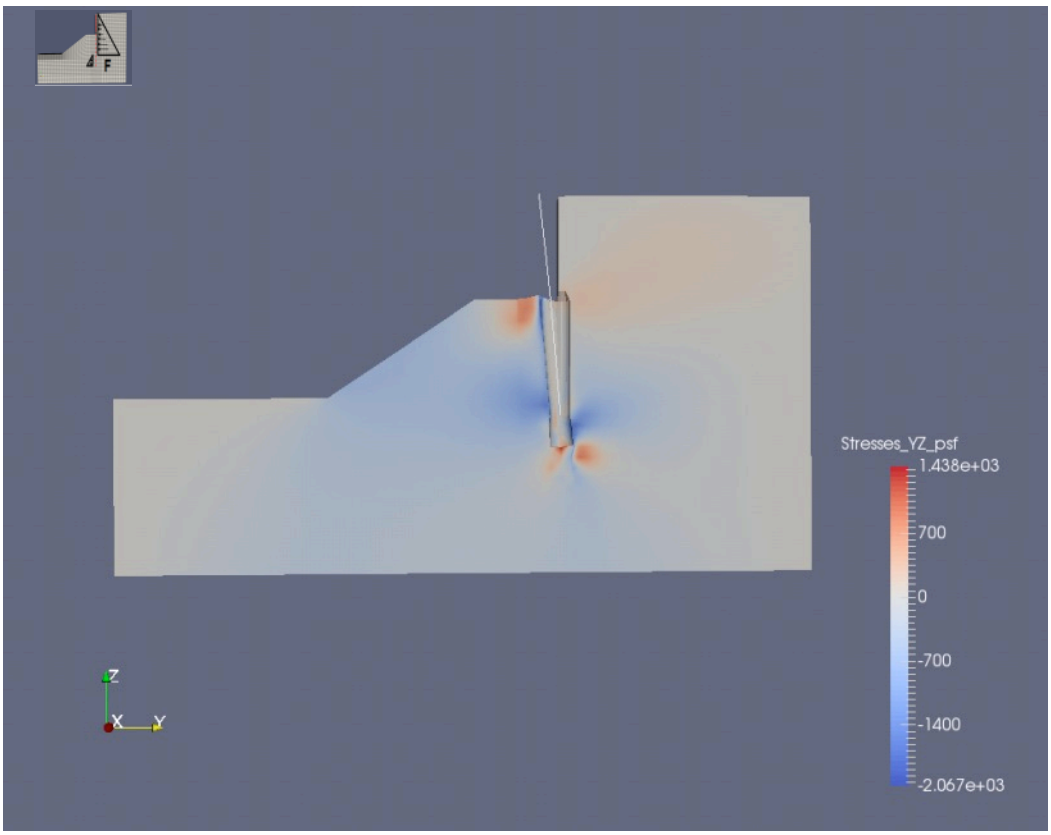

Figure B-5: 3-D model – Elevation view of σ_{YZ} and deformed shape for a pile-head displacement = 2 in. Case: medium-stiff clay, h_w = 10 feet and s = 4d with 3:2 slope and 4d bench

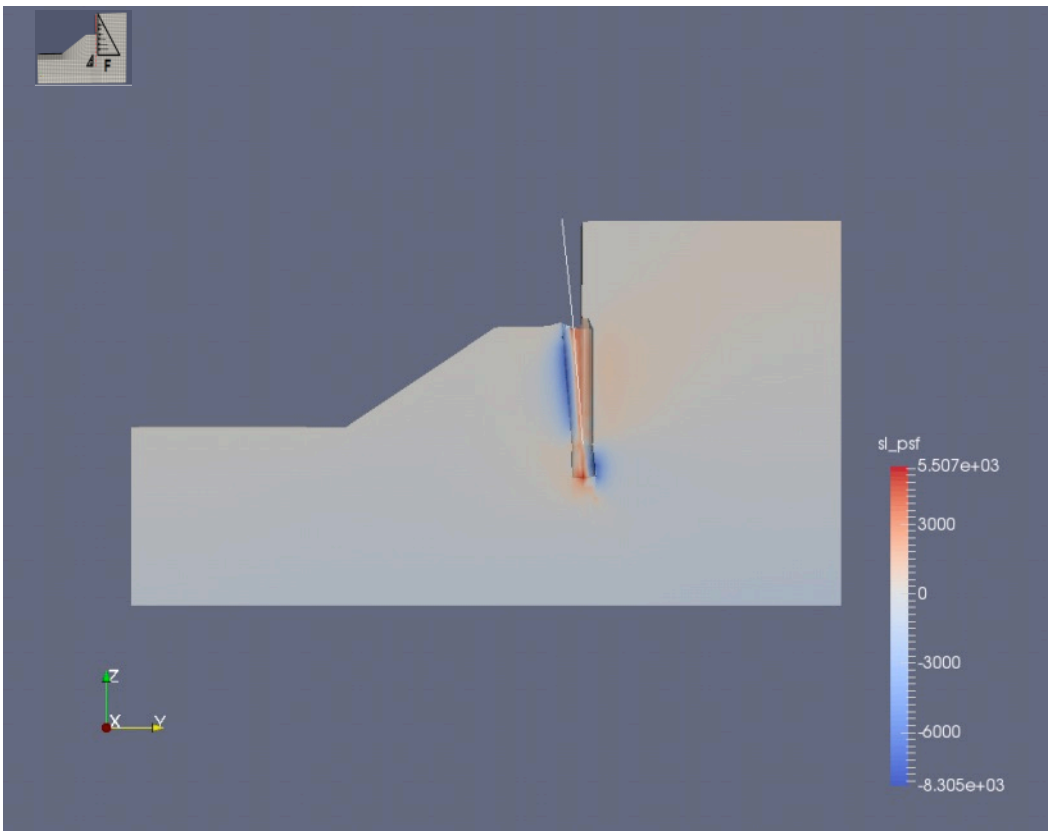

Figure B-6: 3-D model – Elevation view of σ_I and deformed shape for a pile-head displacement = 2 in. Case: medium-stiff clay, h_w = 10 feet and s = 4d with 3:2 slope and 4d bench

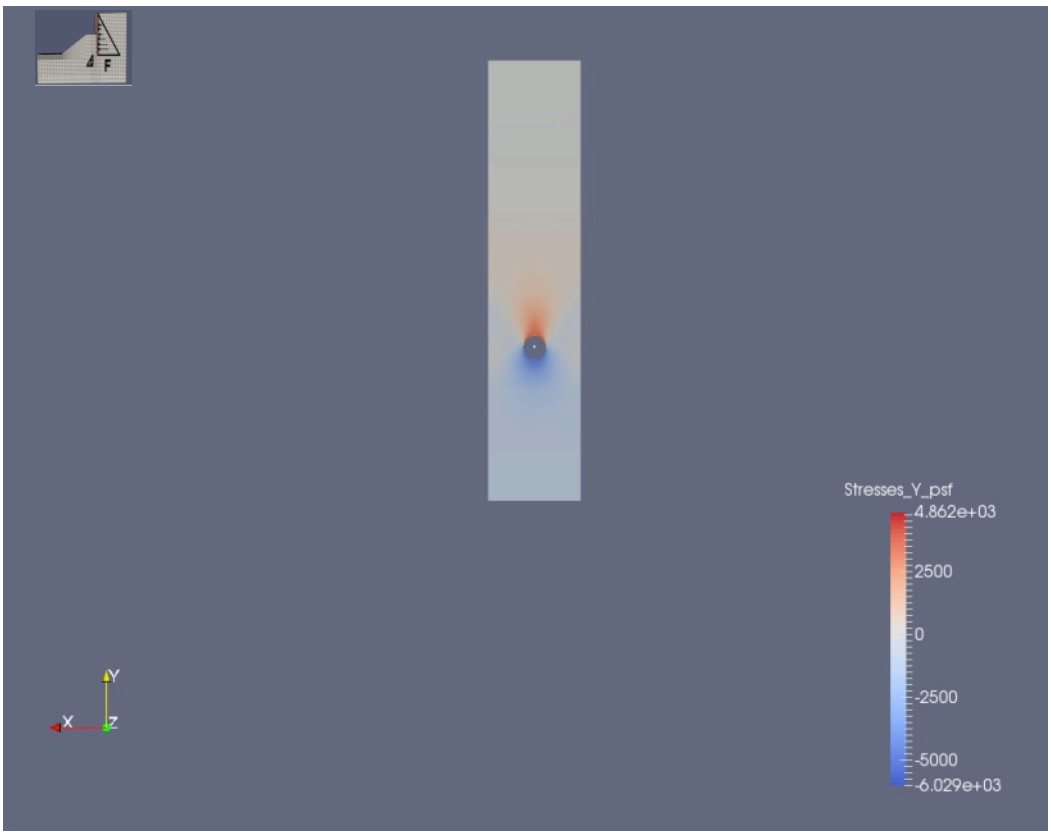

Figure B-7: 3-D model – Plan view of σ_{YY} at depth = -2d for a pile-head displacement = 2 in, for granular cohesive soil, h_w = 10 feet and s = 4d with 3:2 slope and 4d bench

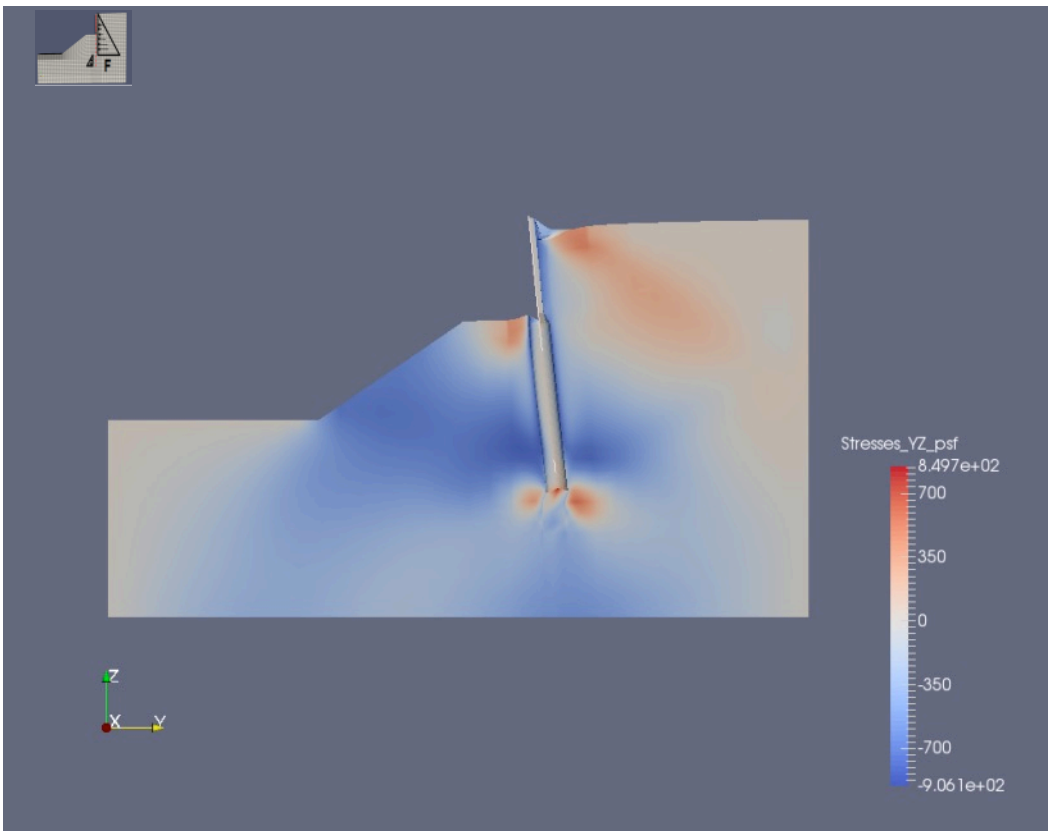

Figure B-8: 3-D model – Elevation view of σ_{YZ} and deformed shape for a pile-head displacement = 2 in, for granular cohesive soil, h_w = 10 feet and s = 4d with 3:2 slope and 4d bench

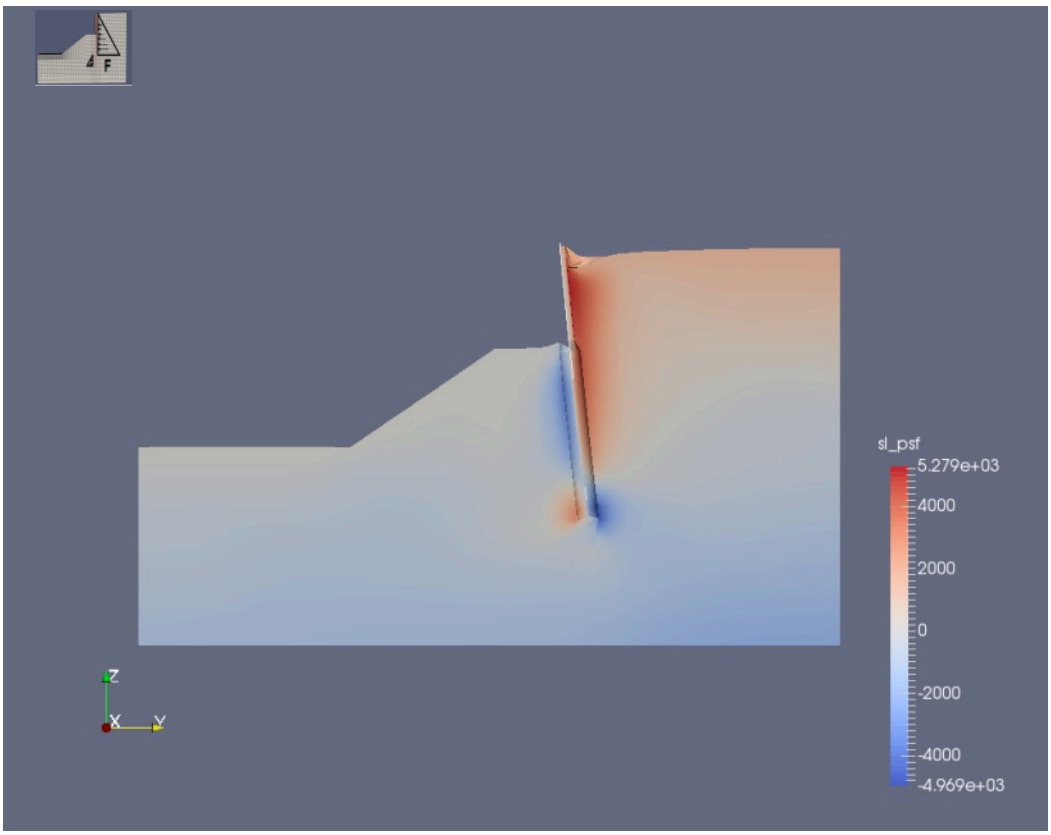

Figure B-9: 3-D model – Elevation view of σ_1 and deformed shape for a pile-head displacement = 2 in, for granular cohesive soil, h_w = 10 feet and s = 4d with 3:2 slope and 4d bench

C. RESULTS FOR MEDIUM-STIFF CLAYS, WITHOUT INTERFACE GAP ELEMENTS

C.1.1 Capacity Curves

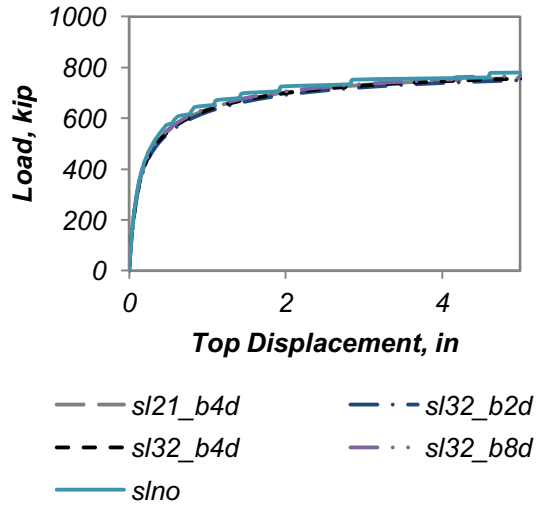

Figure C-1: Capacity curves for medium-stiff clay for 3-D analyses not considering detachment: h_w = 10 feet and s = 4d

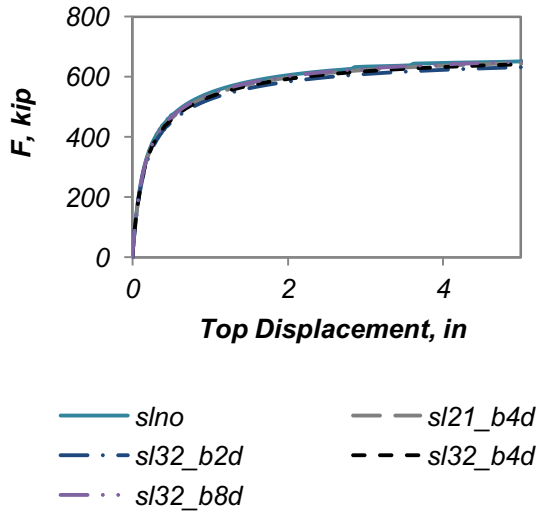

Figure C-2: Capacity curves for medium-stiff clay for 3-D analyses not considering detachment: h_w = 10 feet and s = 3d

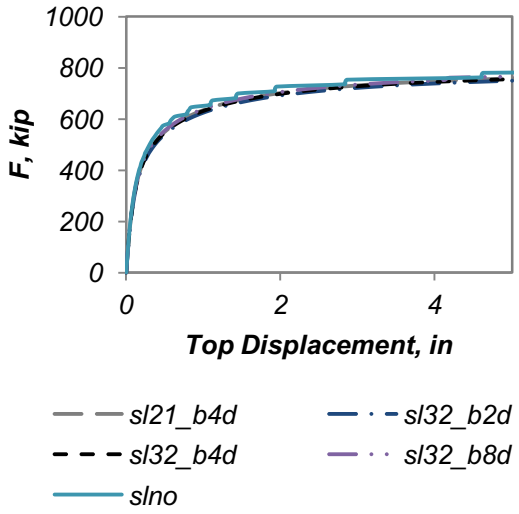

Figure C-3: Capacity curves for medium-stiff clay for 3-D analyses not considering detachment: h_w = 15 feet and s = 4d

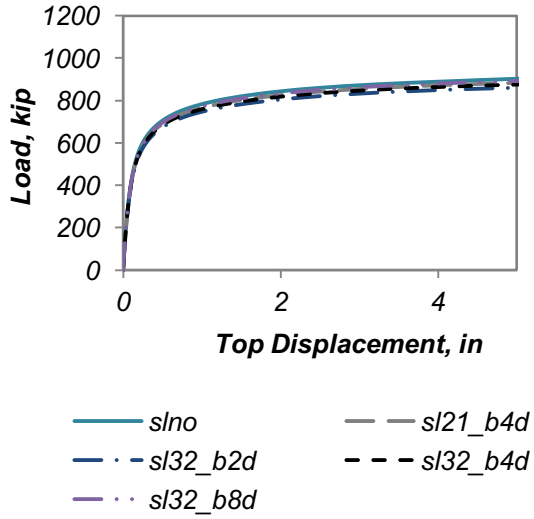

Figure C-4: Capacity curves for medium-stiff clay for 3-D analyses not considering detachment: h_w = 15 feet and s = 3d

C.1.2 Deformed Shape and Stresses

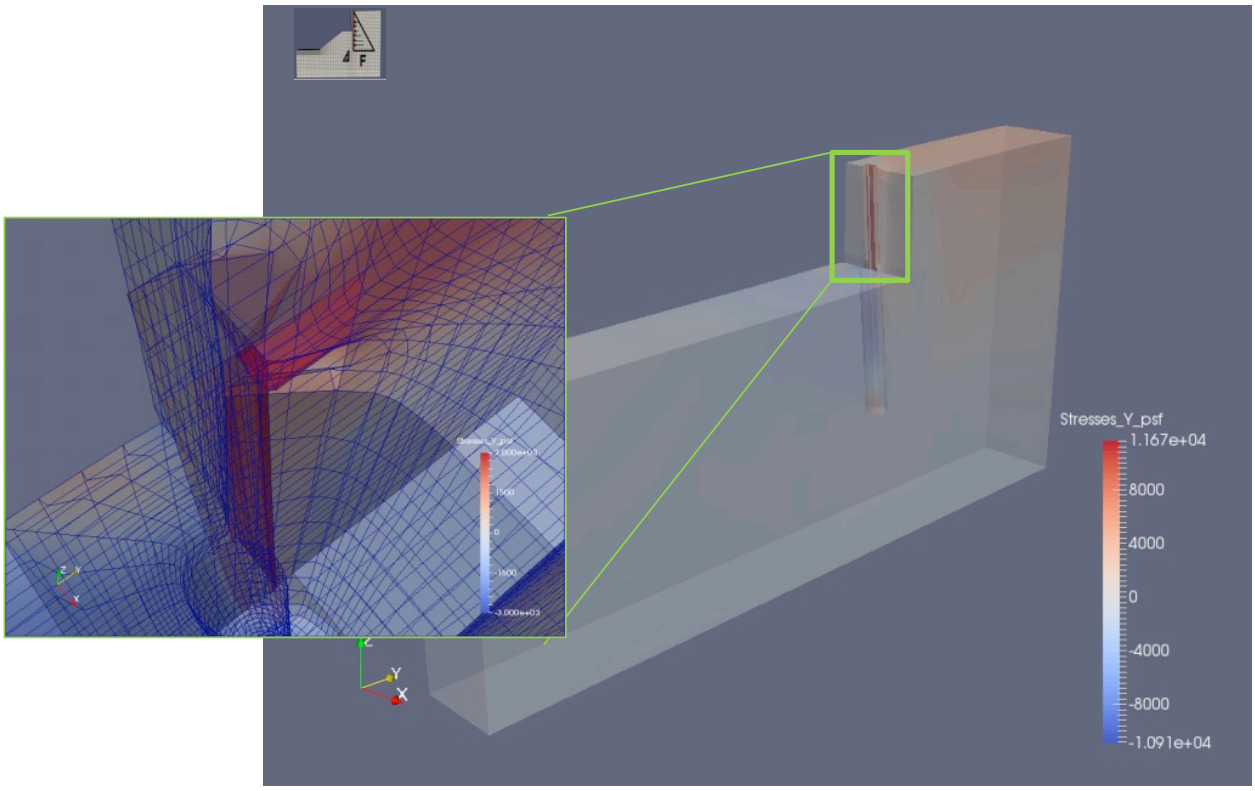

Figure C-5: 3-D model not considering detachment – 3-D view of σ_{YY} and deformed shape for a pile-head displacement = 2 in. Case: medium-stiff clay: h_w = 10 feet, s = 4d, no slope

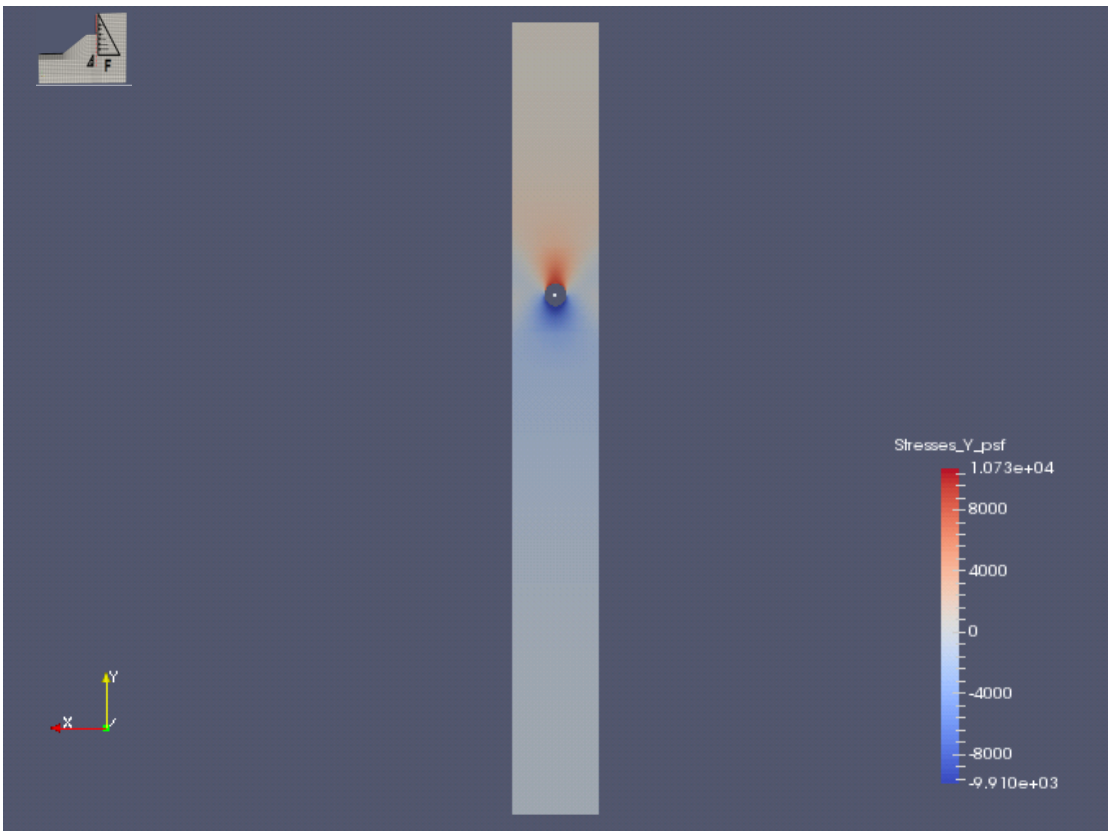

Figure C-6: 3-D model not considering detachment – Plan view of σ_{YY} for a pile-head displacement = 2 in. Case: medium-stiff clay, h_w = 10 feet, s = 4d, no slope

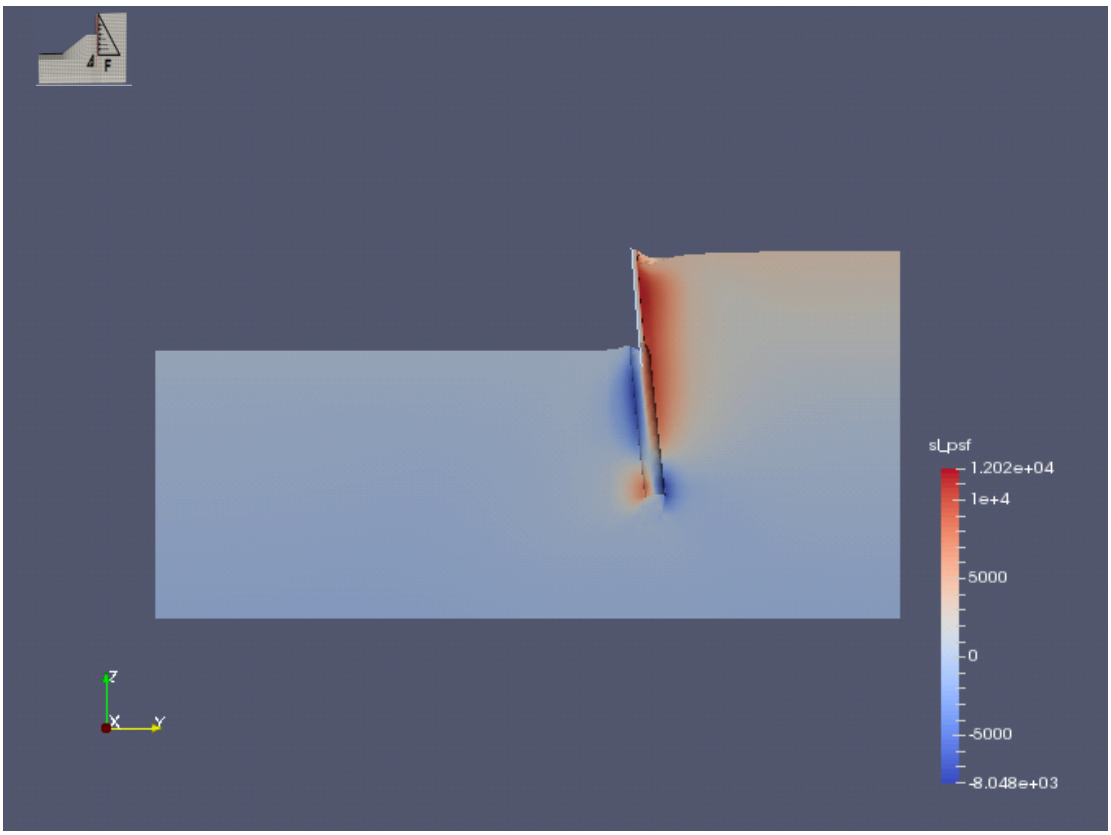

Figure C-7: 3-D model not considering detachment – Elevation view of σ_I and deformed shape for a pile-head displacement = 2 in. Case: medium-stiff clay, h_w = 10 feet, s = 4d, no slope

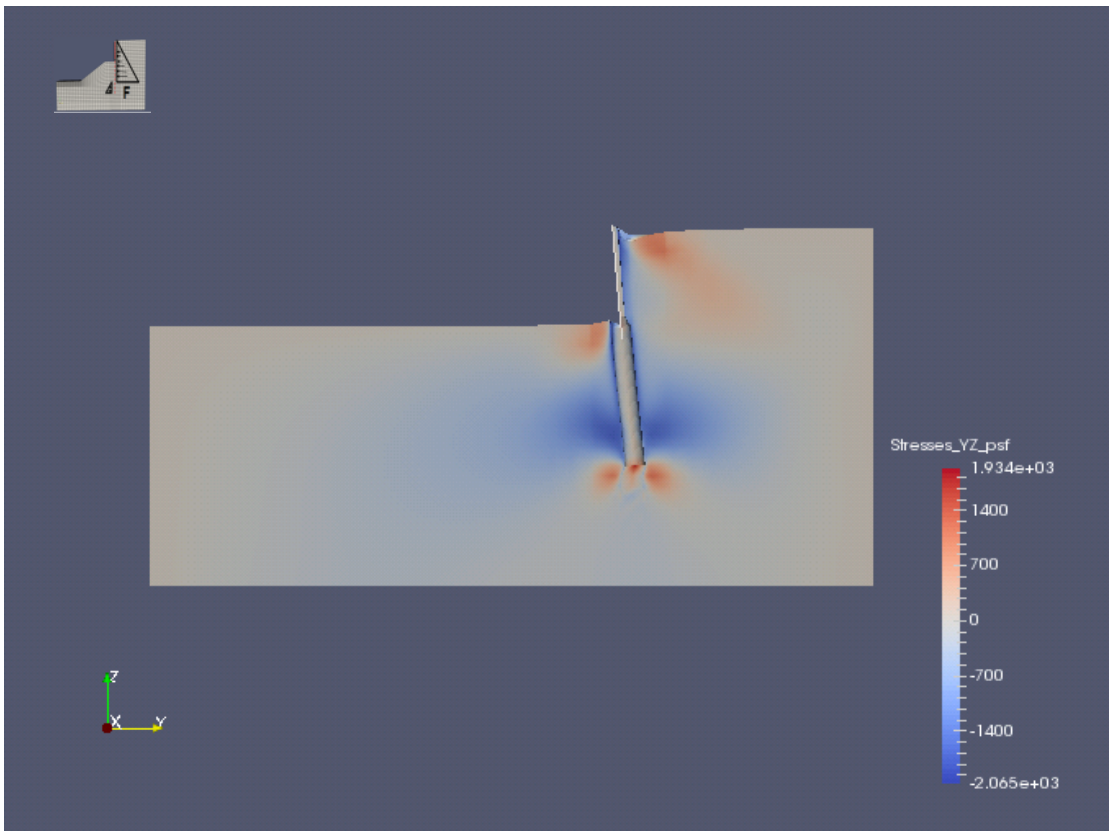

Figure C-8: 3-D model not considering detachment – Elevation view of σ_{YZ} and deformed shape for a pile-head displacement = 2 in. Case: medium-stiff clay, h_w = 10 feet, s = 4d, no slope

C.1.3 Arching Capability Factor Assessment

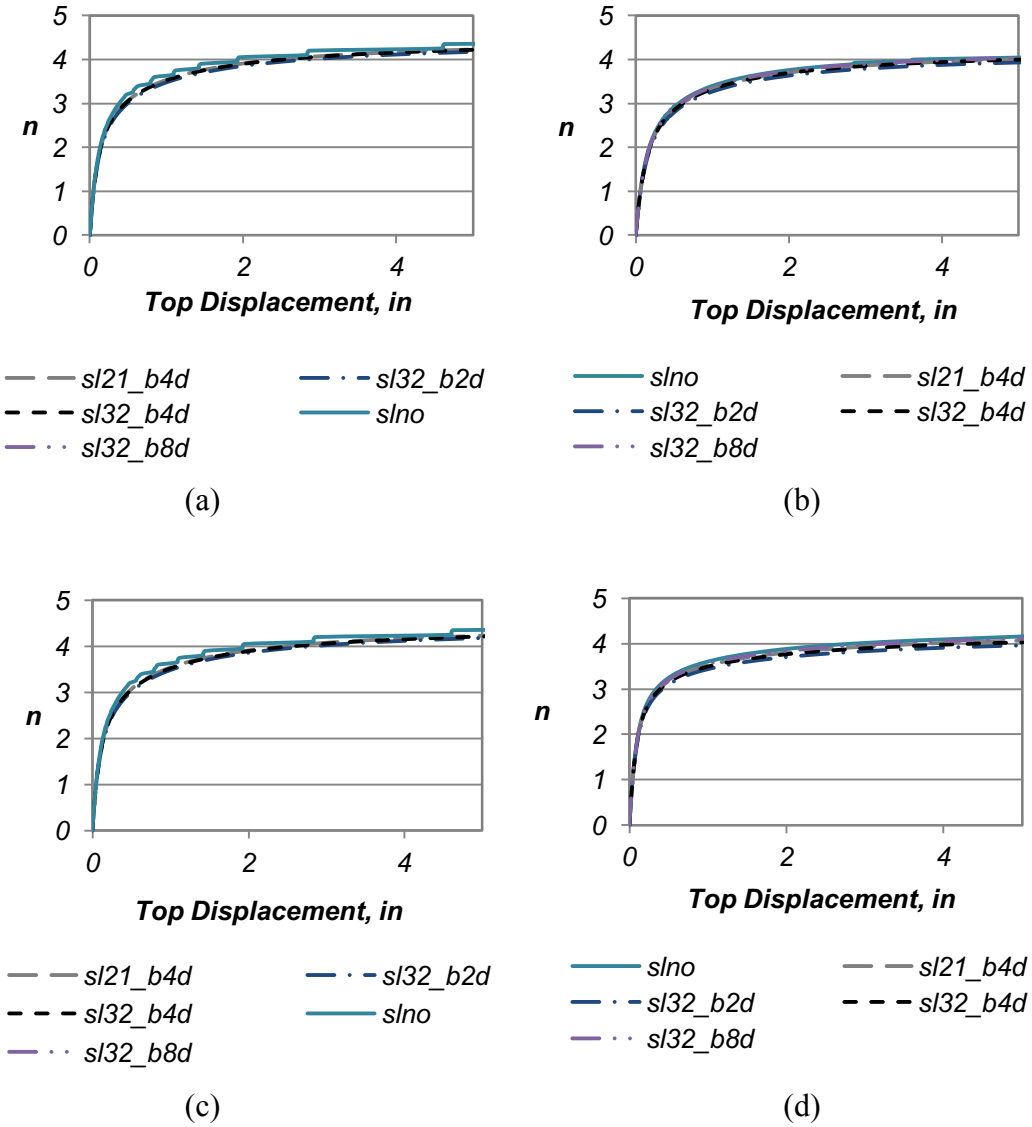

Figure C-9: Arching capability factor assessment for medium-stiff clay not considering detachment: (a) h_w = 10 feet and s = 4d; (b) h_w = 10 feet and s = 3d; (c) h_w = 15 feet and s = 4d; (d) h_w = 15 feet and s = 3d

D. NONLINEAR STATIC PUSHOVER ANALYSIS RESULTS WITH TRIANGULAR PUSHOVER LOAD

D.1 Medium-dense sand

D.1.1 Capacity Curves

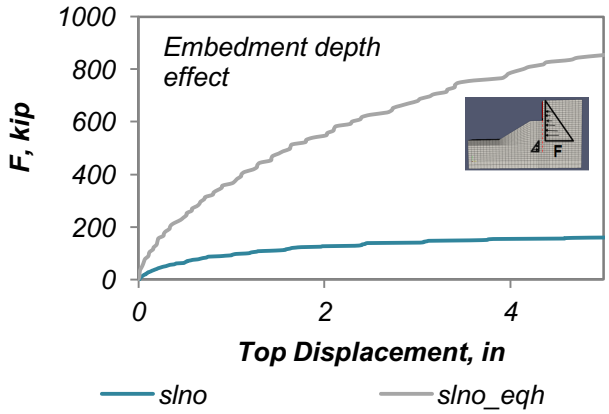

Figure D-1: Effect of embedment depth on capacity curves for medium-dense sand in 3-D analyses: h_w = 10 feet and s = 4d

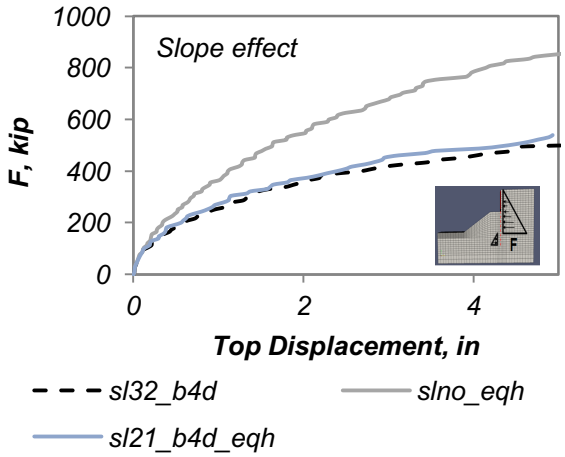

Figure D-2: Effect of slope angle on capacity curves for medium-dense sand in 3-D analyses: h_w = 10 feet and s = 4d

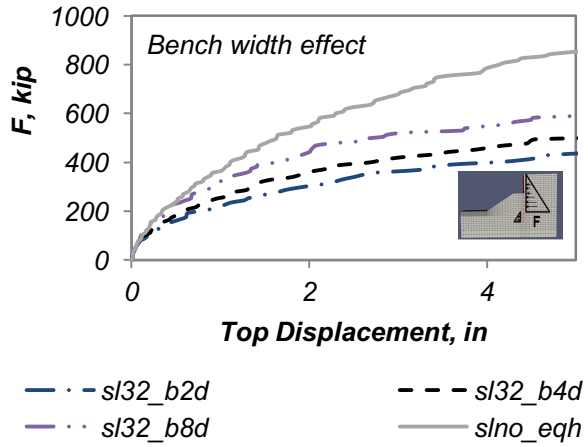

Figure D-3: Effect of bench width on capacity curves for medium-dense sand in 3-D analyses: h_w = 10 feet and s = 4d

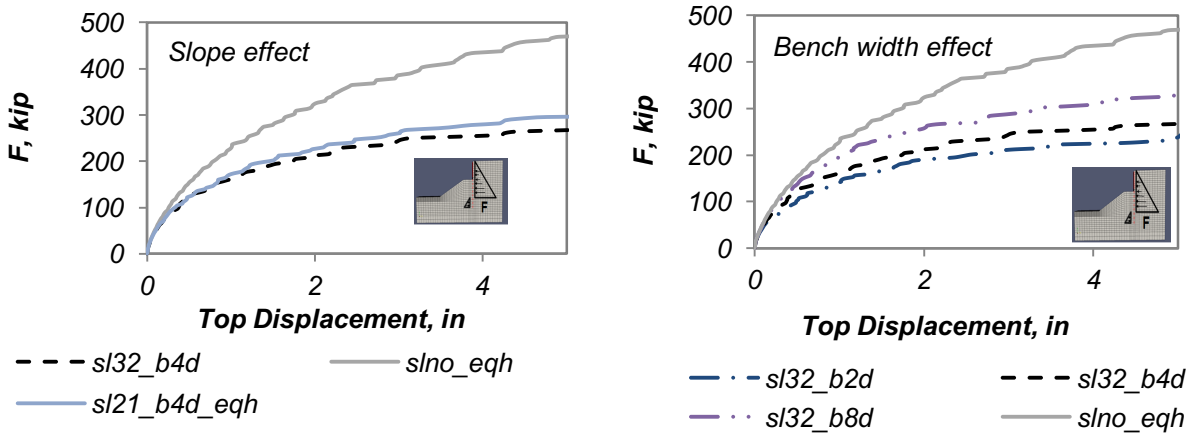

(a) (b)

Figure D-4: Capacity curves for medium-dense sand in 3-D analyses for h_w = 10 feet and s = 3d: (a) slope effect; (b) effect of bench width

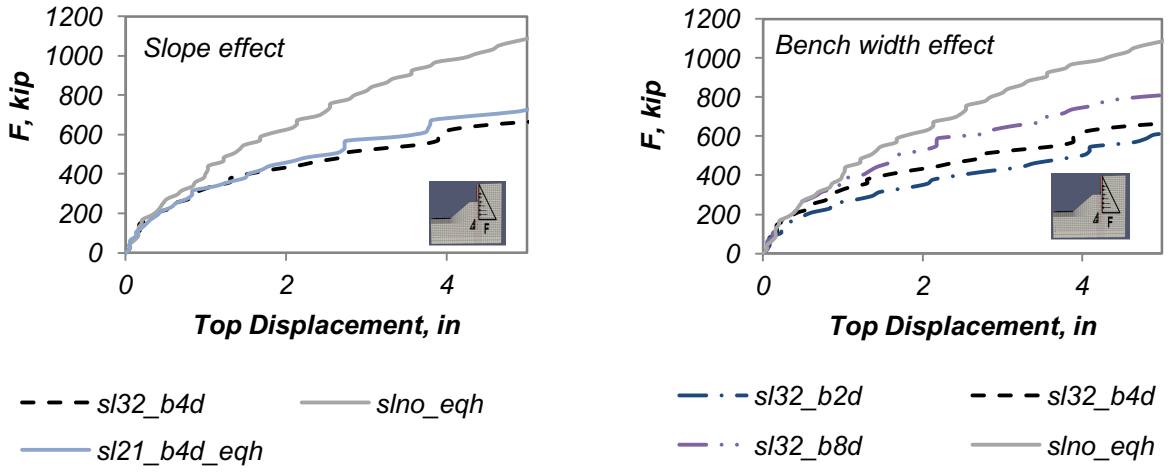

(a) (b)

Figure D-5: Capacity curves for medium-dense sand in 3-D analyses for h_w = 15 feet and s = 4d:(a) slope effect; (b) effect of bench width

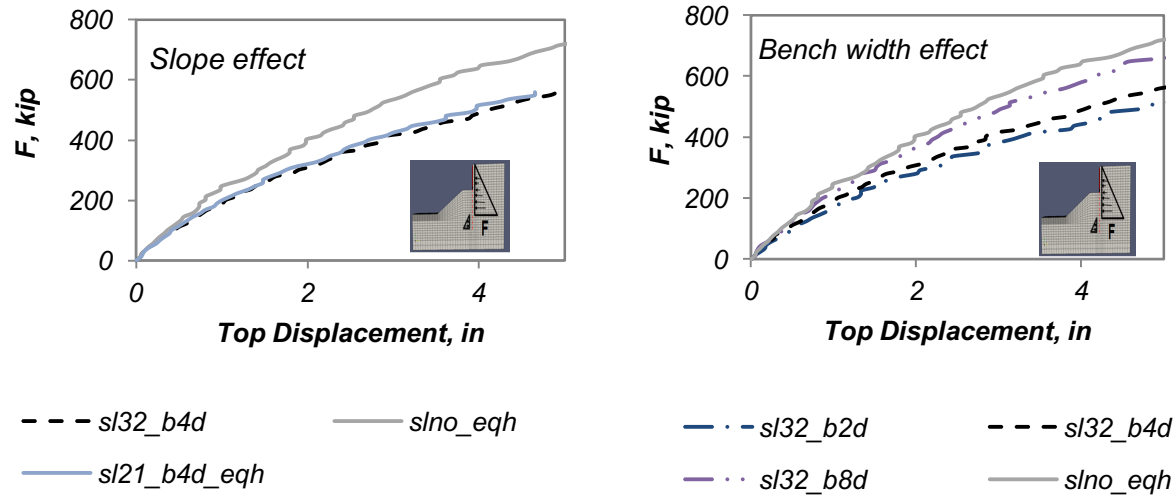

(a) (b)

Figure D-6: Capacity curves for medium-dense sand in 3-D analyses for h_w = 15 feet and s = 3d: (a) slope effect; (b) effect of bench width

D.2 Medium-stiff clay

D.2.1 Capacity Curves

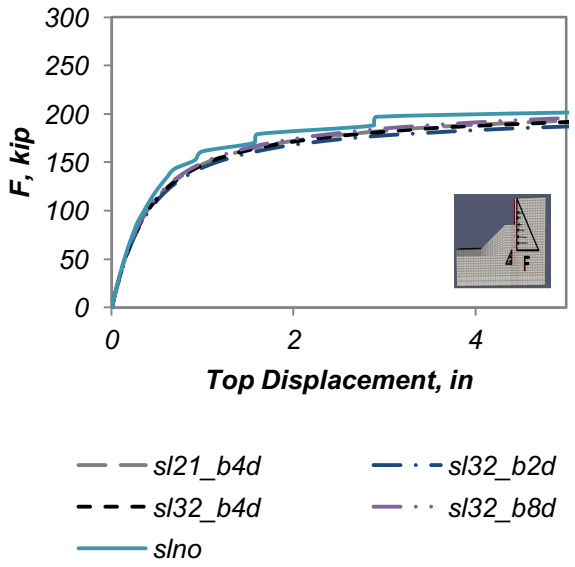

Figure D-7: Effect of bench width for medium-stiff clay for 3-D analyses: h_w = 10 feet and s = 4d

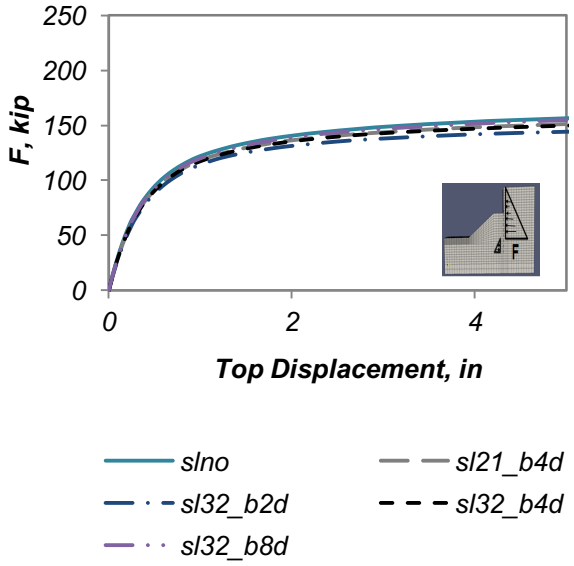

Figure D-8: Effect of bench width for medium-stiff clay for 3-D analyses: h_w = 10 feet and s = 3d

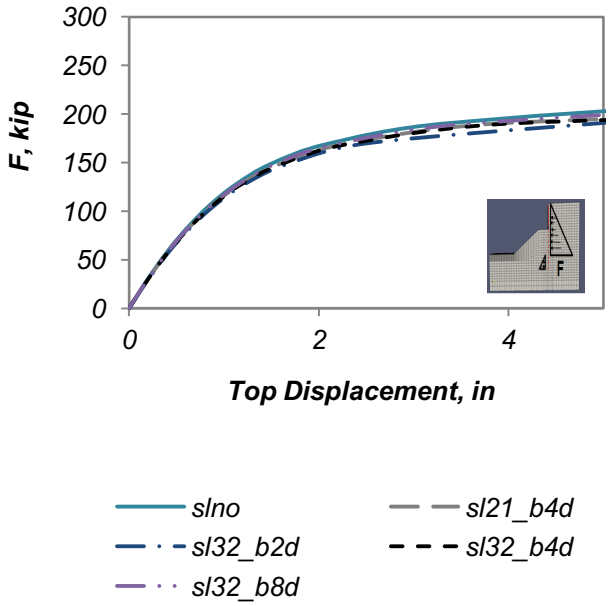

Figure D-9: Effect of bench width for medium-stiff clay for 3-D analyses: h_w = 15 feet and s = 4d

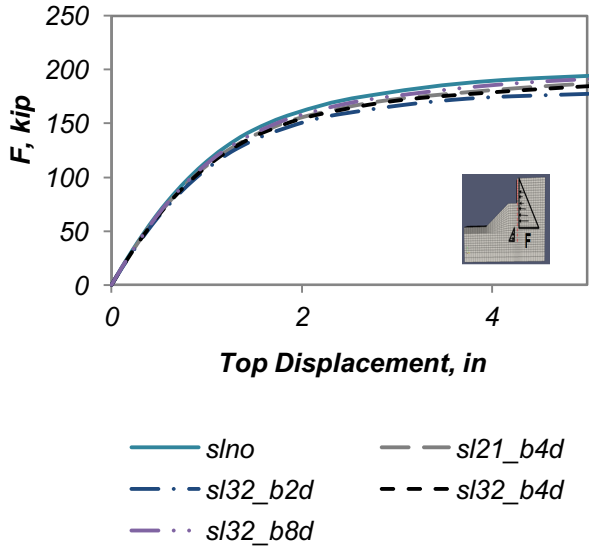

Figure D-10: Effect of bench width for medium-stiff clay for 3-D analyses: h_w = 15 feet and s = 3d

D.3 Granular cohesive soil

D.3.1 Capacity Curves

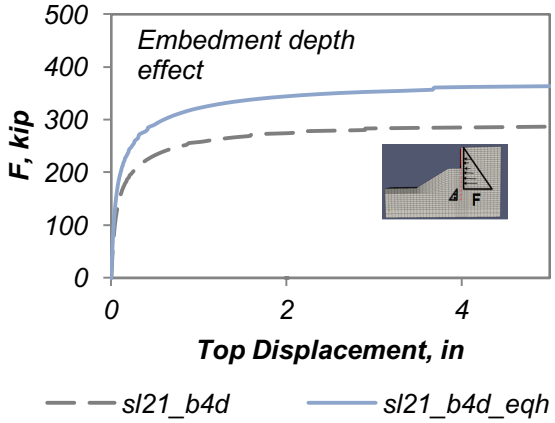

Figure D-11: Effect of embedment depth on capacity curves for granular cohesive in 3-D analyses: h_w = 10 feet and s = 4d

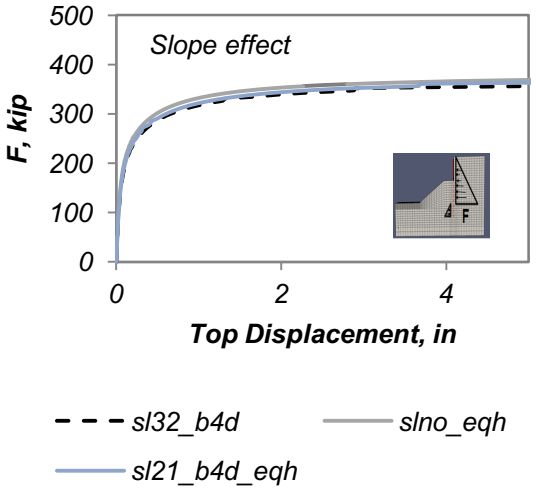

Figure D-12: Effect of slope angle on capacity curves for granular cohesive in 3-D analyses: h_w = 10 feet and s = 4d

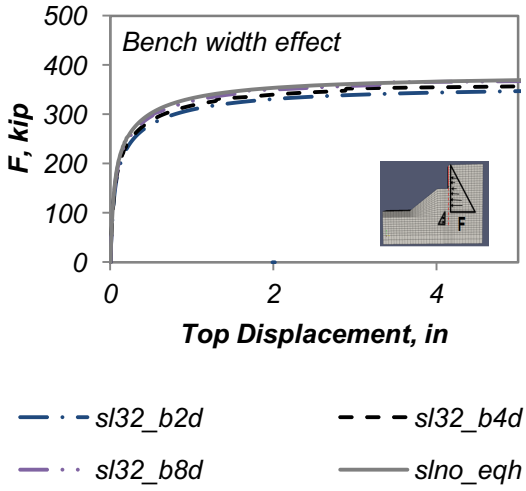

Figure D-13: Effect of bench width on capacity curves for granular cohesive in 3-D analyses: h_w = 10 feet and s = 4d

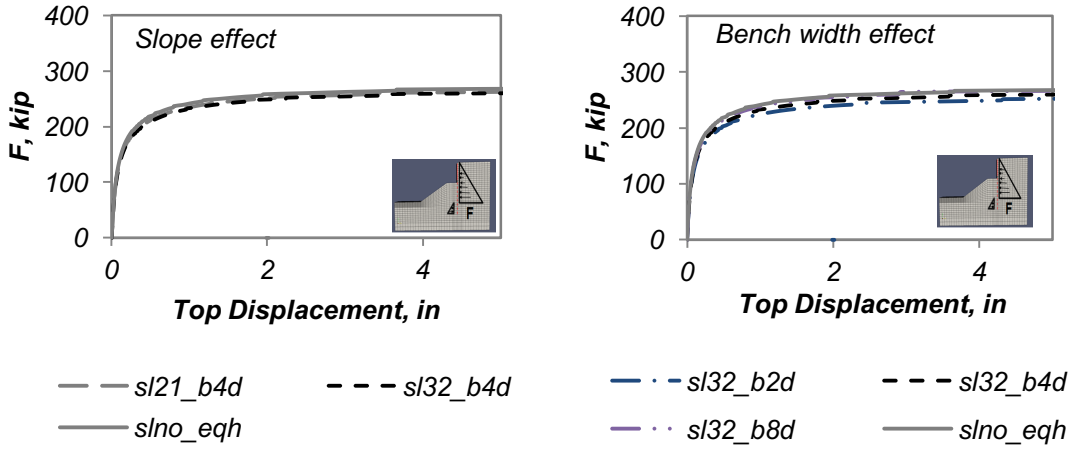

(a) (b)

Figure D-14: Capacity curves for granular cohesive soil in 3-D analyses for h_w = 10 feet and s = 3d: (a) slope effect; (b) effect of bench width

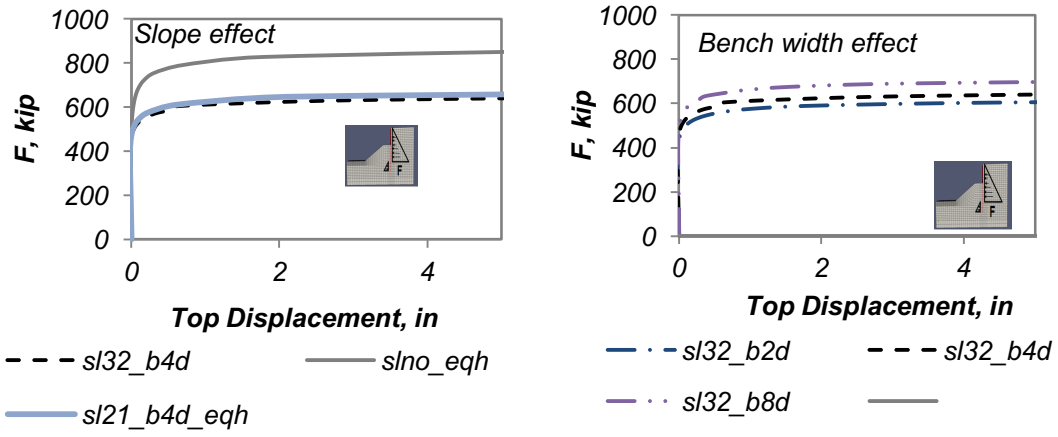

(a) (b)

Figure D-15: Capacity curves for granular cohesive soil in 3-D analyses for h_w = 15 feet and s = 4d: (a) slope effect; (b) effect of bench width

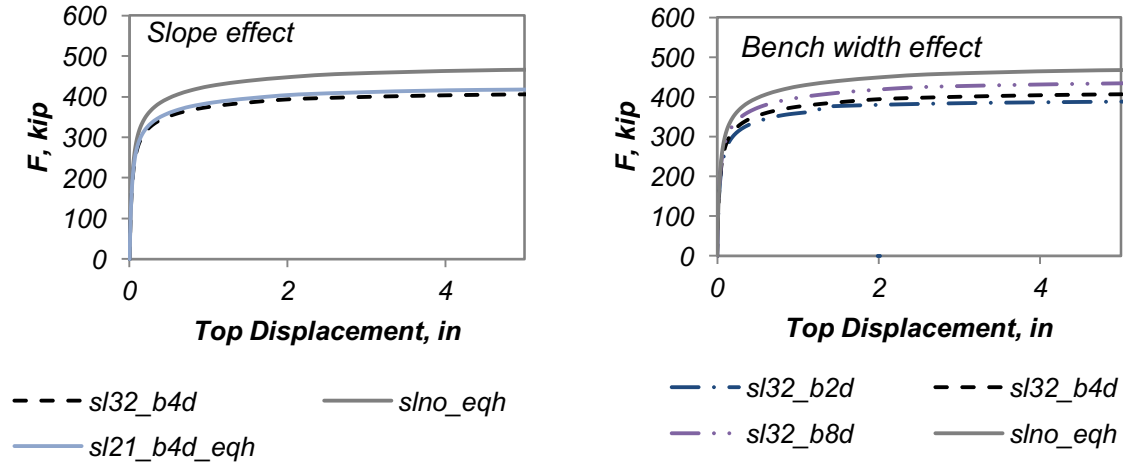

(a) (b)

Figure D-16: Capacity curves for granular cohesive soil in 3-D analyses for h_w = 15 feet and s = 3d: (a) slope effect; (b) effect of bench width

E. PUSHOVER RESULTS FOR 2-D ANALYSES WITH TRIANGULAR LOAD DISTRIBUTION

E.1 Medium-dense sand

E.1.1 Capacity Curves

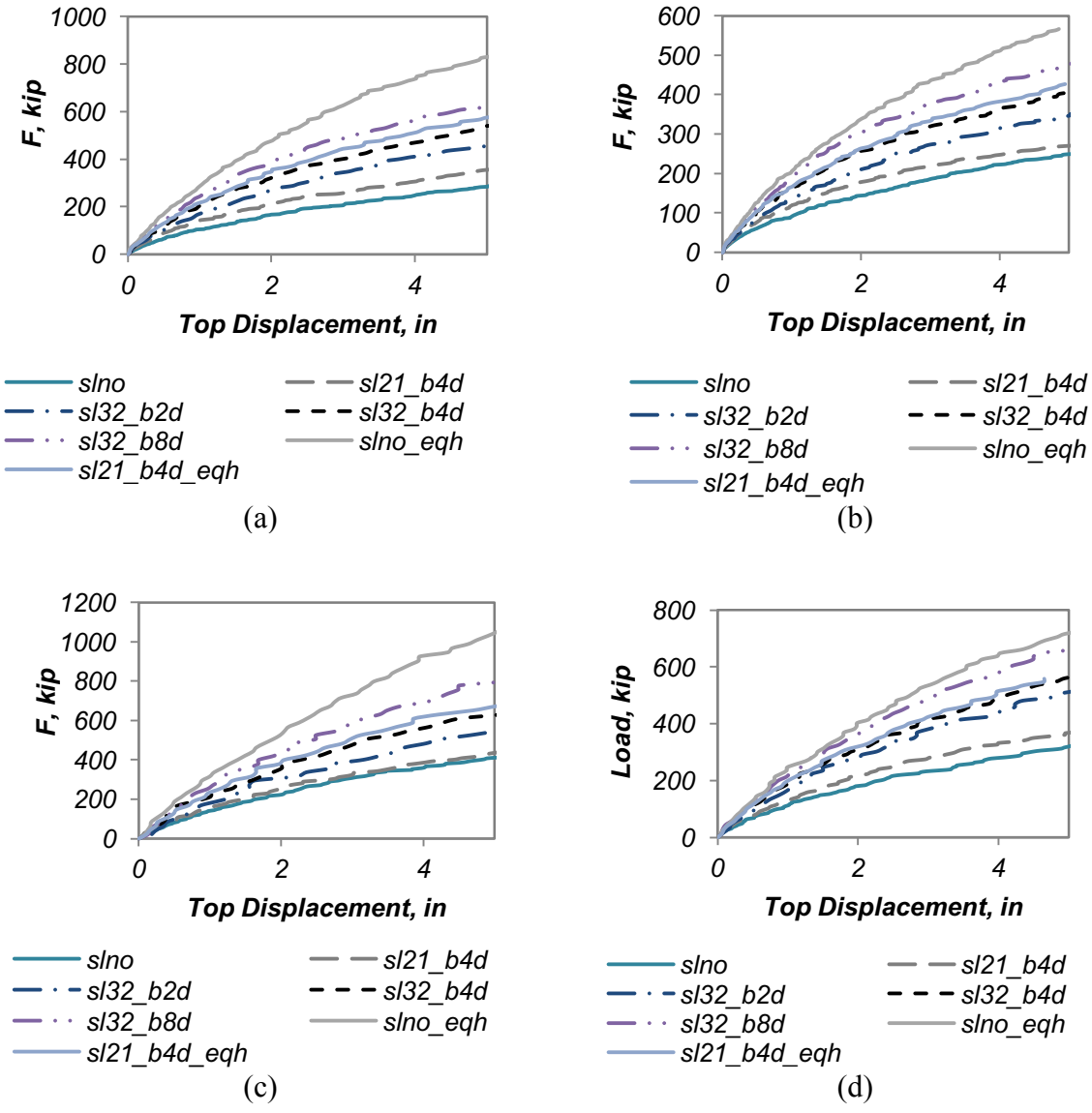

Figure E-1: Capacity curves for medium-dense sand in 2-D analyses: (a) h_w = 10 feet and s = 4d; (b) h_w = 10 feet and s = 3d; (c) h_w = 15 feet and s = 3d; (d) h_w = 15 feet and s = 4d

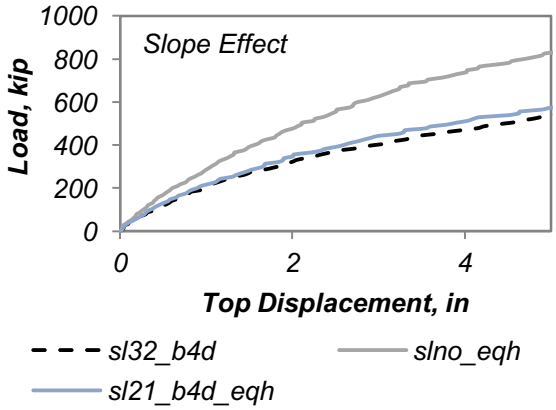

Figure E-2: Effect of slope angle on capacity curves for medium-dense sand in 2-D analyses: h_w = 10 feet and s = 4d

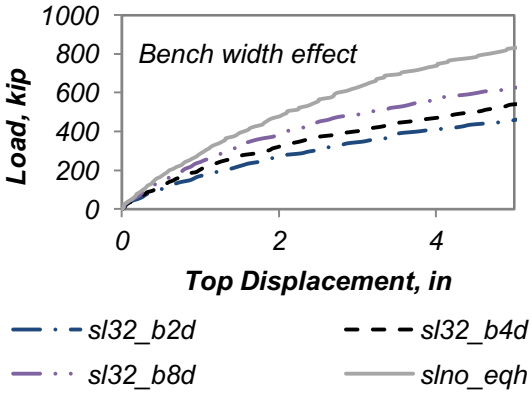

Figure E-3: Effect of bench width on capacity curves for medium-dense sand in 2-D analyses: h_w = 10 feet and s = 4d

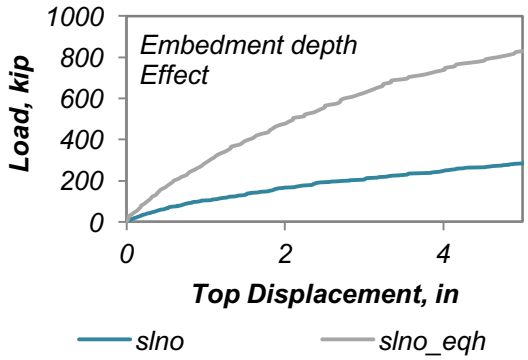

Figure E-4: Effect of embedment depth on capacity curves for medium-dense sand in 2-D analyses: h_w = 10 feet and s = 4d

E.1.2 Deformed Shape and Stresses

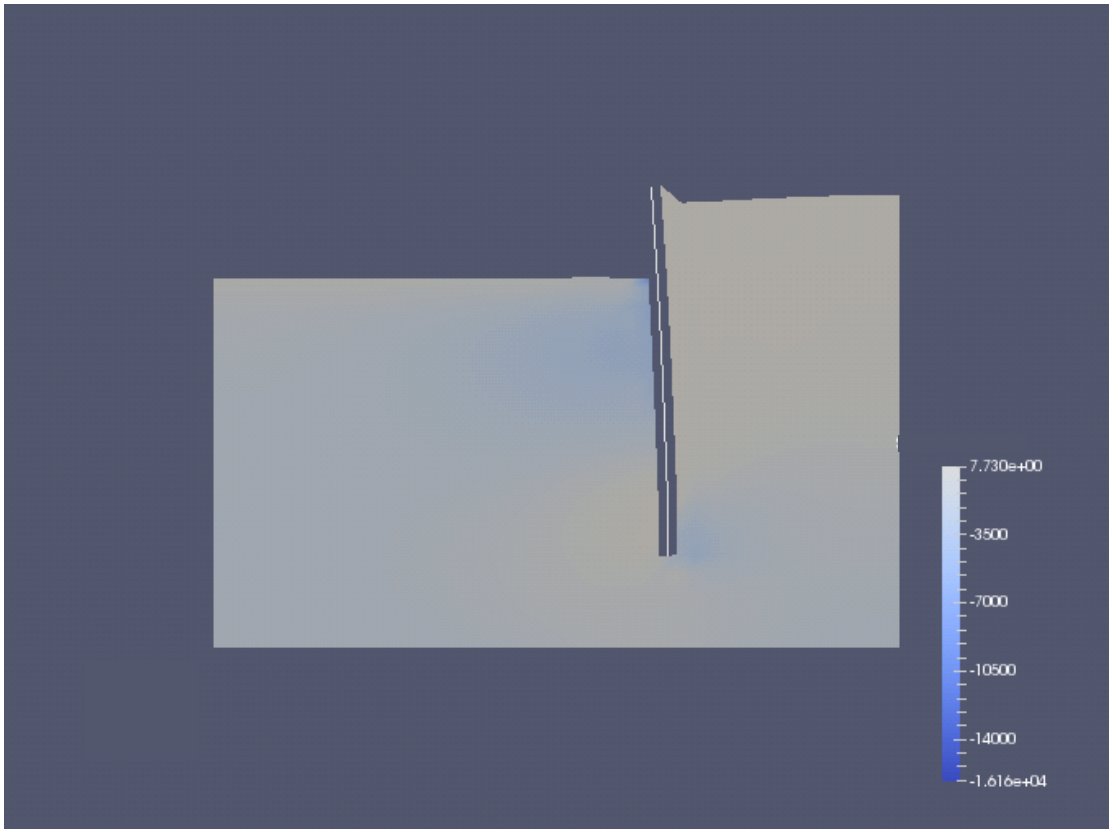

Figure E-5: 2-D model - stresses σ_{YY} and deformed shape for a pile-head displacement = 2 in, for medium-dense sand, h_w = 10 feet, s = 4d, no slope

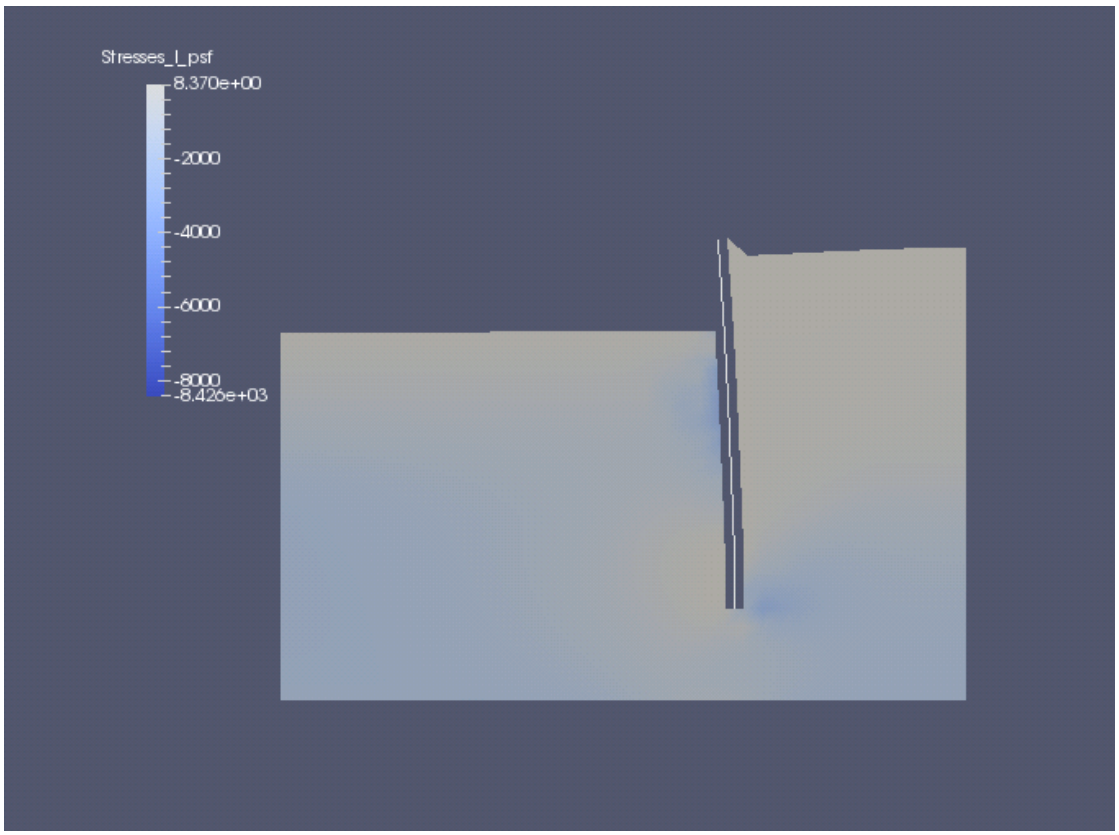

Figure E-6: 2-D model - σ_I at a pile-head displacement = 2 in, for medium-dense sand, h_w = 10 feet, s = 4d, no slope

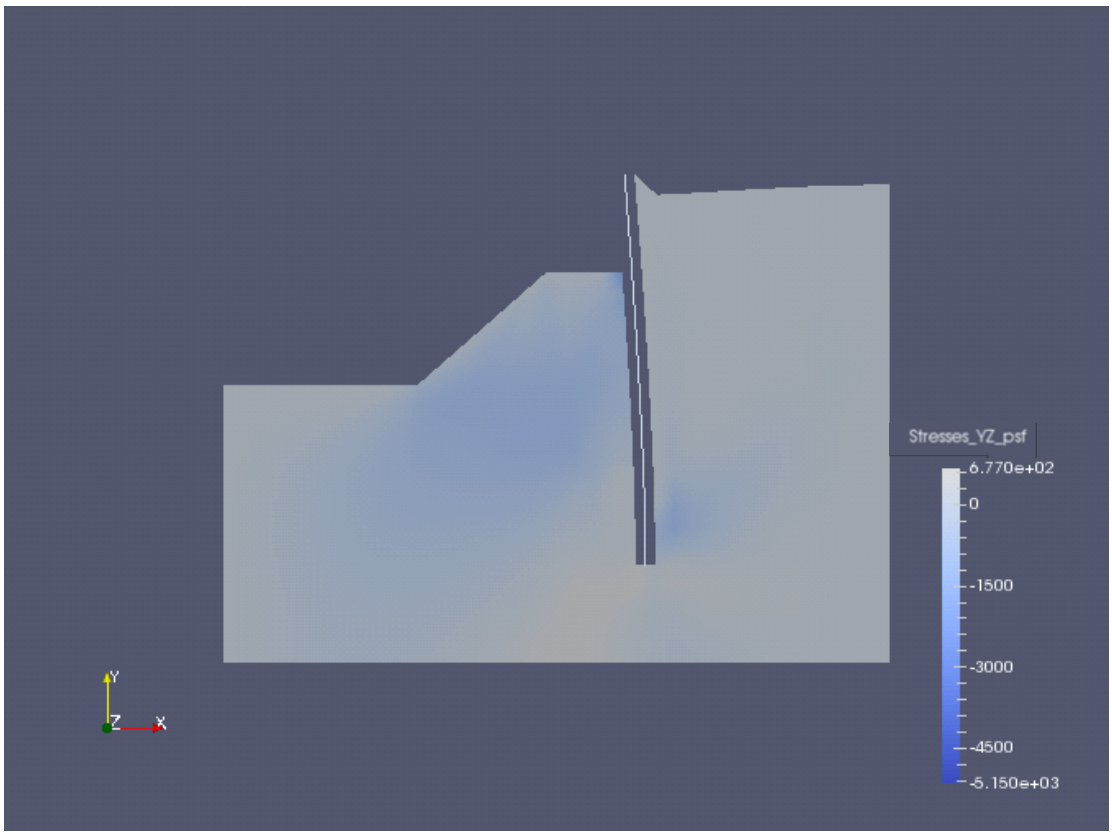

Figure E-7: 2-D model - σ_{YZ} at a pile-head displacement = 2 in, for medium-dense sand, h_w = 10 feet and s = 4d with 3:2 slope and 4d bench

E.1.3 Arching Capability Factor Assessment

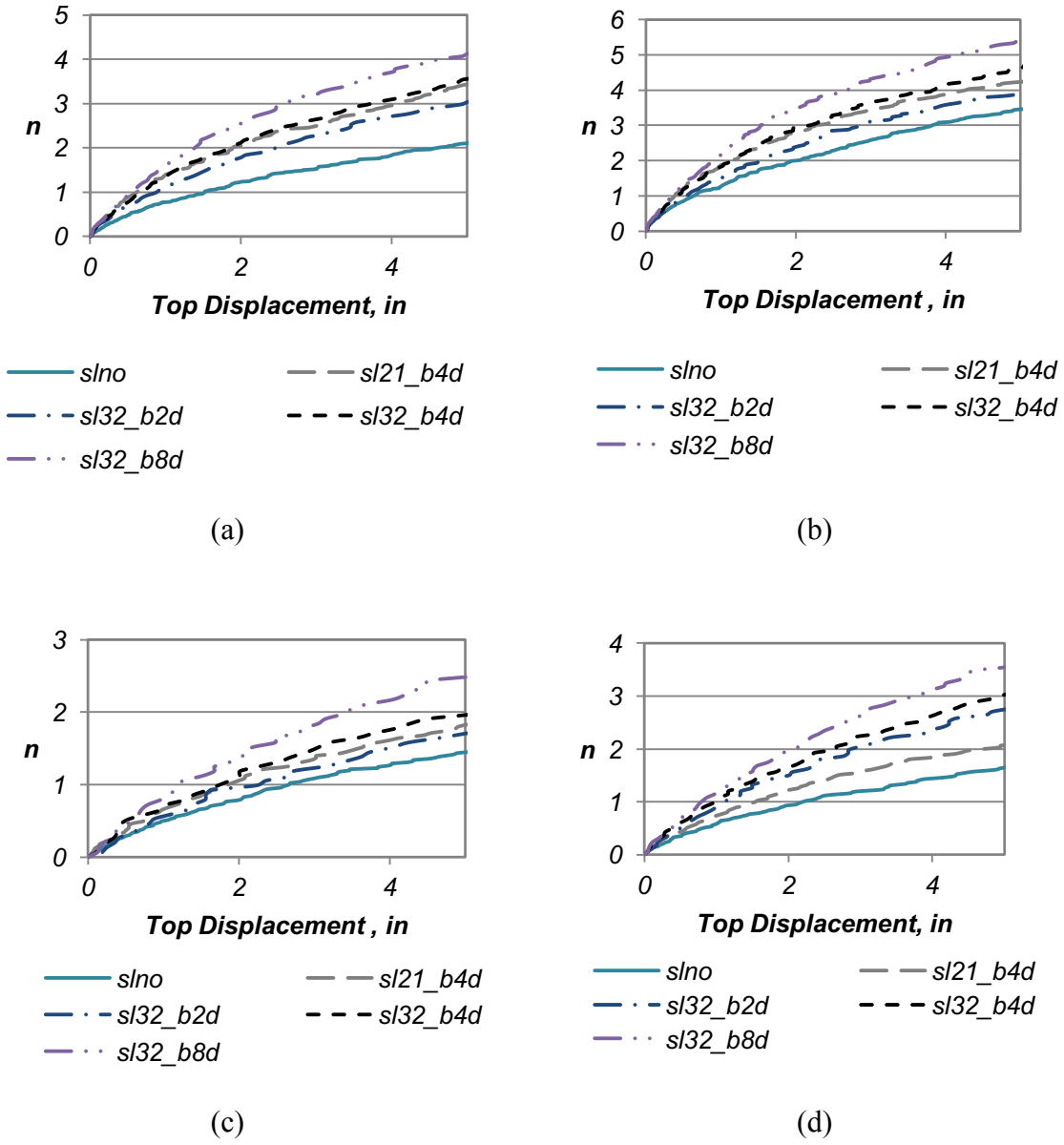

Figure E-8: Arching capability factor assessment for medium dense sand using 2-D analysis: (a) h_w = 10 feet and s = 4d; (b) h_w = 10 feet and s = 3d; (c) h_w = 15 feet and s = 3d; (d) h_w = 15 feet and s = 4d

E.2 Medium-stiff clay

E.2.1 Capacity Curves

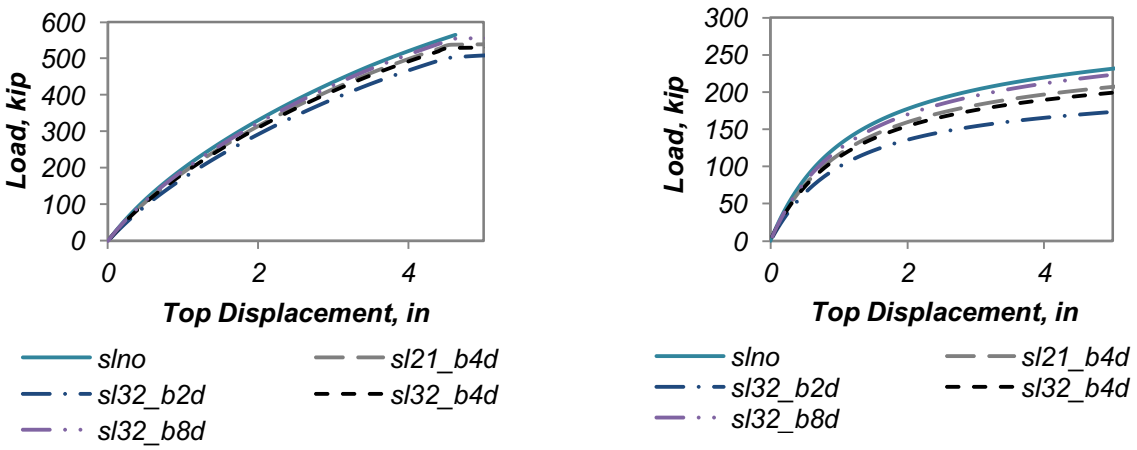

(a)

(b)

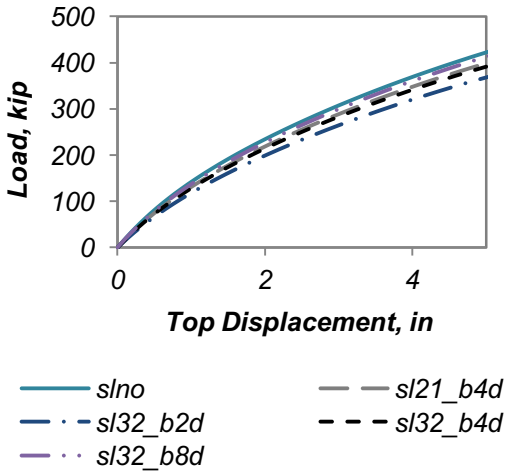

(c)

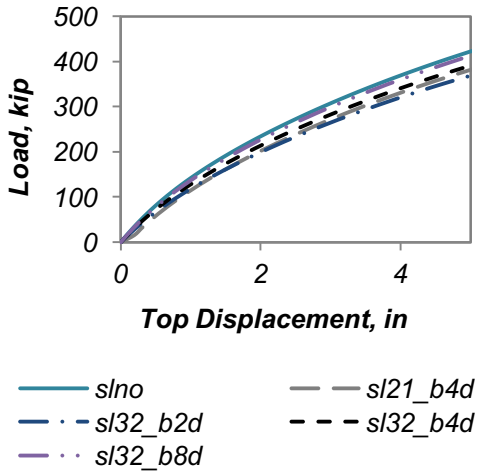

(d)

Figure E-9: Capacity curves for medium-stiff clay for 2-D analyses: (a) h_w = 10 feet and s = 4d; (b) h_w = 10 feet and s = 3d; (c) h_w = 15 feet and s = 3d; (d) h_w = 15 feet and s = 4d

E.2.2 Deformed Shape and Stresses

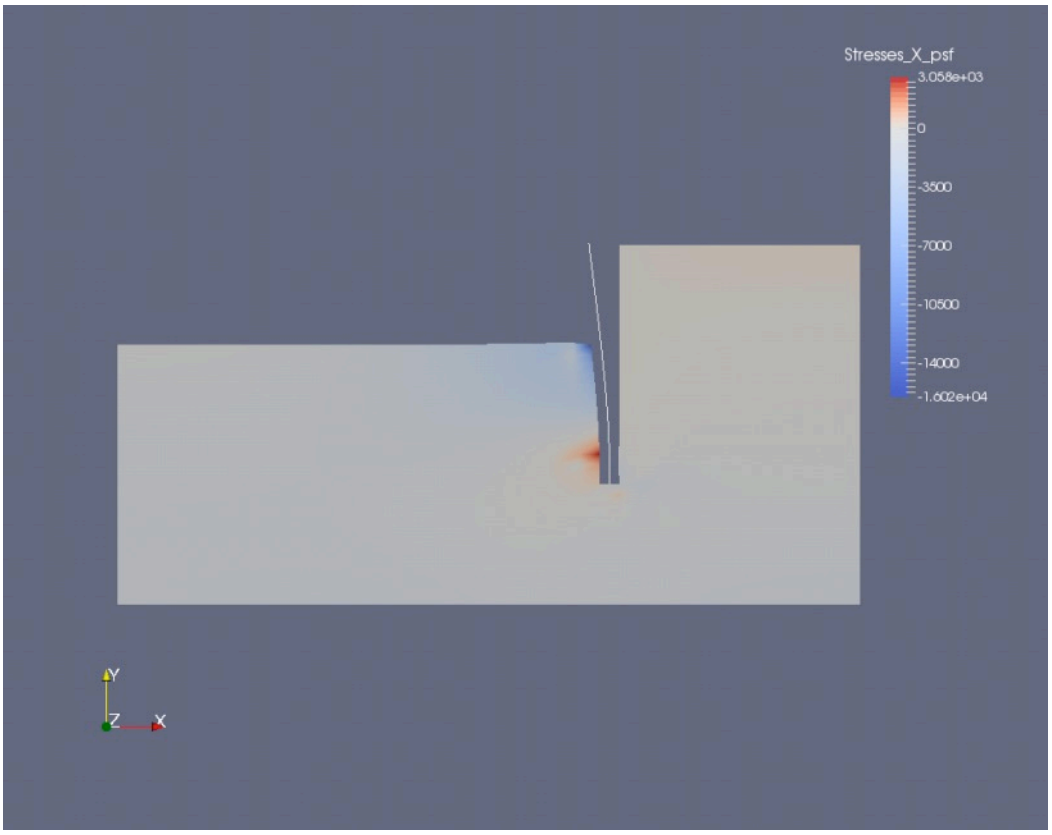

Figure E-10: 2-D model - σ_{XX} direction and deformed shape for a pile-head displacement = 2 in.
Case: medium-stiff clay, h_w = 10 feet, s = 4d, no slope

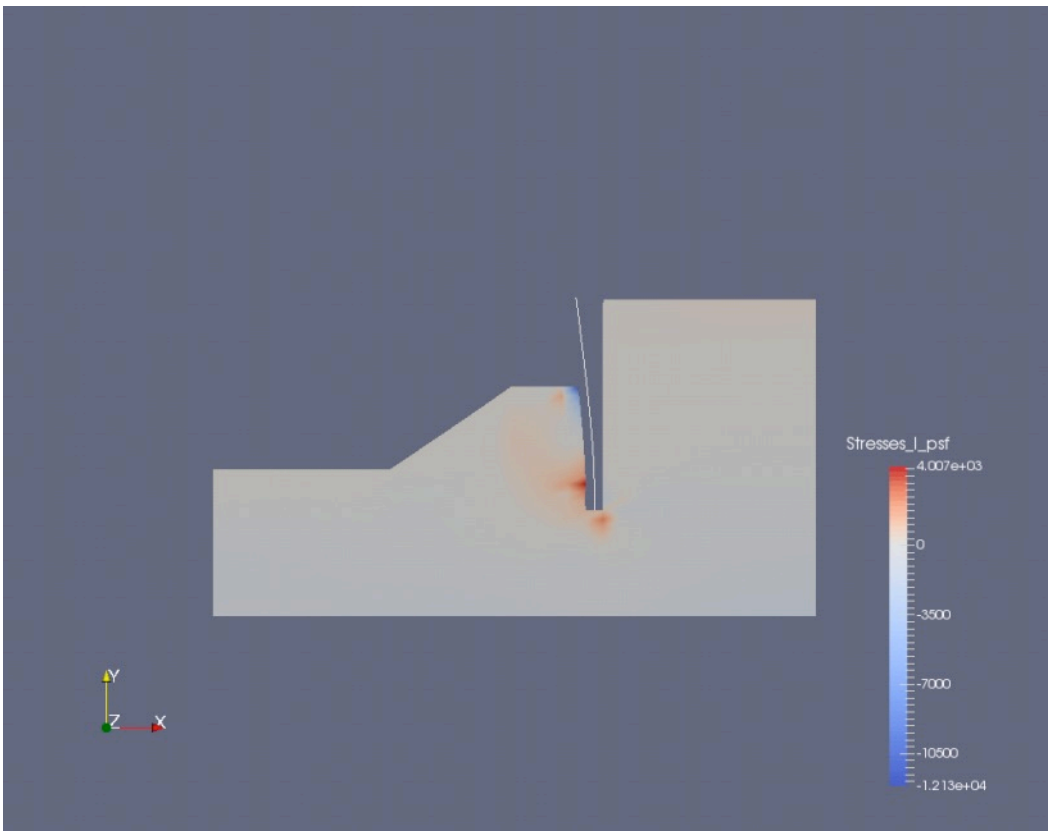

Figure E-11: 2-D model - σ_I for a pile-head displacement = 2 in. Case: medium-stiff clay, h_w = 10 feet and s = 4d with 3:2 slope and 4d bench

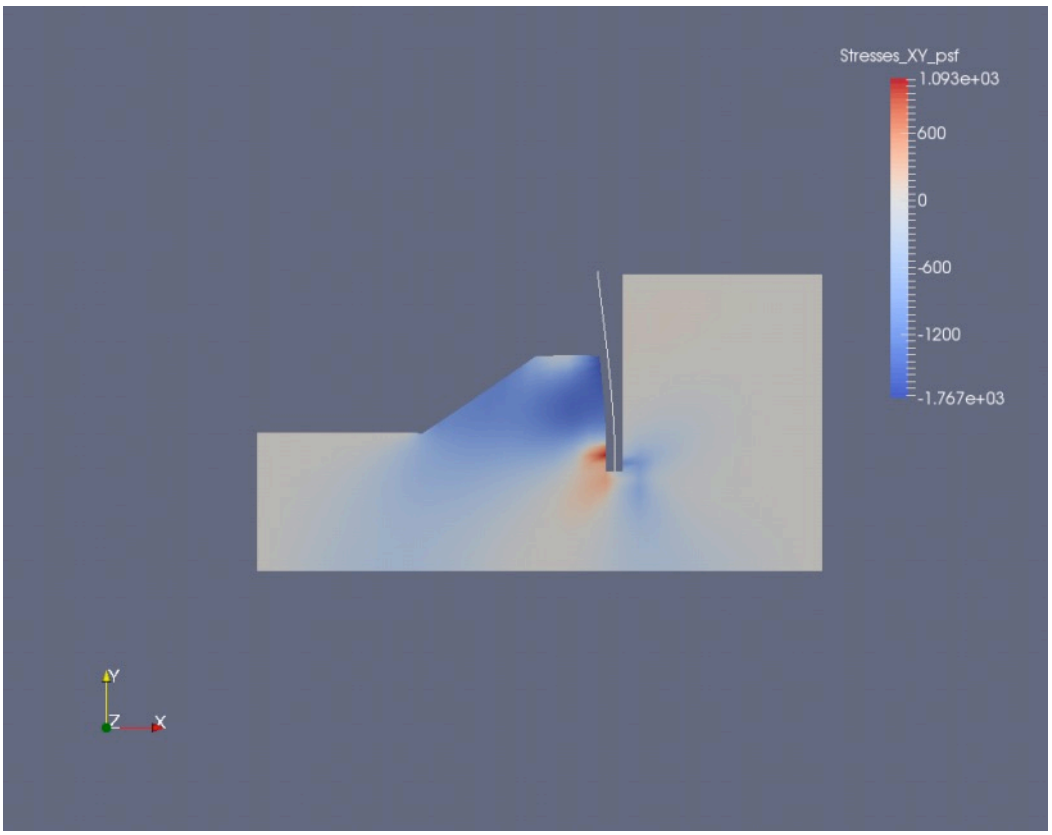

Figure E-12: 2-D model - σ_{XY} and deformed shape for a pile-head displacement = 2 in. Case: medium-stiff clay, h_w = 10 feet and s = 4d with 3:2 slope and 4d bench

E.2.3 Arching Capability Factor Assessment

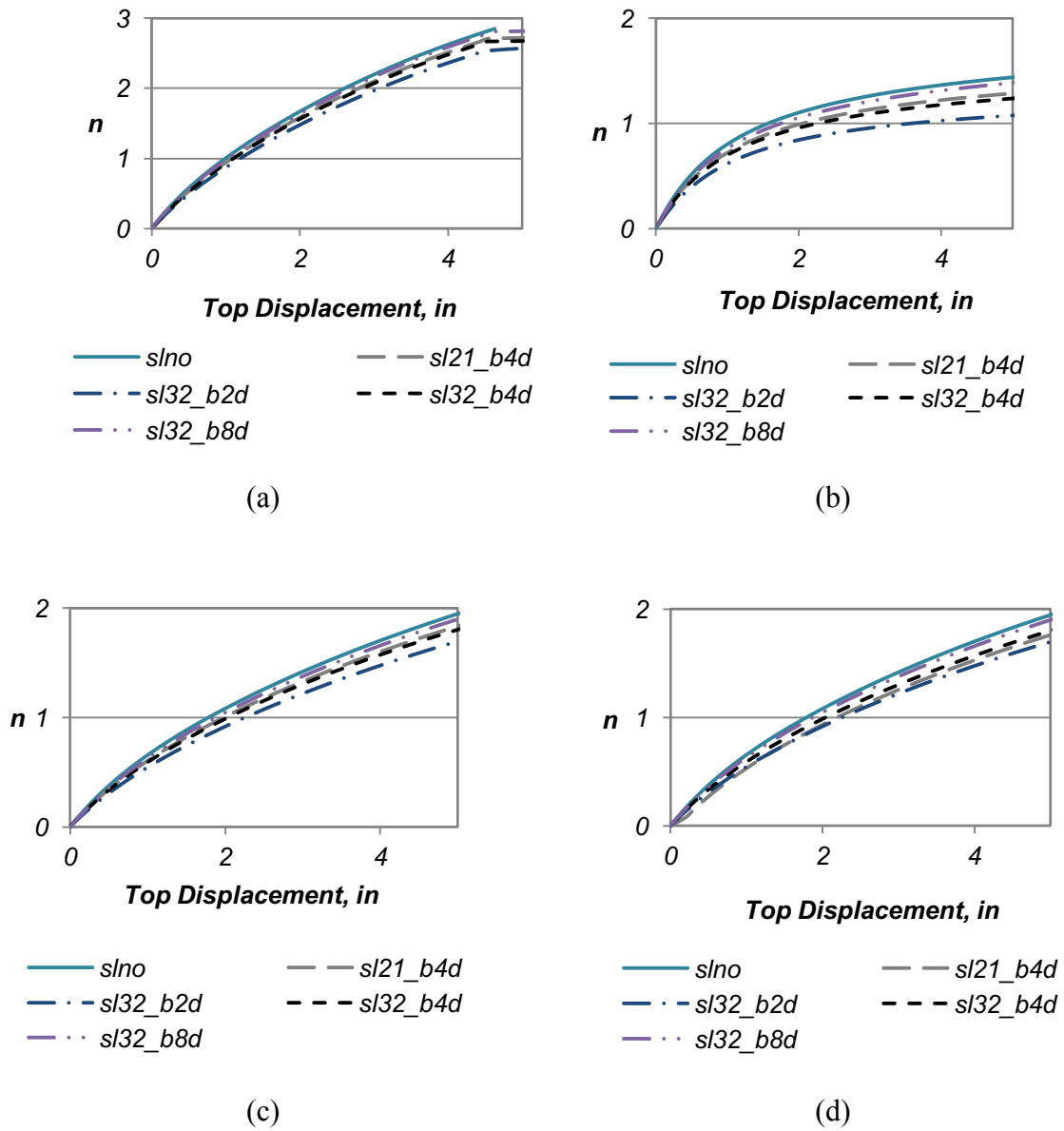

Figure E-13: Arching capability factor assessment for medium-stiff clay using 2-D analysis: (a) h_w = 10 feet and s = 4d; (b) h_w = 10 feet and s = 3d; (c) h_w = 15 feet and s = 3d; (d) h_w = 15 feet and s = 4d

E.3 Granular cohesive soil

E.3.1 Capacity Curves

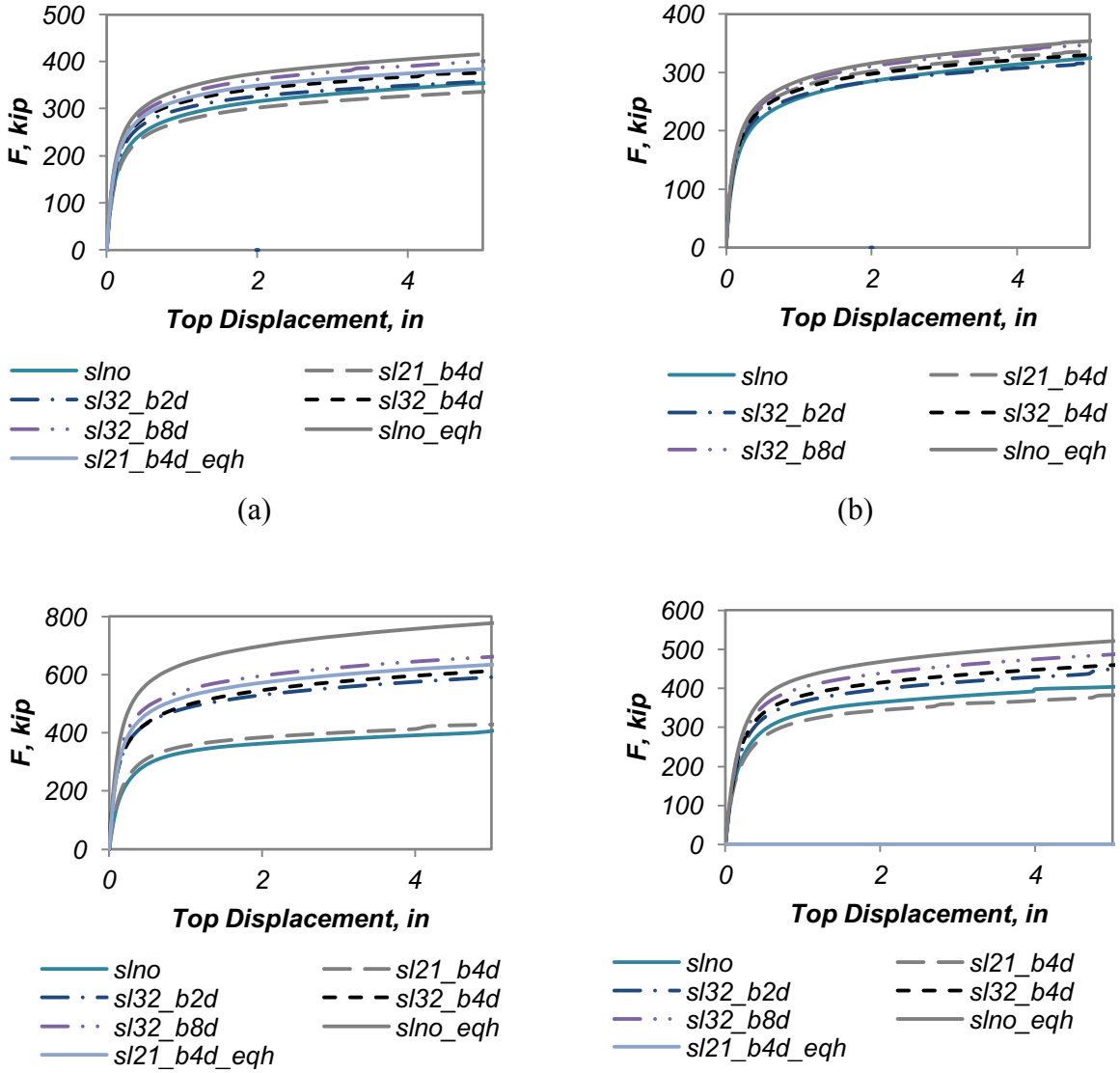

Figure E-14: Capacity curves for granular cohesive soil for 2-D analyses: (a) h_w = 10 feet and s = 4d; (b) h_w = 10 feet and s = 3d; (c) h_w = 15 feet and s = 3d; (d) h_w = 15 feet and s = 4d

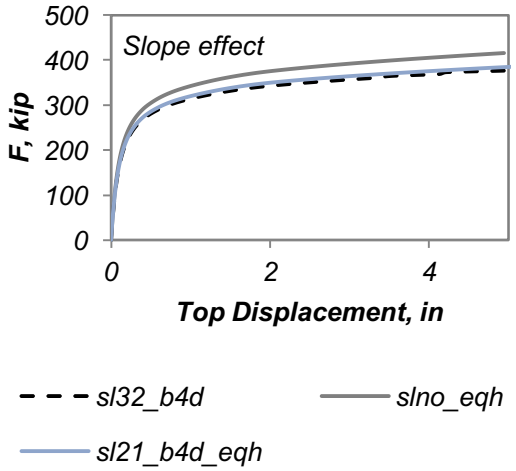

Figure E-15: Effect of slope angle on capacity curves for granular cohesive in 2-D analyses: h_w = 10 feet and s = 4d

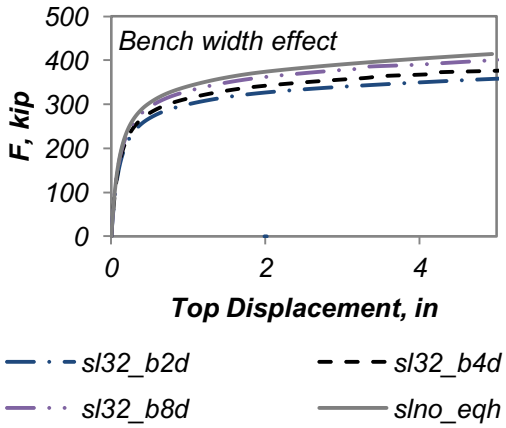

Figure E-16: Effect of bench width on capacity curves for granular cohesive in 2-D analyses: h_w = 10 feet and s = 4d

E.3.2 Deformed Shape and Stresses

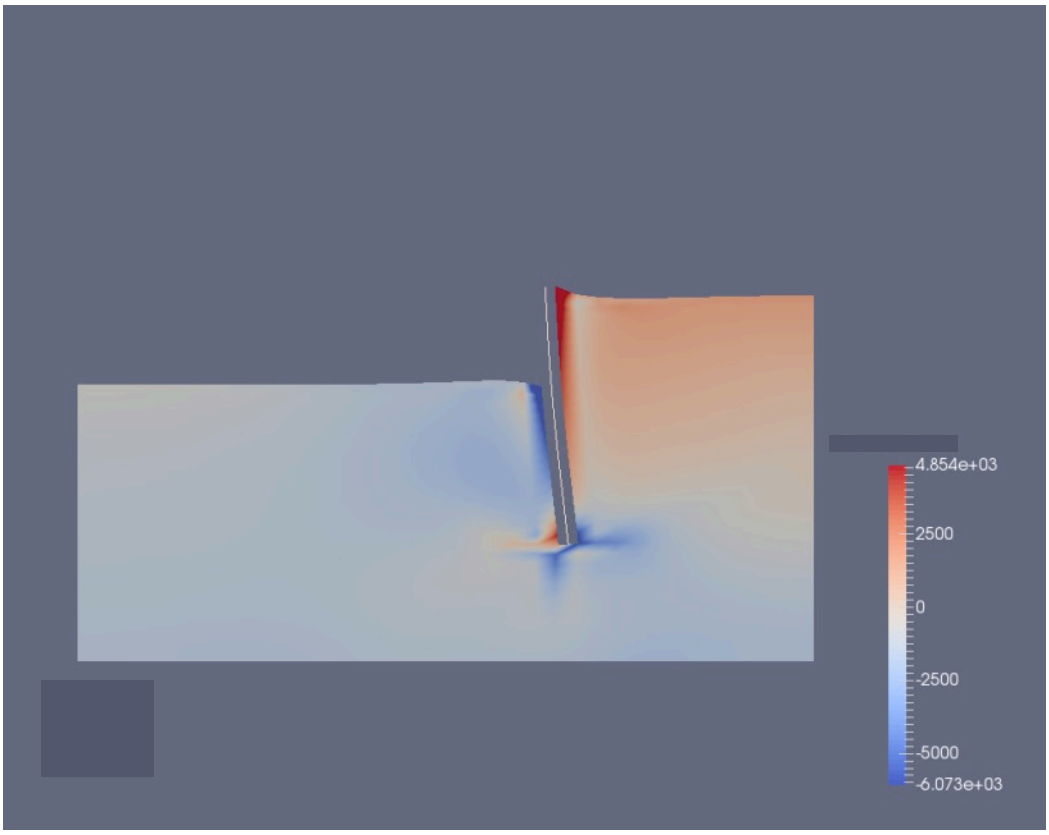

Figure E-17: 2-D model - σ_{YY} at a pile-head displacement = 2 in, for granular cohesive soil, h_w = 10 feet, s = 4d, no slope

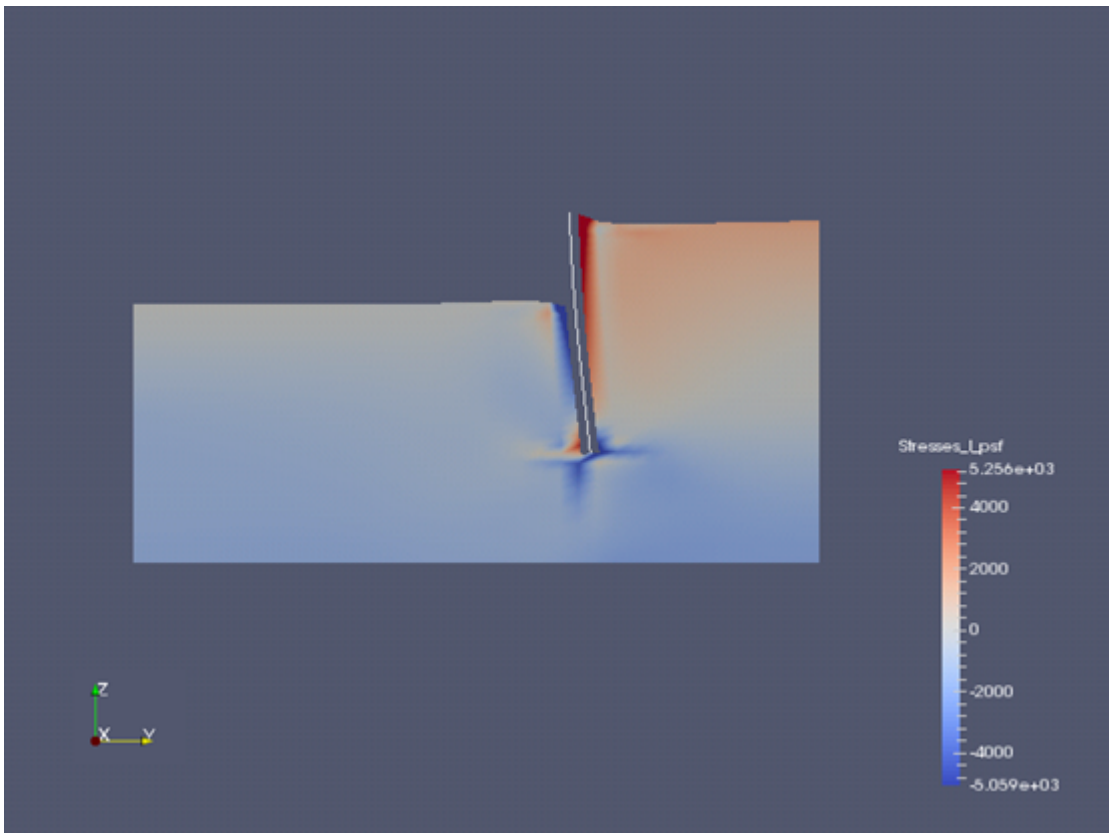

Figure E-18: σ_I at a pile-head displacement = 2 in, for granular cohesive soil, h_w = 10 feet, s = 4d, no slope

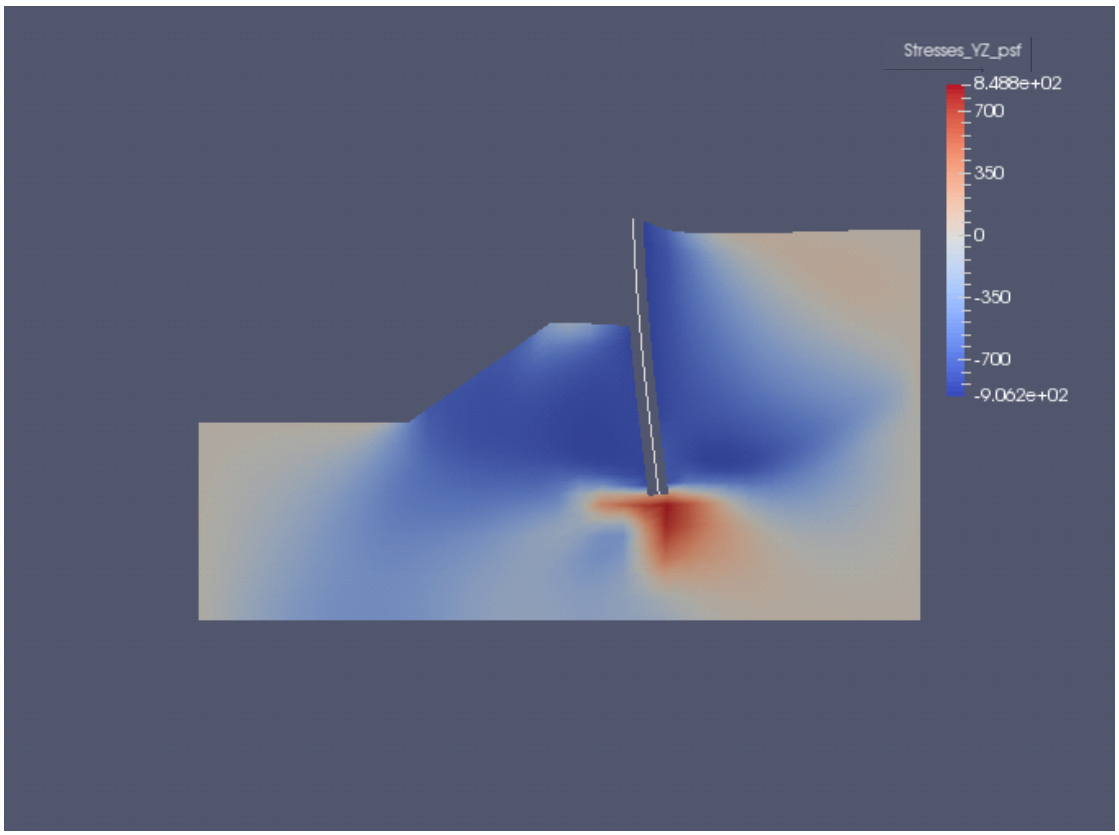

Figure E-19: σ_{YZ} at a pile-head displacement = 2 in, for granular cohesive soil, h_w = 10 feet and s = 4d with 3:2 slope and 4d bench

E.3.3 Arching Capability Factor Assessment

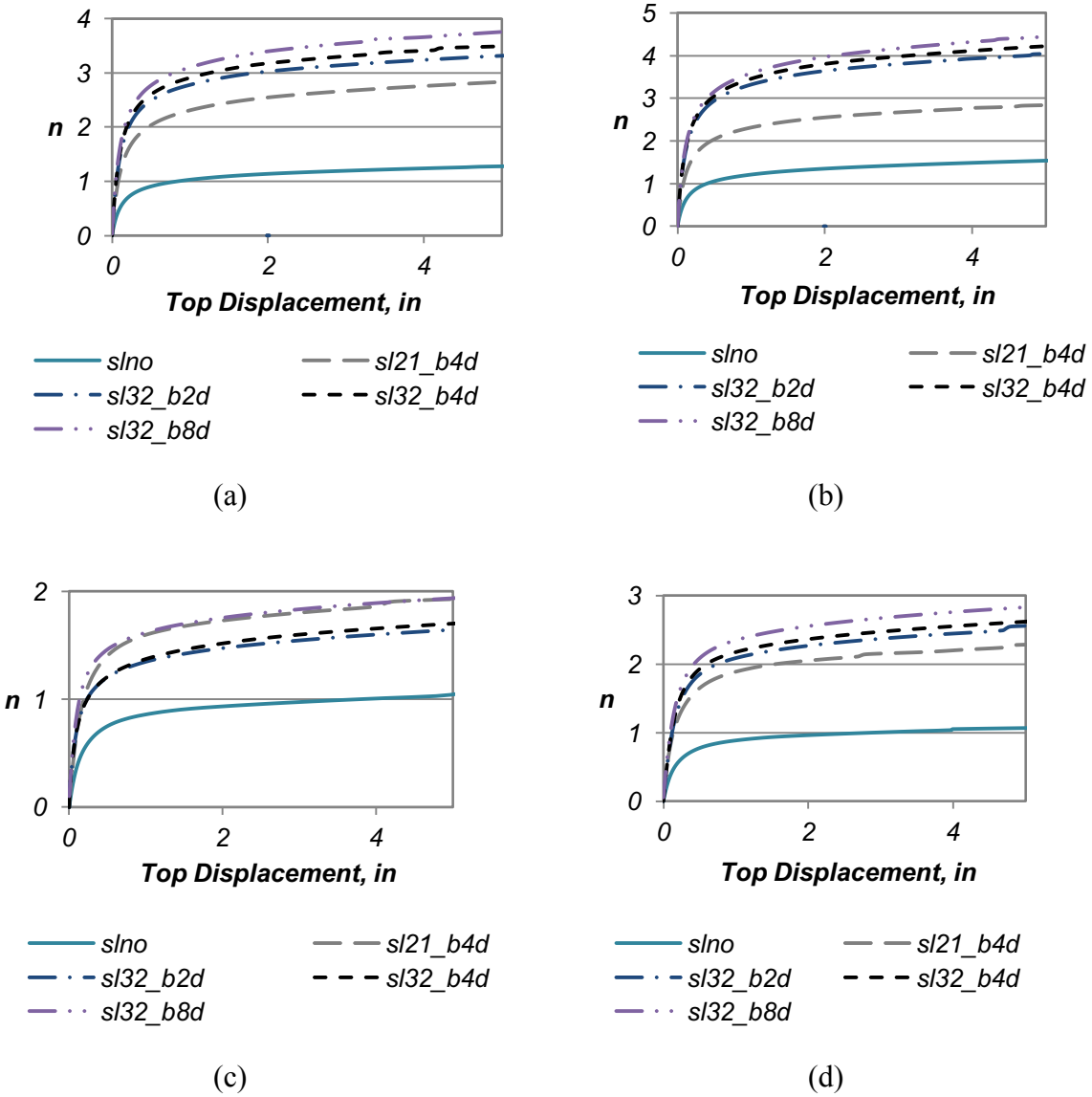

Figure E-20: Arching capability factor assessment for granular cohesive soil using 2-D analysis: (a) h_w = 10 feet and s = 4d; (b) h_w = 10 feet and s = 3d; (c) h_w = 15 feet and s = 4d; (d) h_w = 15 feet and s = 3d